INTERNATIONAL SCIENTIFIC JOURNAL

GEOGRAPHICA PANNONICA

Impact factor: 1.2 | CiteScore: 2.8

Volume 29, Issue 4 (December 2025)

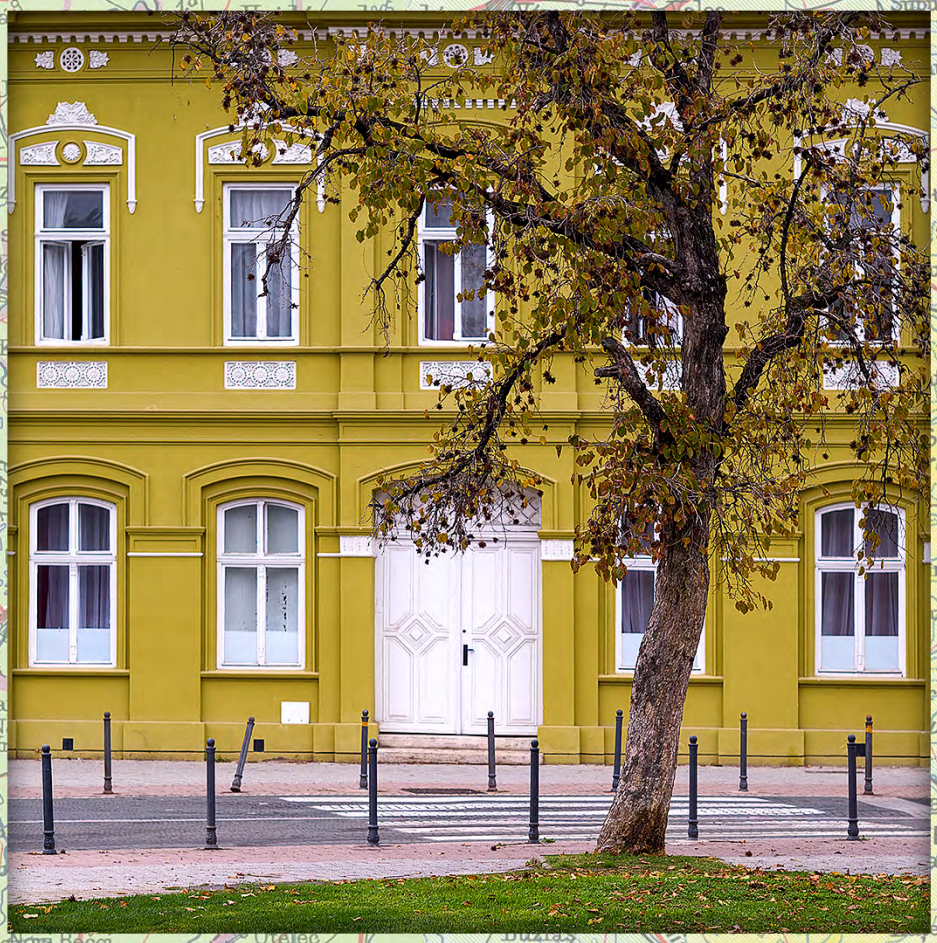

UNIVERSITY OF NOVI SAD, FACULTY OF SCIENCES

DEPARTMENT OF GEOGRAPHY, TOURISM AND HOTEL MANAGEMENT

UNIVERSITY OF NOVI SAD | FACULTY OF SCIENCES
DEPARTMENT OF GEOGRAPHY, TOURISM & HOTEL MANAGEMENT

INTERNATION SCIENTIFIC JOURNAL

GEOGRAPHICA PANNONICA

Impact factor: 1.2 | CiteScore: 2.8 Volume 29, Issue 4, December 2025

ISSN 0354-8724 (hard copy) | ISSN 1820-7138 (online) | UDC 05:91(497.1)=20

ISSN 0354-8724 (hard copy) | ISSN 1820-7138 (online) | UDC 05:91(497.1)=20
UNIVERSITY OF NOVI SAD | FACULTY OF SCIENCES | DEPARTMENT OF GEOGRAPHY, TOURISM & HOTEL MANAGEMENT

INTERNATIONAL SCIENTIFIC JOURNAL

GEOGRAPHICA PANNONICA

EDITORIAL OFFICE

Faculty of Sciences
Department of Geography, Tourism and Hotel Management
Trg Dositeja Obradovića 3, 21000 Novi Sad, Serbia tel. +381 21 450-105 fax +381 21 459-696
Official site: www.dgt.uns.ac.rs

CONTACTS

Lazar Lazić, PhD, full professor
Department of Geography, Tourism and Hotel Management, Serbia, lazar.lazic@dgt.uns.ac.rs

Dragan Milošević, assistant professor
Wageningen University, Netherlands, dragan.milosevic@wur.nl

Official mail of the Journal
gpscijournal@dgt.uns.ac.rs

Internet portal
www.dgt.uns.ac.rs/pannonica.html

Instructions to authors
www.dgt.uns.ac.rs/pannonica/instructions.htm

Contents

INTERNATIONAL SCIENTIFIC JOURNAL | GEOGRAPHICA PANNONICA

Ferenc Ács, Erzsébet Kristóf, Annamária Zsákai
Geographica Pannonica | Volume 29, Issue 4, 282-300

Human Thermal Load of Cfb Climate Summer Weather Based on the Concept of Required Skin Evaporation

Ferenc Ács[A*], Erzsébet Kristóf[A], Annamária Zsákai[B]

[A] Eötvös Loránd University, Faculty of Science, Department of Meteorology, Pázmány Péter sétány 1/A., Budapest, Hungary; ORCID FA: 0000-0002-1611-6839; EK: 0000-0001-9892-9552

[B] Eötvös Loránd University, Faculty of Science, Department of Human Anthropology, Pázmány Péter sétány 1/C, Budapest, Hungary; ORCID AZ: 0000-0001-8880-2056

Received: July 3, 2025| Revised: December 3, 2025| Accepted: December 16, 2025

doi: 10.5937/gp29-59933

Abstract

We analyzed the human thermal load of summer weather in the Cfb climate based on the results of a new model based on the human body energy balance equation and the skin surface evaporation gradient formula. The active surface of the model is the skin surface, the person is lying in a resting position, its skin type is Fitzpatrick skin type IV. For that purpose, longitudinal research method was performed in 2022 in Martonvásár, Hungary (East-Central Europe), comprising 331 observations in which weather conditions and thermal sensation types were recorded simultaneously. The main observation is that in warm climates and/or weather situations, the amount of thermal load can be very simply characterized by latent heat flux density values of the skin evaporation. From a human point of view, the most important characteristics of summer weather in the Cfb climate are as follows: 1) The latent heat flux density of skin surface evaporation varied between 10 and 300-350 Wm^{-2}, while the operative temperature ranged between 25 °C and 80 °C. 2) The relationship between skin surface evaporative resistance and operative temperature can be characterized by an exponential function. In cases of thermal sensation type "neutral", skin surface evaporative resistance values are mostly above 0.5 $hPa \cdot m^2 \cdot W^{-1}$. Observations made by people with different skin types are essential to generalize the results.

Keywords: Cfb climate; summer weather; human thermal load; required skin evaporation; evaporative resistance of skin

Introduction

Experiencing thermal load is deeply subjective (von Humboldt, 1845), especially during the summer season when the excess of heat approaches its maximum values (Hantel & Haimberger, 2016). Table 1 gives a brief overview of the climatological methods for characterizing heat excess. As we see, the examination of heat-excess can be linked, but does not necessarily have to be linked to living beings. Even today, the statistical analysis of data in space and time is a frequently used methodology. The analysis of heatwaves and warm extremes has grown in popularity recently (Basarin et al., 2020). The vast majority of the studies are not related to the living world (Bokros & Lakatos, 2022; Megyeri-Korotaj et al., 2023; Boras et al., 2022), but it should be emphasized that several studies have dealt with the investigation of the relationship between heat waves and mortality, or illnesses (Fouilett et al.,

* Corresponding author: Ferenc Ács; e-mail: acs@caesar.elte.hu

2006; Páldy et al., 2018; Khosla & Guntupalli, 1999). Among the many climate indices, the tourism climate index (TCI) should be mentioned (Mieczkowski, 1985). The index is applied to actual conditions and tries to express the simultaneous, integrated effect of several meteorological elements on the tourist's comfort in a quantified form. It should be mentioned that there are newer modified versions of this index (Kovács et al., 2017). However, in TCI the human being is not specified.

Table 1. Brief overview of the climatological methods for characterizing environmental heat excess.

Methods	**Chosen features**		
	Climatic characteristic	**Living being**	**The size of the living community**
Data analysis	heat waves, warm extremes, climate indices		
Heat index	thermal load in warm period	human	group of people
Köppen's method	seasonality	vegetation	biome size
Physiologically equivalent temperature	thermal load	human	group of people
Universal Thermal Climate Index	thermal stress	human	group of people
Concept of the required skin evaporation	thermal load in warm period	human	individuals

In contrast to extreme events and targeted applications, climate has annual and/or seasonal characteristics. The most common method for describing the annual characteristics of the climate (averages and fluctuations) is the method of the Köppen (Köppen, 1936). Köppen's method is vegetation-based (Köppen, 1900), it is designed for biome-scale applications. In Köppen's climate formula, the 3rd symbol (*a* – hot summer, *b* – warm summer, *c* – cool summer, *d* – extremely continental) characterizes the type of summer heat availability (Kottek et al., 2006), which is independent from the type of the biome. In summary: Köppen's method do characterize summer, but only for orientation.

In contrast to Köppen's method, the heat index (HI) only focuses on the summer period. The thermal load subject is a human. This "standard human" represents a group of people. In the case of HI, it is 170 cm tall, weighs 67 kg, walks in the shade at a speed of 1.5 ms^{-1} in a light breeze of 2.7 ms^{-1}, wearing long pants and a short-sleeved shirt (Mohan et al., 2014). The human characteristics are not taken into account in calculating HI values, but they are included implicitly in the categorization of heat risk. The method requires only 2 input data: air temperature and relative humidity. It is described and applied, for instance, in Hungary in the period 1971-2020 by Bátori (2022). In the United States, HI is also used in meteorological operational practice.

In our days and age, the use of energy balance-based methods in biometeorological applications has become widespread (Potchter et al., 2018). By calculating the energy balance of the human body covered with clothing, the effect of human characteristics on thermal load can also be analyzed. Thus, these methods make it possible to simulate the subjective

experience of the climate (von Humboldt, 1845). Among these, the two most popular methods are the PET (Physiologically Equivalent Temperature) and UTCI (Universal Thermal Climate Index) methods. Both methods use "standardized human", the advantage is that the thermal load is to be applied to a group of people, the disadvantage is that the subjective nature disappears in the characterization of the human-climate relationship. We emphasize that the climate is what we perceive it to be. It should be noted that the "standardized human" in the PET, UTCI, and HI methods are different and tend to be men. In the Austria-Hungary region, the PET index was used most often (Matzarakis et al., 2005; Matzarakis & Gulyás, 2006). There is also a study that focus on estimating the thermal load in the summer months (Gulyás & Matzarakis, 2009). However, the assessment of summer warm extremes using the PET or UTCI methods is becoming widespread (Basarin et al., 2020; Błazejczyk et al., 2014; Pecelj et al., 2019).

The simplest energy balance-based method is the one that uses the concept of required skin evaporation (Parsons, 1997). The method can only be used in climatic or weather conditions that cause excess heat. If there is no heat storage, then the skin evaporation (practically sweating as his value changes) that compensates for the excess heat is the required skin evaporation, and therefore this must be determined as a residual term in the energy balance equation. Although the method is very simple, it is less widely used due to the more complicated determination of other terms that make up the energy balance. To the best of our knowledge, there are no studies dealing with quantification of summer excess heat based on the concept of required skin evaporation. This study aims to fill this gap.

The specific objectives of this study are as follows: to characterize the relationship between 1) latent heat flux density of required skin evaporation (λE_{tot}^{req}) and operative temperature (T_o), 2) λE_{tot}^{req} and thermal perception types and 3) skin evaporative resistance (r_{skin}) and T_o. 4) We also aimed to test the behavior of the model to changes in skin albedo. Finally, 5) we also talk about the applicability of the model. It should be noted that the longitudinal experiment is performed in lowland area of the Pannonian region (Hungary, Martonvásár) in the summer of 2022. The person was wearing minimal summer clothing and was always in a lying position.

Methodology

The study is conducted using the longitudinal research method. An important part of the study is the observation of thermal perception. Since thermal perception observations occurred, information about skin type is also essential. Fitzpatrick skin typing method is used for characterizing skin type. Human thermal load is characterised by latent heat flux density of the required skin evaporation. Thermal perception type results were derived by strict application of an observation protocol. Finally, thermal load and thermal sensation type results are carefully checked and filtered. The listed methodological elements are now described one by one.

Longitudinal observations

The basic methodology of this study is longitudinal observation. One person (hereafter observer) performed long-term, concurrent thermal load estimations and thermal perception observations in the summer of 2022. There were a total of 331 observations. The methodological elements used by the observer during each observation are described below.

Basic equations of the model

If there is no heat storage (constant surface temperature), the energy balance of the skin surface of the human body can be written as follows,

$$R_n + M - \lambda E_r - H_r - W - H_s - \lambda E_{tot} = 0, \quad (1)$$

where R_n is the net radiation energy flux density [Wm^{-2}], M is the metabolic energy flux density [Wm^{-2}], λE_r is respiratory latent heat flux density [Wm^{-2}], H_r is respiratory sensible heat flux density [Wm^{-2}], W is mechanical work flux density [Wm^{-2}], which refers to the activity being carried out, H_S is sensible heat flux from the skin surface [Wm^{-2}] and λE_{tot} is latent heat flux density of the skin evaporation [Wm^{-2}]. In this model, M = 55 Wm^{-2} and W = 0 Wm^{-2} since the person is in a lying position.

The latent heat flux density of skin surface evaporation can also be expressed using the gradient formula,

$$\lambda E_{tot} = \frac{\frac{\rho \cdot c_p}{\gamma} \cdot [e_S(T_s) - e_a]}{r_{skin} + r_{Ha}}, \quad (2)$$

where ρ is air density [kgm^{-3}], c_p is specific heat at constant pressure [$Jkg^{-1}°C^{-1}$], γ is psychrometric constant [$hPa°C^{-1}$], T_{skin} is skin surface temperature (34 °C) (Campbell & Norman, 1997), $e_S(T_{skin})$ [hPa] is saturation vapor pressure at T_{skin}, e_a is actual vapor pressure [hPa], r_{skin} is the evaporative resistance of skin surface [sm^{-1}] and r_{Ha} is the aerodynamic resistance for expressing convective heat exchange effect [sm^{-1}].

Applying the model conditions, we can express λE_{tot} and r_{skin} from equations (1) and (2),

$$\lambda E_{tot} = R_n + M - \lambda E_r - H_r - H_s, \quad (3)$$

$$r_{skin} = \frac{\frac{\rho \cdot c_p}{\gamma} \cdot [e_S(T_s) - e_a]}{R_n + M - \lambda E_r - H_r - H_s} - r_{Ha}, \quad (4)$$

When estimating λE_{tot}^{req}, we use not only equation (3), but also equation (4). Namely, $\lambda E_{tot}^{req} = \lambda E_{tot}$ if $r_{skin} \geq 0$.

Parametrizations

Radiation: R_n is parameterised as simply as possible,

$$R_n = S \cdot (1 - \alpha_{skin}) + \epsilon_a \sigma T_a^4 - \epsilon_{skin} \sigma T_{skin}^4, \quad (5)$$

where *S* is incoming solar radiation [Wm^{-2}], σ is Stefan-Boltzmann constant [$Wm^{-2}K^{-4}$], ϵ_a is emissivity of the cloudy sky, T_a is air temperature [°C], α_{skin} is skin surface albedo and ϵ_{skin} is emissivity of the skin surface. In this study, $\alpha_{skin} = 0.27$ (concentration of melanosomes in epidermis is 2.5%, (Nielsen et al., 2008)), $\epsilon_{skin} = 1$. S is estimated according to the work of Ács et al. (2025),

$$S = Q_0 \cdot [\alpha + (1 - \alpha) \cdot rsd], \quad (6)$$

where Q_0 is solar radiation constant [$MJ \cdot m^{-2} \cdot hour^{-1}$] referring to clear sky conditions and a 1-hour time period, α is the corresponding dimensionless constant referring to the same hour

and *rsd* is relative sunshine duration. ϵ_a depends on clear sky emissivity ϵ_{cs} and cloudiness N (0 for cloudless and 1 for completely overcast conditions),

$$\epsilon_a = \epsilon_{cs} \cdot (1 - N^{1.6}) + 0.9552 \cdot N^{1.6}, \quad (7)$$

$$\epsilon_{cs} = 0.51 + 0.066 \cdot \sqrt{e_a}\,. \quad (8)$$

ϵ_{cs} and ϵ_a are given according to Brunt (1932) and Konzelmann et al. (1994), respectively. Heat flux densities: λE_r and H_r depend upon M, they are parameterized according to Fanger (1970) as follows,

$$\lambda E_r = 1.72 \cdot 10^{-5} \cdot M \cdot (5867 - e_{ap}), \quad (9)$$

$$H_r = 1.4 \cdot 10^{-3} \cdot M \cdot (T_s - T_a), \quad (10)$$

where e_{ap} is actual vapor pressure [Pa]. H_S is expressed as

$$H_s = \rho \cdot c_p \cdot \frac{T_s - T_a}{r_{Ha}}, \quad (11)$$

r_{Ha} depends upon wind velocity (Campbell & Norman, 1997),

$$r_{Ha}[sm^{-1}] = 7.4 \cdot 41 \cdot \sqrt{\frac{D}{U_{0.5}}}, \quad (12)$$

where D is the diameter of the cylindrical body used to approach the body of the observer (Campbell & Norman, 1997), $U_{0.5}$ is the wind speed at 0.5 m height (sunbed height).

Operative temperature: It depends upon air temperature, net radiation flux density and wind speed (Campbell & Norman, 1997) as follows,

$$T_o = T_a + \frac{R_n}{\rho \cdot c_p} \cdot r_{Ha}. \quad (13)$$

Estimation of thermal sensation

Each thermal sensation observation is performed according to the following observation protocol: 1) the observer always started the observation with a "neutral" thermal sensation, that is, he started from a place of about 24–26 °C, 2) all observations were made wearing the same sports garment, which was (the observer was male) put on immediately before starting the observation (we emphasize that the observer was not wearing other clothing than the sports garment), 3) the observer always performed the observation in a supine position for at least 10 minutes lying on the sunbed shown in Figure 1, 4) the beach pillow was always stored in a place where the thermal sensation was "neutral" and 5) all data were registered immediately (observed thermal sensation type and the meteorological variables) after the observation.

Figure 1. The observer during a thermal perception observation. His anthropometric data are as follows: body mass 89 kg, body height 190 cm, and age 67 years

As we can see, we used the human body's thermal sensors as a monitoring tool. This has advantages and disadvantages. A major advantage is that the thermal sensation is human-based, as every living being (species, individual) experiences and perceives the same thermal supply differently. Its disadvantage is that it is difficult to quantify, i.e. it is less exact, and it is subjective. The variability of subjectivity is not great, we can state this based on our experience. The fact that the thermal sensation is described in words rather than numbers should not be considered a disadvantage.

Management of thermal sensation and thermal load data

Weather and thermal sensation data are collected concurrently. The following data management protocol was applied after each observation: 1) Human thermal load characteristics (latent heat flux density of the skin evaporation and evaporative resistance of the skin) were calculated immediately after each observation, 2) the cases when the method was not applicable ($r_{skin} < 0$) were eliminated, 3) the consistency between thermal load characteristics and thermal perception types observed was checked and 4) we have always tried to interpret the relationships that cause thermal load. The printed list of output variables calculated with the model is shown in Figure 2.

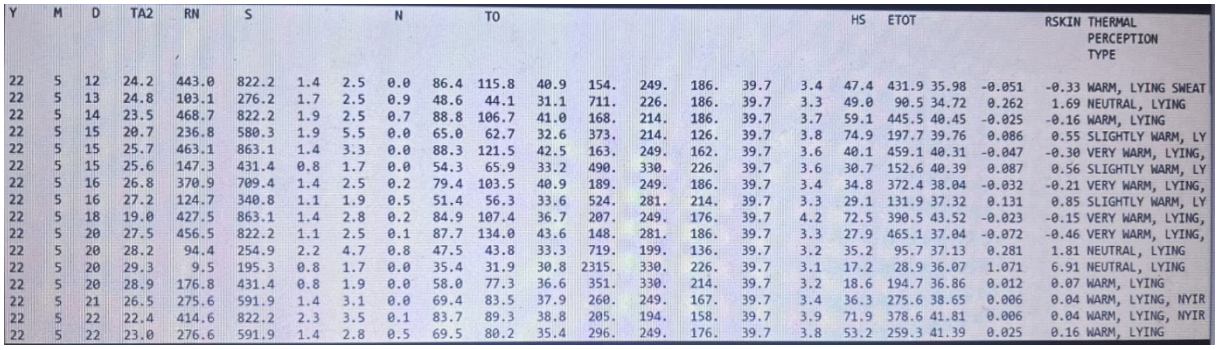

Y	M	D	TA2	RN	S			N		TO						HS	ETOT		RSKIN	THERMAL PERCEPTION TYPE
22	5	12	24.2	443.0	822.2	1.4	2.5	0.0	86.4	115.8	40.9	154.	249.	186.	39.7	3.4	47.4	431.9	35.98	-0.051	-0.33 WARM, LYING SWEAT
22	5	13	24.8	103.1	276.2	1.7	2.5	0.9	48.6	44.1	31.1	711.	226.	186.	39.7	3.3	49.0	90.5	34.72	0.262	1.69 NEUTRAL, LYING
22	5	14	23.5	468.7	822.2	1.9	2.5	0.7	88.8	106.7	41.0	168.	214.	186.	39.7	3.7	59.1	445.5	40.45	-0.025	-0.16 WARM, LYING
22	5	15	20.7	236.8	580.3	1.9	5.5	0.0	65.0	62.7	32.6	373.	214.	126.	39.7	3.8	74.9	197.7	39.76	0.086	0.55 SLIGHTLY WARM, LY
22	5	15	25.7	463.1	863.1	1.4	3.3	0.0	88.3	121.5	42.5	163.	249.	162.	39.7	3.6	40.1	459.1	40.31	-0.047	-0.30 VERY WARM, LYING,
22	5	15	25.6	147.3	431.4	0.8	1.7	0.0	54.3	65.9	33.2	490.	330.	226.	39.7	3.6	30.7	152.6	40.39	0.087	0.56 SLIGHTLY WARM, LY
22	5	16	26.8	370.9	709.4	1.4	2.5	0.2	79.4	103.5	40.9	189.	249.	186.	39.7	3.4	34.8	372.4	38.04	-0.032	-0.21 VERY WARM, LYING,
22	5	16	27.2	124.7	340.8	1.1	1.9	0.5	51.4	56.3	33.6	524.	281.	214.	39.7	3.3	29.1	131.9	37.32	0.131	0.85 SLIGHTLY WARM, LY
22	5	18	19.0	427.5	863.1	1.4	2.8	0.2	84.9	107.4	36.7	207.	249.	176.	39.7	4.2	72.5	390.5	43.52	-0.023	-0.15 VERY WARM, LYING,
22	5	20	27.5	456.5	822.2	1.1	2.5	0.1	87.7	134.0	43.6	148.	281.	186.	39.7	3.3	27.9	465.1	37.04	-0.072	-0.46 VERY WARM, LYING,
22	5	20	28.2	94.4	254.9	2.2	4.7	0.8	47.5	43.8	33.3	719.	199.	136.	39.7	3.2	35.2	95.7	37.13	0.281	1.81 NEUTRAL, LYING
22	5	20	29.3	9.5	195.3	0.8	1.7	0.0	35.4	31.9	30.8	2315.	330.	226.	39.7	3.1	17.2	28.9	36.07	1.071	6.91 NEUTRAL, LYING
22	5	20	28.9	176.8	431.4	0.8	1.9	0.0	58.0	77.3	36.6	351.	330.	214.	39.7	3.2	18.6	194.7	36.86	0.012	0.07 WARM, LYING
22	5	21	26.5	275.6	591.9	1.4	3.1	0.0	69.4	83.5	37.9	260.	249.	167.	39.7	3.4	36.3	275.6	38.65	0.006	0.04 WARM, LYING, NYIR
22	5	22	22.4	414.6	822.2	2.3	3.5	0.1	83.7	89.3	38.8	205.	194.	158.	39.7	3.9	71.9	378.6	41.81	0.006	0.04 WARM, LYING, NYIR
22	5	22	23.0	276.6	591.9	1.4	2.8	0.5	69.5	80.2	35.4	296.	249.	176.	39.7	3.8	53.2	259.3	41.39	0.025	0.16 WARM, LYING

Figure 2. A cutout image of the model results. Notations: Y - year, M - month, D - day, TA2 - air temperature [°C], RN - radiation balance [Wm^{-2}], S - global radiation [Wm^{-2}], N - cloudiness, TO - operative temperature [°C], HS - sensible heat flux density from the skin surface [Wm^{-2}], ETOT - latent heat flux density of skin surface evaporation [Wm^{-2}] and RSKIN - skin surface resistance to evaporation [$hPa \cdot m^2 \cdot W^{-1}$]

The designation of the selected variables can be found in the title of Figure 2. Looking at Figure 2, we can notice negative r_{skin} values (penultimate column).

Fitzpatrick skin typing method

Fitzpatrick skin typing method (Fitzpatrick, 1975) is a well-known method for classifying human skin types. It uses three input variables: skin color (a numerical value on a scale 1-30), eye color (a numerical value on a scale 1-16) and hair color when the person is young (a numerical value on a scale 1-10). The classification is done based on the sum of the points. The scores and Fitzpatrick skin types are presented in Table 2.

Table 2. Fitzpatrick skin types

Type	Scores	Skin color characterization	Skin tone
I	0-6	Caucasian, blond/red hair, freckles, fair skin, blue eyes	very fair
II	6-13	Caucasian	fair
III	14-20	Darker Caucasian, light Asian	fair to medium
IV	21-27	Mediterranean, Asian, Hispanic	medium

V	28-34	Middle Eastern, Latin, light-skinned black, Indian	olive to dark
VI	35+	Dark-skinned black	very dark

Location

The region and the location are presented in Figure 3. Town Martonvásár is located in the lowland area of Hungary. Within Martonvásár, the observations took place in the garden of a family house, the basic tools required for the observation are also shown in Figure 3 (on the right).

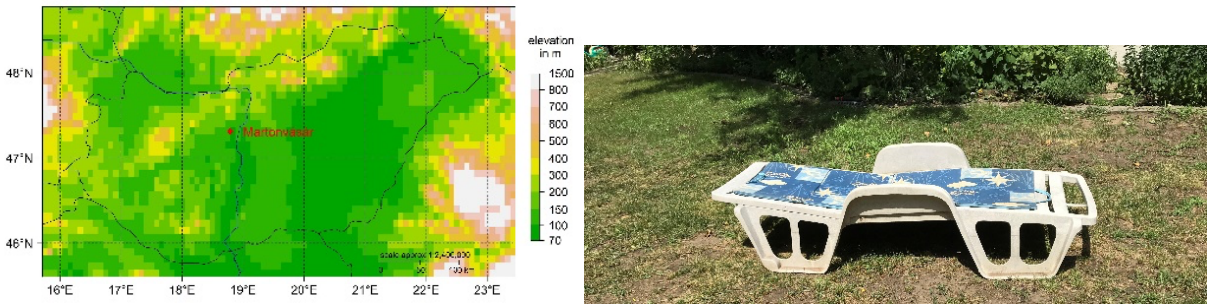

Figure 3. On the left, the location of the observation is Martonvásár, it is presented on a topographical map of Hungary. On the right, the sunbed and the beach pillow for monitoring the thermal sensation without observer in the garden of the observer's house

Martonvásár is located in the Central Transdanubian Region. This region is hilly, so the variety of meso- and microclimates is somewhat greater than in the plain areas. The Köppen method does not see this variability, but neither does the variability of summer heat supply conditions, especially in terms of human thermal load. The following observations and analyses are intended to fill this gap.

Data

Weather and human data are used.

Human data

Two human data types are used: a) data needed for identifying skin type (skin color, eye color and hair color at a young age) and b) data characterizing thermal perception type. Data for identifying skin type are presented in Table 3.

Table 3. Input variables for determining Fitzpatrick skin type and the Fitzpatrick skin type of the observer

Person	Skin color (scale 1-30)	Eye color (scale 1-16)	Youthful hair color (scale 1-10)	Sum of points	Fitzpatrick skin type and its description
Observer	7	8	8	23	IV, moderate brown skin

Thermal perception data are registered on a 7-grade scale, which contains the following grades: “very warm”, “warm”, “slightly warm”, “neutral”, “cool”, “cold”, “very cold”. In this study, by definition, we only used the first 4 thermal perception types. The method is not applicable to cold thermal perception types. We can see that the terminology used to indicate thermal perception types is somewhat different from the commonly used terminology (Enescu, 2019). We did not distinguish between "very warm" and "unbearably warm/hot". Further discussion of human data can be found in the section Results.

Weather data

We used the following weather data: air temperature, relative humidity of air, average wind speed, wind gust speed, air pressure, relative sunshine duration and cloudiness. All the elements, except for the last two, were measured by the automatic station of the company Időkép. The data are taken from the website of the company Időkép (https://www.idokep.hu/). The beeline distance between the station and the observer's location (garden of a family house) is shorter than 3 km. Cloud cover and relative sunshine duration data are provided by the observer. Cloud cover is estimated visually in tenths. Relative sunshine duration refers to the observer's body because the human body's thermal load is to be estimated. In 2022, there were 331 observations made between May 12 and September 18. The observations not only recorded many cases, but also cases with the lowest and highest heat loads, so multi-year observations were not necessary.

Among weather elements, more attention will be paid to air temperature, incoming solar radiation and relative air humidity. The air temperature values obtained during thermal perception observations are shown in Figure 4.

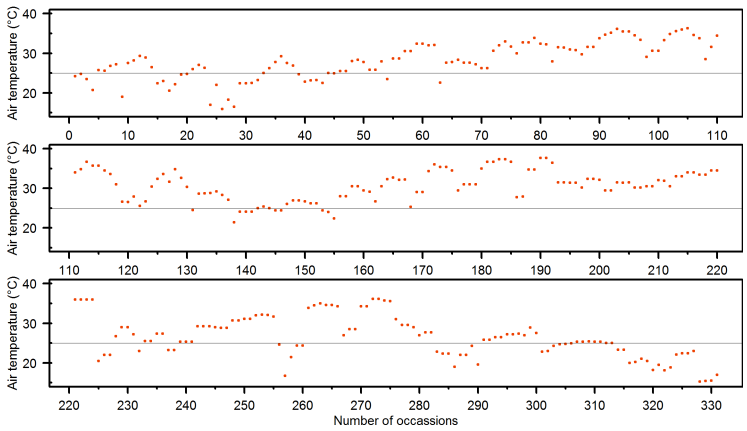

Figure 4. The air temperature values during thermal perception observations

We can see that the lowest air temperature values were around 16 °C (minimum is 15.9 °C), the highest around 37 °C (maximum is 37.2 °C). In the vast majority of the cases, air temperature was higher than 25 °C. In summer, in addition to temperature, incident solar radiation also plays a decisive role. The values of incident solar radiation estimated during the observations are shown in Figure 5.

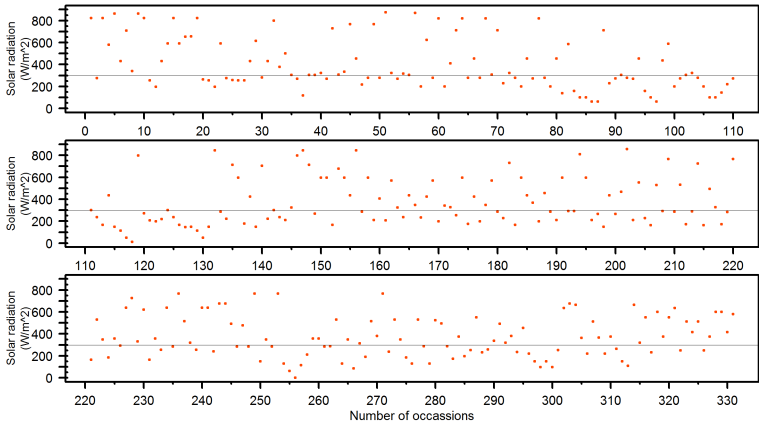

Figure 5. The incoming solar radiation values during thermal perception observations

The smallest value was 49 Wm^{-2}, the largest value was 870 Wm^{-2}. In the vast majority of cases the values exceeded 300 Wm^{-2}. Due to the estimation of skin surface evaporation, air humidity is an important input data. The evolution of these data during the observation period is shown in Figure 6.

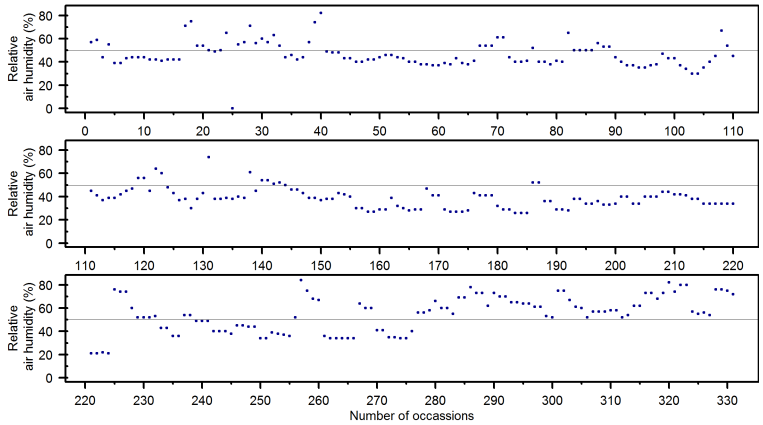

Figure 6. The relative air humidity values during thermal perception observations

The values varied between 20-80% (minimum value was 21%, maximum value was 88%), but the majority of values were below 50%. Wind speed values (not presented here) varied within wide limits. Average wind speed values varied between 0.5-8 ms^{-1}, wind gust speed values between 1.4-13.3 ms^{-1}. The highest wind speed values were in the afternoon on July 10. In the majority of the cases, average wind speed varied between 1.5-3 ms^{-1}.

Results

Several results are presented and discussed. Firstly, we give some basic information regarding M and the skin type of the observer. After this we characterize the relationship between λE_{tot} and operative temperature as well as the relationship between thermal perception types and λE_{tot}. The relationship between r_{skin} and operative temperature is also presented and analysed. Finally, we examined the sensitivity of λE_{tot} to changes in skin albedo and we will talk also about the applicability of the model.

Observer's M value and skin type

When choosing the observer's M value of, we took into account the values of the observer's heart rate (58-65 BPM (beats per minute)), as well as the value range of resting metabolic heat flux density (M_r) (ISO8996, 2004). M_r's range is 55-70 Wm^{-2}. The M_r value of the observer was chosen to be low, because his resting heart rate values are lower. Based on the information presented in Tables 2 and 3, the observer's skin type is skin type IV on the Fitzpatrick skin type scale. The skin color characterization of this skin type is "Mediterranean, Hispanic". This additional information about skin type is given because we made thermal perception observations.

Relationship between skin evaporation and operative temperature

The scatter chart of λE_{tot}–T_o relationship is presented in Figure 7.

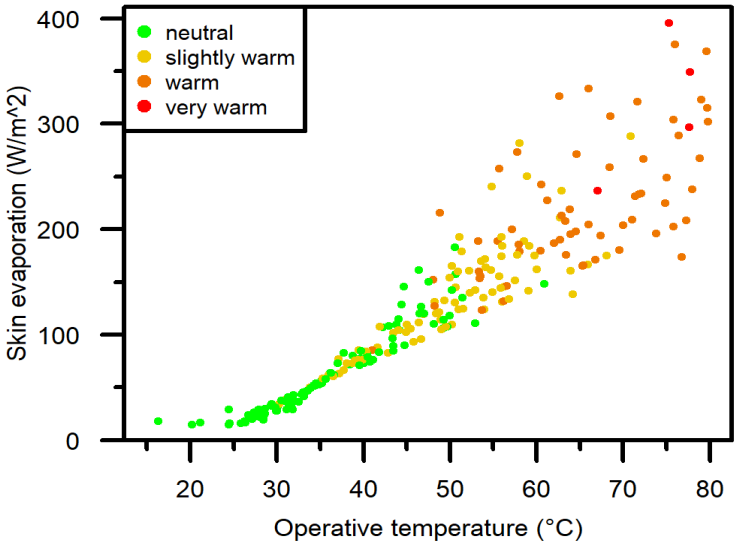

Figure 7. Scatter chart of the latent heat flux density of skin surface evaporation as a function of operative temperature at actual average air humidity and wind speed. Thermal perception types experienced during the observations can also be seen based on the coloring of points

λE_{tot} is the sum of evaporation from dry skin λE_{ds} and sweaty skin λE_{sw}. It should be mentioned that λE_{sw} can be estimated as the difference between λE_{tot} and λE_{ds}. λE_{ds} can be parameterized, for instance, as a function of T_{skin} (Parsons, 2003). The point cloud can be

divided into 2 parts. In the range 25 °C < T_o < 45 °C, the change of λE_{tot} as a function of T_o can be considered linear, the maximum values of λE_{tot} are around 100 Wm^{-2}, the thermal perception types are "neutral" (smaller T_o) and "slightly warm" (larger T_o). In the range 45 °C < T_o < 80 °C, the scatter of the points is significant, and the amount of scatter increases with increasing T_o. The maximum values of λE_{tot} are around 300-400 Wm^{-2}. For T_o = 70 °C, λE_{tot} is scattered between 170 and 320 Wm^{-2}. We can see that in the case of thermal perception types "warm" and "very warm", the points characterizing the λE_{tot}-T_o relationship are irregularly scattered and cannot be characterized by a regression relationship.

Relationship between thermal perception types and skin evaporation
The relationship between thermal perception types and λE_{tot} is presented in Figure 8.

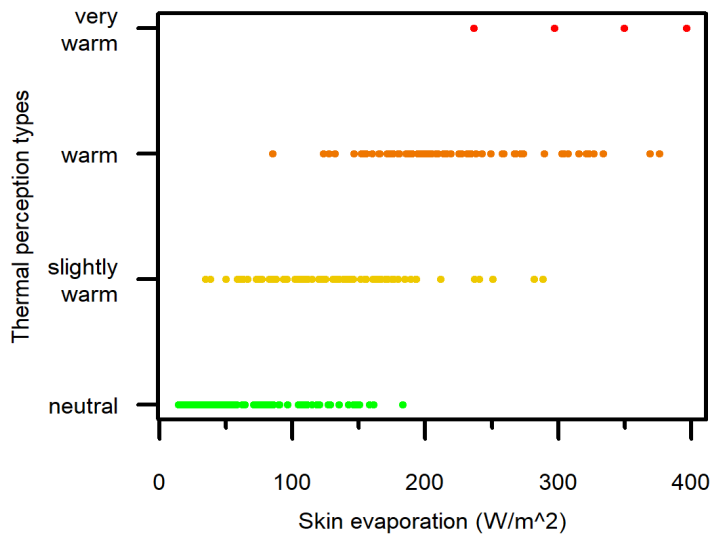

Figure 8. Scatter chart of thermal perception as a function of latent heat flux density of skin surface evaporation

In the range 20 $Wm^{-2} \leq \lambda E_{tot} <$ 160 Wm^{-2} (except for 1 observation), thermal perception type is “neutral”. In the range 50 $Wm^{-2} \leq \lambda E_{tot} <$ 200 Wm^{-2} (except for 8 observations), thermal perception type is “slightly warm”. It can be seen that there is a large overlap between the thermal perception types "neutral" and "slightly warm". Thermal perception type “warm” appeared in the range 130 $Wm^{-2} \leq \lambda E_{tot} <$ 340 Wm^{-2} (except 3 observations). Thermal perception type “very warm” is becoming to be typical in the range 340 $Wm^{-2} < \lambda E_{tot}$. This range is the same as the $T_o \geq$ 75-80 °C range. Note that we did not distinguish between thermal perception types "very warm" and "hot" or "unbearably hot". These latter thermal perception types occur when air temperature is at least 25 °C and incoming solar radiation is at least 700 Wm^{-2}.

Relationship between evaporative resistance of skin and operative temperature
The scatter chart of evaporative skin resistance–operative temperature relationship is presented in Figure 9.

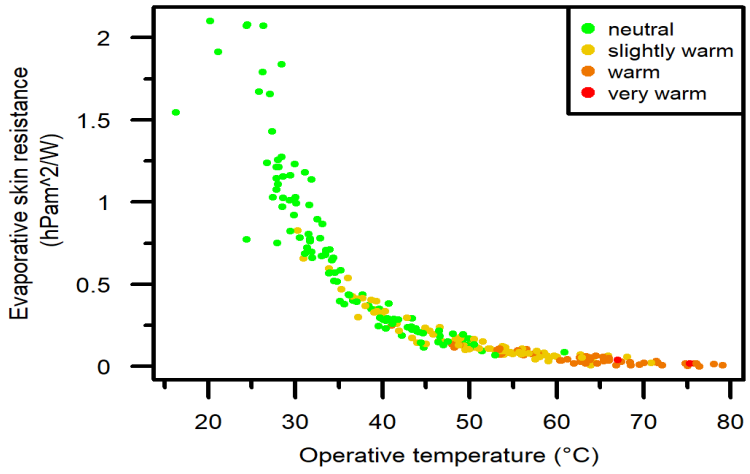

Figure 9. Scatter chart of the evaporative skin resistance as a function of operative temperature at actual average air humidity and wind speed. Thermal perception types experienced during the observations can also be seen based on the coloring of points

Each point in the figure represents an observation. The change of r_{skin} as a function of T_o is clearly visible. The points can be approximated by the following exponential function:

$$r_{skin} = 19.17 \cdot e^{-0.1017 \cdot To}.$$

In the range 30 °C ≤ T_o < 35 °C, r_{skin} decreases sharply with increasing T_o. The perceived thermal sensation type is mostly "neutral". In the range 35 °C ≤ T_o < 50 °C, the rate of reduction of r_{skin} with increasing T_o is much smaller than in the former case. The thermal sensation types are mostly "slightly warm" and "neutral". A reduction of r_{skin} as a function of T_o can still be observed in the range 50 °C ≤ T_o < 70 °C. The thermal perception types are mostly "slightly warm" and "warm". In this range, the thermal perception type "very warm" was also registered once. In the range 70 °C ≤ T_o, the reduction of r_{skin} as a function of T_o is practically negligible, r_{skin} can be taken as constant, its value is equal to or less than 0.005 $hPa \cdot m^2 \cdot W^{-1}$. In this range, the thermal perception type "very warm" appears and its frequency increases considerably with increasing T_o.

Sensitivity of skin evaporation and evaporative resistance of skin to skin albedo
The comparison of λE_{tot} values for lower (0.13) and higher (0.27) skin surface albedo values is shown in Figure 10.

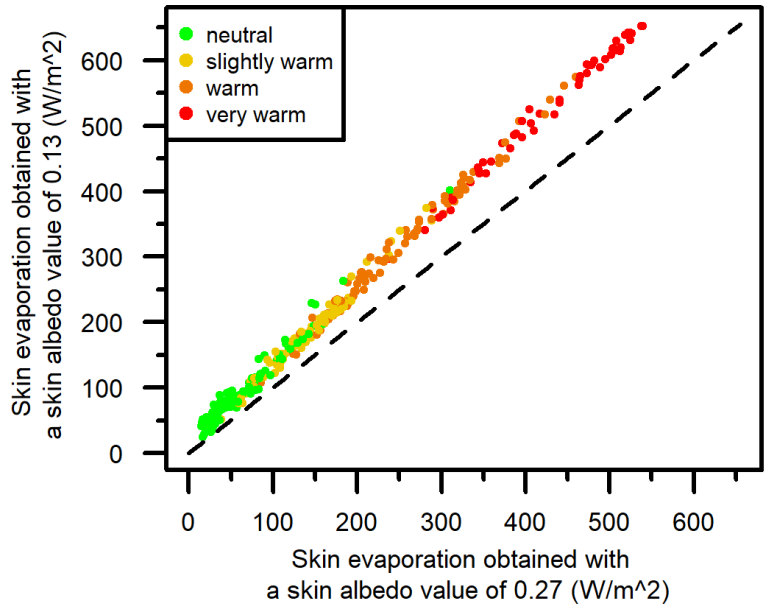

Figure 10. Scatter chart of latent heat flux density of skin evaporation simulated by lower (albedo value 0.13) and higher (albedo value 0.27) skin albedo values. Thermal perception types experienced during the observations can also be seen based on the coloring of points

Since λE_{tot} is calculated as the residual term of the energy balance equation, it makes sense that $\lambda E_{tot}^{0.13} > \lambda E_{tot}^{0.27}$. The $\lambda E_{tot}^{0.13}$ - $\lambda E_{tot}^{0.27}$ differences increase with increasing λE_{tot} moving towards warm thermal perception types. Thus, for instance, in the thermal perception type "very warm", $\lambda E_{tot}^{0.13}$ - $\lambda E_{tot}^{0.27}$ differences are around 100 Wm^{-2}. This change is also beautifully reflected in the ratio of r_{skin} values (Figure 11).

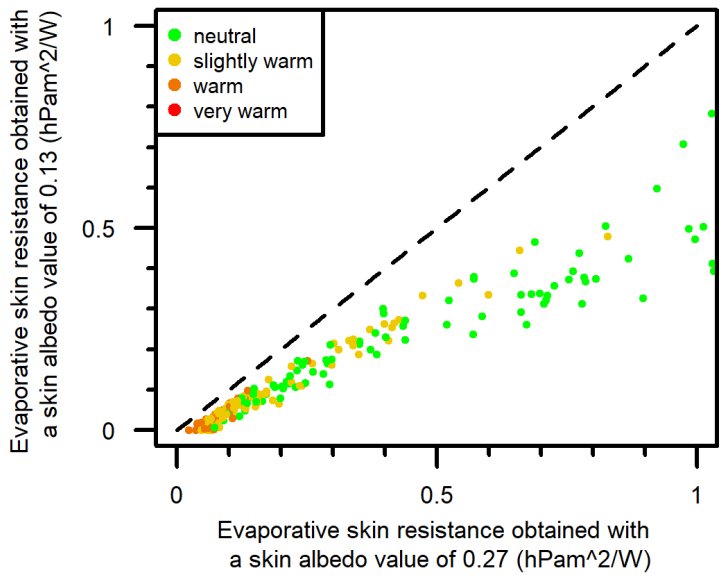

Figure 11. Scatter chart of the skin evaporative resistance simulated by lower (albedo value 0.13) and higher (albedo value 0.27) skin albedo values. Thermal perception types experienced during observations can also be seen based on the coloring of points.

Based on the model, it makes sense that $r_{skin}^{0.13}$ is smaller than $r_{skin}^{0.27}$ because $\lambda E_{tot}^{0.13}$ is larger than $\lambda E_{tot}^{0.27}$. It can be seen that the $r_{skin}^{0.13}/r_{skin}^{0.27}$ ratio decreases moving from the thermal perception type "very warm" to the thermal perception type "neutral". This ratio is the smallest when the thermal perception type is “neutral”. This ratio is higher in the "warm-neutral" situations and lower in the "cold-neutral" situations. The “warm-neutral” thermal perception type is the "slightly warm" side of the “neutral” thermal perception type, and conversely, the “cold-neutral” thermal perception type is the "cool" side of the "neutral" thermal perception type. Note that $r_{skin}^{0.27}$ is almost double of $r_{skin}^{0.13}$ in the thermal perception range “cold-neutral”. It is interesting to see that the albedo value of the skin surface determines the magnitude of evaporative resistance (r_{skin} value) when the thermal sensation type is "neutral".

Applicability of the model

By definition, the model cannot be applied if the r_{skin} value is negative. This can happen in two cases: when 1) the first term of eq. (4) is smaller than the r_{Ha} term and when 2) the first term of eq. (4) has a negative sign. The first case occurs when the R_n values are very large; the second case occurs when the R_n values are very small. In both cases, incoming solar radiation is a determining factor. When solar radiation is high, above 700 Wm^{-2}, the R_n values are around 400 Wm^{-2}, and when wind speed is lower or moderate, the first term of eq. (1) will be smaller than the r_{Ha} term. Of course, air temperature is at least around 20-25 °C. In these cases, the thermal perception type "very warm" is the most common. When solar radiation is low, about 100 Wm^{-2}, or even smaller, R_n values can be around 0 or even negative, and thus

the denominator of the first term of eq. (4) can become negative. In such cases, the thermal perception type is "neutral".

Discussion

The presented model is obviously simple. It uses the concept of required sweating (Parsons, 1997) as well as the evaporation gradient formula. The use of the gradient formula is also an important part of the model, so we can also estimate the value of the skin surface evaporative resistance, which is naturally always greater than or equal to zero. With this methodological innovation, we have made the concept of required skin surface evaporation completely universal, as the concept not only fulfills the energy balance, but also the physical laws characterizing the transfer of water vapor (Monteith, 1965). Another unique feature of the model is that the active surface is the skin surface (not the clothing surface). Therefore, we preferred to look at a person in a lying position. Thanks to this, human variability is not determined by the variability of metabolic heat flux density values, but by the variability of skin types. That's why it was important to specify the skin type of the person suffering from heat stress.

Nowadays, only fewer studies link information from climate type and human thermal load (e.g. Yang & Matzarakis, 2019; Blazejczyk et al., 2015; Ács et al. 2020; Ács, 2024). In all of these studies, the persons, or the "standard human" wear clothing, i.e., the active surface used in the model is the clothing surface. To the best of our knowledge, the skin surface has not yet been used as an active surface. It should be emphasized that, according to Monteith (1965), every surface type has an evaporative resistance value. From this perspective, our approach is entirely justifiable - even if it is not common. Due to the above, our results are new and provide a human-based characterization of the summer weather conditions of the Cfb climate. The λE_{tot} values varied between 10 and 300-350 Wm^{-2}, meanwhile 25 °C < T_o < 80 °C. It should also be noted that the simulated λE_{tot} results were not verified by comparing them with other measurement or model calculation results. However, the λE_{tot} results were always compared with the observed thermal sensation type results, and their consistency was perfect. Note, when T_o is around 35 °C (we referred to this as a "warm neutral" thermal sensation), the λE_{tot} values are around 50 Wm^{-2}. In these cases, λE_{sw} is comparable with λE_{ds}. Of course, we are aware that the λE_{tot}-thermal sensation type relationship could be very individual. It is more individual than the clothing resistance-thermal sensation relationship (Ács et al., 2022), since this relationship also depends on skin type.

As a fact, we can state that only results of one observer are presented. This can even be considered as a serious shortcoming. We tried to compensate for this deficiency by specifying the observer's skin type. Based on this, it is obvious that observations of people with other skin types are also needed for the method to be used more generally. At the same time, it should also be emphasized that, to the best of our knowledge, this longitudinal research is the first of its kind.

Finally, the study – both its methodology and its results – brings people closer to outdoor conditions characterized by sunlight, primarily through understanding the relationship between thermal load and thermal perception. This type of awareness encourages a healthier lifestyle, which is also proclaimed globally by the United Nations, see SDG (Sustainable Development Goals) 3 entitled as “Ensure healthy lives and well-being for all at all ages”. The study and its results also raise awareness of the importance of self-knowledge. In this regard, it is also worth mentioning that the Fitzpatrick skin type test is considered a standard skin type test method.

Conclusion

In this study, the active surface is the skin surface of the human body, as the clothing worn is minimal in accordance with behavioral norms. Accordingly, we observed a lying person whose body is under the influence of excess heat caused by the summer weather conditions of the Cfb climate. According to the results of a new model based on the human body energy balance equation and the skin surface evaporation gradient formula, the following main conclusions can be drawn: 1) The concept of "required skin evaporation" can be successfully applied to quantitatively characterize human heat excess by linking „required skin evaporation" and thermal perception information. 2) Since the albedo of the skin surface depends on the skin type, the "required skin evaporation" concept (calculation of λE_{tot} and r_{skin}) is more sensitive to higher than lower thermal loads.

It should be emphasized that the application of the concept does not require the parameterization or characterization of thermoregulatory processes.

References

Ács, F. (2024). On the Comparison of Generic and Human-based Climate Classification Methods. *Research Advances in Environment, Geography and Earth Science*, *7*, 64–78. https://doi.org/10.9734/bpi/raeges/v7/1631

Ács, F., Kristóf, E., & Zsákai, A. (2025). Human thermal load of foggy and cloudless mornings in the cold season. *Geofizika*, 42(1), 1-24, https://doi/org/10.15233/gfz.2025.42.1

Ács, F., Zsákai, A., Kristóf, E., Szabó, A. I., & Breuer, H. (2020). Carpathian Basin climate according to Köppen and a clothing resistance scheme. *Theoretical and Applied Climatology, 141*, 299–307. https://doi.org/10.1007/s00704-020-03199-z

Ács, F., Zsákai, A., Kristóf, E., Szabó, A.I., & Breuer, H. (2022). Individual local human thermal climates in the Hungarian lowland: Estimations by a simple clothing resistance-operative temperature model. *International Journal of Climatology*, *43*(3), 1273–1292. https://doi.org/10.1002/joc.7910

Basarin, B., Lukić, T., & Matzarakis, A. (2020). Review of Biometeorology of Heatwaves and Warm Extremes in Europe. *Atmosphere*, *11*(12), 1276. https://doi.org/10.3390/atmos11121276

Bátori, L. (2022). Examination of the impact of climate change on sport on the example of the heat index. In International Conference *National Higher Education Environmental Science Student Conference*, June 3-5, Shanghai.

Błażejczyk, K., Baranowski, J., Jendritzky, G., Błażejczyk, A., Bröde, P., & Fiala, D. (2015). Regional features of the bioclimate of Central and Southern Europe against the background of the Köppen-Geiger climate classification. *Geographia Polonia*, *88*, 439–453. 10.7163/GPol.0027

Bokros, K., & Lakatos, M. (2022). Analaysis of hot spells in Budapest from the early 20th century to the present. *Légkör, 67*(4), 208–218. (in Hungarian)

Boras, M., Herceg-Bulić, I., Zgela, M., & Nimac, I. (2022). Temperature characteristics and heat load in the City of Dubrovnik. *Geofizika, 39*(2), 259–279. https://doi.org/10.15233/gfz.2022.39.16.

Brunt, D. (1932). Notes on radiation in the atmosphere. *Quaterly Journal of Royal Meteorological Society, 58*(247), 389–420.10.1002/qj.49705824704.

Campbell, G. S., & Norman, J. M. (1997). *An introduction to environmental biophysics* (2nd ed.). Springer.

Enescu, D. (2019). Models and Indicators to Assess Thermal Sensation under Steady-State and Transient Conditions. *Energies*, *12*(5), 841. https://doi.org/10.3390/en12050841

Fanger, P. O. (1970). *Thermal comfort: Analysis and applications in environmental engineering*. Danish Technical Press.

Fitzpatrick, T. B. (1975). "Soleil et peau" [Sun and skin]. *Journal de Médecine Esthétique* (in French), *2*, 33–34.

Fouilett, A., Rey, G., Laurent, F., Pavillon, G., Bellec, S., Guihenneuc-Jouyaux, C., Clavel, J. Jougla, & E. Hemon D. (2006). Excess mortality related to ´ the August 2003 heat wave in France. *International Archives of Occupational and Environmental Health*, *80*(1), 16–24.

Gulyás, Á. & Matzarakis, A. (2009). Seasonal and spatial distribution of physiologically equivalent temperature (PET) index in Hungary. *Időjárás, 113*(3), 221–231.

Hantel, H., & Haimberger, L. (2016). *Grundkurs Klima*. Springer Spektrum. https://doi.org/10.1007/978-3-662-48193-6

ISO 8996. (2004). *Ergonomics of the thermal environment – Determination of metabolic rate* (2nd ed.). International Organization for Standardization.

Khosla, R., & Guntupalli, K.K. (1999). Heat-related illnesses. *Critical care Clinics, 15*(2), 251–263. 10.1016/s0749-0704(05)70053-1

Konzelmann, T., van de Wal, R. S., Greuell, W., Bintanja, R., & Henneken, E. A. (1994). Abe-Ouchi, A. Parameterization of global and longwave incoming radiation for the Greenland Ice Sheet. *Global Planetary Change, 9*(1-2), 143–164. 10.1016/0921-8181(94)90013-2.

Kottek, M., Grieser, J., Beck, C., Rudolf, B., & Rubel, F. (2006). World Map of the Köppen-Geiger classification updated. *Meteorologische. Zeitschrift*, *15*(3), 259–263.

Kovács, A., Németh, Á., Unger, J., & Kántor, N. (2017). Tourism climatic conditions of Hungary – present situation and assessment of future changes. *Időjárás*, *121*(1), 79–99.

Köppen, W. (1900). Versuch einer Klassifikation der Klimate, vorzugsweise nach ihren Beziehungen zur Pflanzenwelt. *Geographische Zeitschrift*, *6*(11), 593–611.

Köppen, W. (1936). *Das geographische System der Klimate*. Gebrüder Borntraeger.

Matzarakis, A., & Gulyás, Á. (2006). A contribution to the thermal bioclimate of Hungary: Mapping of the physiologically equivalent temperature. In A. Kiss, G. Mezősi, & Z. Sümeghy (Eds.), *Landscape, environment and society: Studies in honour of professor Ilona Bárány-Kevei on the occasion of her birthday* (pp. 479–488). University of Szeged.

Matzarakis, A., Rudel, E., Zygmuntowski, M., & Koch, E. (2005). Thermal Human Bioclimate Conditions for Austria and the Alps. *Croatian Meteorological Journal*, *40*, 190–193.

Megyeri-Korotaj, O.A., Bán, B., Suga, R., Allaga-Zsebeházi, G., & Szépszó, G. (2023). Assessment of Climate Indices over the Carpathian Basin Based on ALADIN5.2 and REMO2015 Regional Climate Model Simulations. *Atmosphere*, *14*, 448, https://doi.org/10.3390/

Mieczkowski, Z.T. (1985). The tourism climatic index: a method of evaluating world climates for tourism. *Canadian Geographic*, 29, 220–233.

Mohan, M., Gupta, A. & Bhati, S. (2014). A modified approach to analyse thermal comfort classification. *Atmospheric and Climate Sciences*, 4, 7–19. 10.4236/acs.2014.41002

Monteith, J. L. (1965). Evaporation and environment. In *Proceedings of the 19th Symposium of the Society for Experimental Biology* (pp. 205–236). Cambridge University Press.

Nielsen, K. P., Zhao, L., Stamnes, J. J., Stamnes, K., & Moan, J. (2008). The optics of human skin: Aspects important for human health. In E. Bjertnes (Ed.), *Solar radiation and human health* (pp. 35–46). The Norwegian Academy of Science and Letters.

Páldy, A., Bobvos, J., & Málnási, T. (2018). The impact of climate change on human health and health care system in Hungary. *Magyar Tudomány*, *179*(9), 1336–1348. 10.1556/2065.179.2018.9.7

Parsons, K. C. (2003). *Human thermal environments* (2nd ed.). Taylor & Francis.

Parsons, R. A. (1997). Evaporative heat loss from skin. In *1997 ASHRAE Handbook* (Chapter 8: Thermal Comfort, p. 8.3). Frank M. Coda.

Potchter, O., Cohen, P., Lin, T.P., & Matzarakis, A. (2018). Outdoor human thermal perception in various climates: a comprehensive review of approaches, methods and quantification. *Science of The Total Environment*, 631–632, 390–406. 10.1016/j.scitotenv.2018.02.276

von Humboldt, A. (1845). *Kosmos: Entwurf einer physischen Weltbeschreibung* [Cosmos: A sketch of the physical description of the universe] (in German). Cotta.

Yang, S.Q., & Matzarakis, A. (2016). Implementation of human thermal comfort information in Köppen-Geiger climate classification— the example of China. *International Journal of Biometeorology*, *60*, 1801–1805. 10.1007/s00484-016-1155-6

INTERNATIONAL SCIENTIFIC JOURNAL | GEOGRAPHICA PANNONICA

When Ungauged Micro-Watersheds Conceal Danger: A Morphometric and Morphodynamic Analysis of Flood Risk. Case Study: The City of Aïn M'lila, Algeria

Nedjoua Cemali[A*] , Sihem Ramoul[B]

[A] Faculty of Earth Sciences and Architecture, Larbi Ben M'hidi University, Oum El Bouaghi, Algeria

[B] Faculty of Earth and Universe Sciences, Department of Geography and Spatial Planning, Moustapha Ben Boulaïd University, Batna, Algeria

Received: July 30, 2025| Revised: December 15, 2025| Accepted: December 16, 2025

doi: 10.5937/gp29-60528

Abstract

Extreme weather events-particularly episodes of intense rainfall-are increasingly disrupting hydrological regimes and triggering frequent, destructive floods, especially in urban environments. These floods have severe repercussions on populations, infrastructure, and economic activities. While large river basins are typically monitored and extensively studied, small ungauged urban catchments remain poorly documented despite their critical role in generating localized hydrological hazards. This study focuses on a small ungauged watershed located in Aïn M'lila (northeastern Algeria), which experiences recurrent flash floods that frequently lead to urban inundation. In the absence of hydrological instrumentation, the objective is to generate insight into the watershed's hydrological functioning and the associated geomorphological impacts using alternative, integrative methods. The approach combines morphometric analysis, a morphodynamic reading of surface flow dynamics, and targeted field observations of flood traces and erosion patterns. This methodological framework offers a more precise characterization of the watershed's specific features, enhances understanding of its behavior during extreme rainfall events, and provides a transferable basis for flood risk assessment in other similarly data-scarce urban contexts. This study contributes in three concrete ways: (1) by demonstrating a reproducible workflow that integrates 30 m DEM-based morphometry with field-scale morphodynamic observations for ungauged urban micro-watersheds; (2) by providing quantified morphometric metrics linked to hydrological response indicators (e.g., drainage density, time of concentration) and interpreting their physical meaning for flash-flood generation; and (3) by combining spatial evidence with participatory survey data to inform practical recommendations for low-cost monitoring and urban planning interventions.

Keywords: Floods; Small ungauged watersheds; Morphometric analysis; Morphodynamic interpretation; Flood risk; Urban environments; Aïn M'lila

[*] Corresponding author: Nedjoua Cemali; e-mail: nedjoua.cemali@gmail.com

Introduction

In developing countries, river basins play a strategic role in territorial planning and the management of water resources. Major basins -such as the Nile, Congo, and Niger in Africa- serve as natural units for water governance, often transcending administrative boundaries. These large-scale systems are essential pillars for irrigated agriculture, potable water supply, hydroelectric power generation, and ecosystem regulation.

At the same time, small sub-catchments-integral components of larger basins-are increasingly recognized for their importance in decentralized and participatory natural resource management. Their reduced scale allows for more precise integration of local specificities, particularly in relation to erosion control, flood mitigation, and water accessibility. This dual dynamic highlights the need to reconcile macro-scale planning with locally grounded interventions for effective water governance.

In the Mediterranean region, watersheds display distinct climatic and hydrological characteristics, including limited water resources, long dry summers, and high-intensity rainfall events that often trigger sudden floods (Merheb et al., 2016). Within this context, small catchments are especially sensitive hydro-geomorphological units (Seethapathi et al., 2008).

In recent years, flooding has become a central concern in debates on climate change impacts. Numerous studies have highlighted the intensification of extreme precipitation and the increasing frequency of flood events across various regions, particularly in the Mediterranean (Tramblay & Somot, 2018). In Algeria, the growing occurrence of extreme hydro-meteorological events has been accompanied by a steady increase in the availability of climatic and hydrological data, particularly for large, gauged basins. This wealth of data has sparked considerable scientific interest, as reflected in the extensive hydrological modeling literature by researchers such as Meddi, Bouanani, and Elahcene (e.g., Meddi et al., 2009; Achite, 2023; Elahcene, 2013).

However, this focus on well-documented catchments has contributed to the marginalization of small, ungauged watersheds, particularly those located on urban fringes or in neglected rural areas. Despite the absence of hydrometeorological time series, these basins are capable of generating intense hydrological responses, including flash floods that can inflict significant downstream damage. Their hydrological potential—exacerbated by the effects of climate change—remains significantly underestimated in risk management frameworks precisely due to the lack of available data.

Climate change further amplifies the vulnerability of small, ungauged catchments through both the intensification of extreme rainfall events (IPCC, 2021) and shifts in hydrological regimes (Özcan et al., 2025). In North Africa, climate projections for 2050 forecast an increase in the frequency and intensity of extreme precipitation directly linked to global warming (World Bank, 2020). In Tunisia, for instance, 100-year daily rainfall totals are projected to increase by approximately 20%. While the frequency of such events may decrease in Morocco and Algeria, their rising intensity significantly heightens flood risk (World Bank, 2020). These climatic shifts pose major threats to agricultural systems, infrastructure, and the sustainable management of water resources.

Despite the growing literature on well-instrumented basins, there remains a knowledge gap in how to generate actionable, quantitative flood-risk insight for small (<25 km²), ungauged urban watersheds using accessible geospatial data and direct field evidence. This study aims to (i) quantify key morphometric indicators from a 30 m DEM and interpret their hydrological implications for flash-flood generation; (ii) integrate morphodynamic field

evidence and a targeted participatory survey to validate flow paths and propose pragmatic risk-reduction measures.

This study aims to draw attention to the hydrological risks posed by small, ungauged watersheds risks that remain largely overlooked by local stakeholders and researchers due to data scarcity. Despite their capacity to generate substantial runoff during heavy rainfall events, these basins are still widely neglected in risk prevention and management strategies (Jakubínský et al., 2014).

Drawing on a rainfall event that occurred in June 2023 in the city of Aïn M'lila, this study employs a suite of accessible tools—including morphometric and morphodynamic analyses, slope and hydrography mapping, flood trace identification, and field photography. The objective is to transform fragmented data into structured and actionable knowledge. This research provides a foundation for further academic inquiry into small, data-scarce watersheds and aims to raise awareness among local decision-makers regarding their significance. Ultimately, it advocates for the integration of these overlooked hydrological systems into land-use planning and risk prevention policies.

Study Area

The watershed under investigation is located within the municipality of Aïn M'lila, which is administratively part of the Oum El Bouaghi province in northeastern Algeria. It is a small, ungauged catchment situated directly upstream of the urban area of Aïn M'lila, contributing significantly to the city's flood exposure.

A land-cover classification performed on the Landsat (2024) image indicates that the basin comprises approximately: built-up/urban areas 48.32% (compact urban centre and expanding residential zones), green spaces/vegetation 39.71% (annual crops, gardens, and sparse vegetation), and bare soil 11.84%. This quantitative description highlights the significant extent of urbanization, which is central to understanding runoff generation in the basin.

The study area is characterized by a semi-arid Mediterranean climate, with marked seasonal and interannual variability in precipitation. Meteorological data from the Fourchi station (altitude Z = 775 m; coordinates X = 849.85, Y = 346.6) indicate a mean annual rainfall of 366.3 mm for the period 1976–2010, with significant fluctuations ranging from 187 mm in the driest years to 791.7 mm in exceptionally wet years. Winter and spring are the wettest seasons, receiving 115.12 mm and 116.23 mm, respectively, while the dry season occurs from June to August, with the lowest rainfall in June (6.11 mm). Other months with relatively low precipitation include September (36.4 mm), December (38.12 mm), and March (40.8 mm). Extreme events include daily rainfall reaching up to 125 mm, which is a major factor triggering flash floods in the micro-catchment.

This watershed functions as a tributary within the larger Oued Boumerzoug basin, of which it is a sub-affluent. Despite its modest surface area of 24.83 km², this micro-basin plays an active hydrological role-particularly during episodes of intense rainfall-when it serves as a conduit for rapid surface runoff toward the urbanized downstream zones (*see* Figure 1):

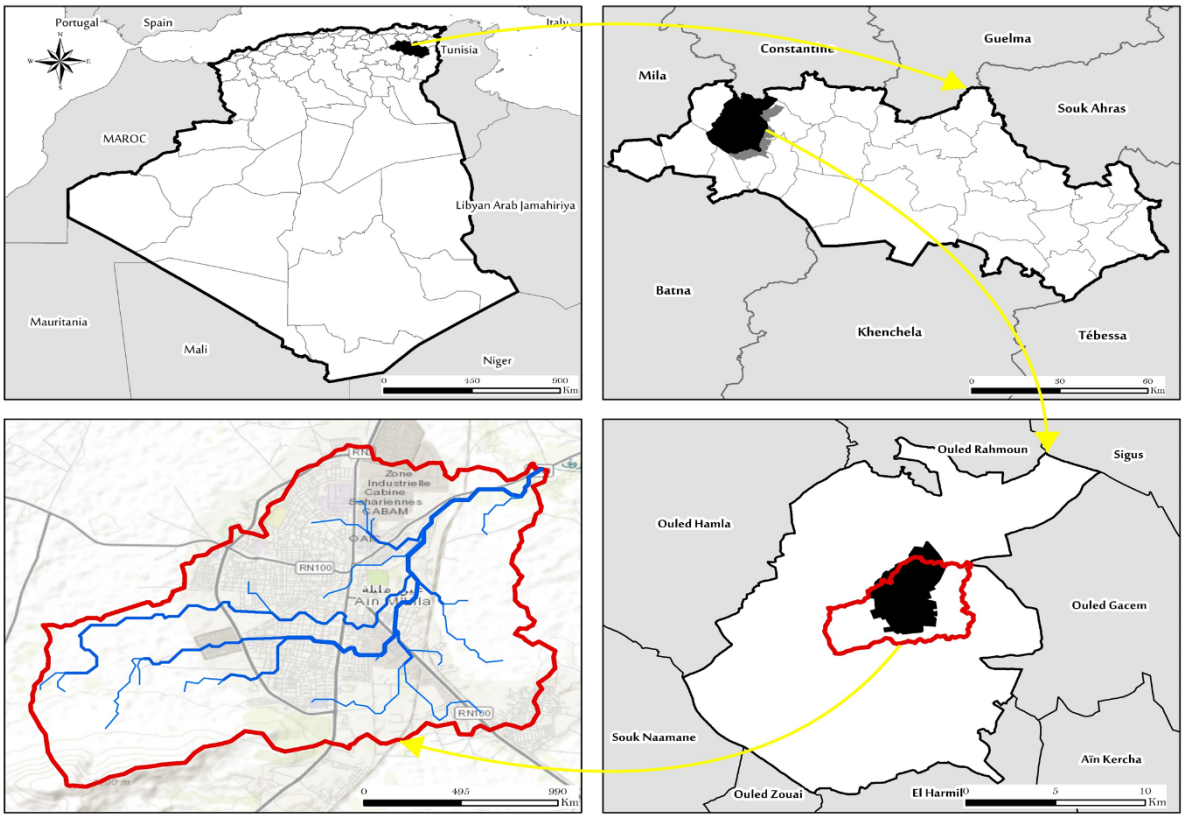

Figure 1. Geographic location of the study area

Data and Methodology

Urban streams are highly dependent on the hydrological behavior of their contributing catchments. As such, analyzing these upstream basins is an essential step in evaluating hydrological risks that may affect urban environments. In the present study, the case of the stream running through the city of Aïn M'lila is particularly illustrative, as it lacks both hydrometric and meteorological monitoring stations—making any attempt at data-driven hydrological analysis considerably more complex.

To address this limitation, the evaluation was based on a combined morphometric and morphodynamic analysis of the watershed. This integrated approach provides an initial understanding of the hydrological functioning and dynamic behavior of the studied urban micro-watershed.

The methodological framework adopted for assessing hydrological risk was structured into three complementary stages (*see* Figure 2):

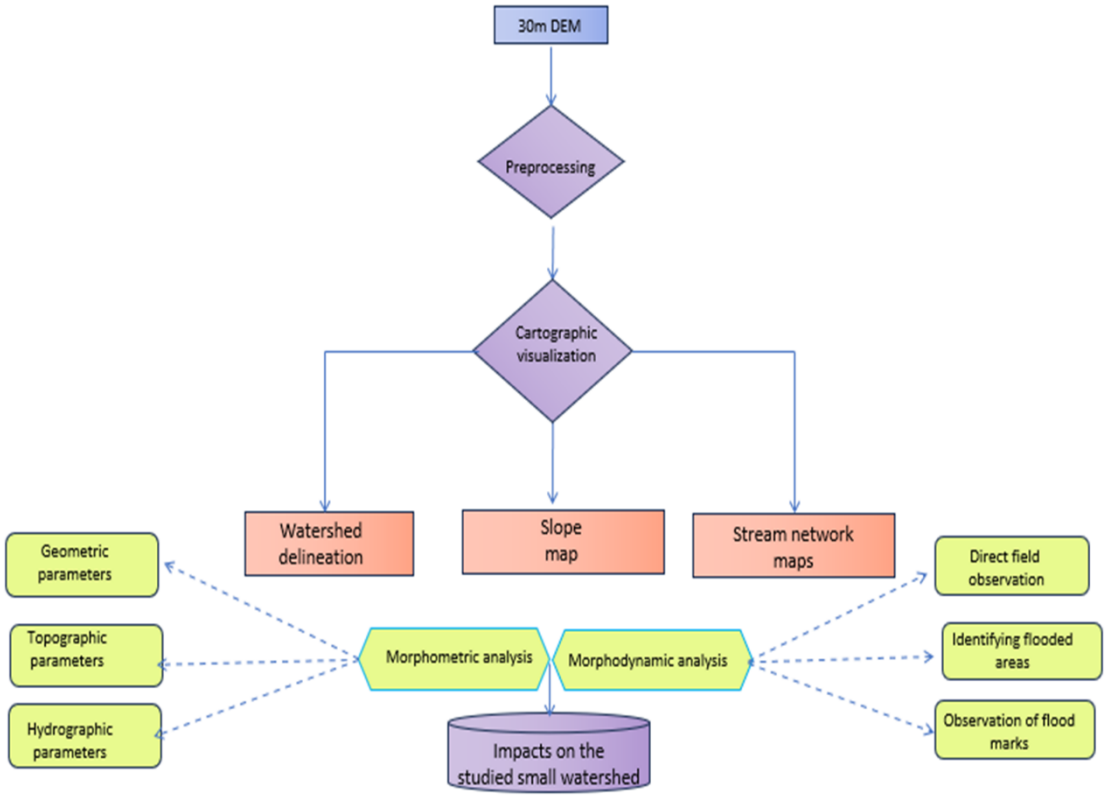

Figure 2. Schematic overview of the methodology used

Watershed Delineation and Morphometric Extraction

The watershed was delineated using a 30-meter resolution Digital Elevation Model (DEM) within ArcGIS 10.8. From this model, automated delineation of the catchment area was performed, and thematic maps were generated, including slope maps, elevation maps, and hydrographic network maps. Flow direction and flow accumulation were computed using the Hydrology tools of ArcGIS. A flow-accumulation threshold of 500 cells (45 hectares) or an alternative physical threshold of contributing area of approximately 0.45 km² was applied to extract the primary channel network in this micro-watershed. The threshold selection was tested sensibly by varying the accumulation threshold and visually validating network continuity against high-resolution satellite imagery and field-observed channels.

However, using a 30 m resolution DEM in the context of small urban catchments carries important limitations. A 30 m DEM is generally regarded as relatively coarse or medium resolution: the comparatively large cell size tends to smooth microtopographic variations, which can lead to under-detection of narrow thalwegs and to an overall simplification of the drainage network. This smoothing also causes a generalization of local slopes and curvatures, reducing the precision of derived slope, flow direction, and flow accumulation products; as a consequence, locations of flow convergence, overland flow paths, and small-scale connectivity can be misrepresented. For hydrological analyses in small urban basins—where microtopography and narrow channels strongly influence runoff concentration and flood routing—these effects can result in biased assessments of flow pathways and flood-prone areas, and therefore must be explicitly considered when interpreting results obtained from a 30 m DEM.

Morphometric Analysis
This step involved the calculation of several geometric, topographic, and hydrographic indices. These indicators allow for an indirect estimation of the basin's hydrological responsiveness to intense rainfall events.

Morphodynamic Interpretation of a Flood Event and Participatory Survey
A field campaign was conducted in the most flood-affected areas, particularly in the Regaizi neighborhood. This phase involved identifying the main post-flood morphodynamic features—such as riverbank erosion, alluvial deposits, and alterations to the hydrographic network. Simultaneously, semi-structured interviews were conducted with local residents to document observed flood dynamics, perceptions of risk, and associated socio-economic impacts. This integrated approach made it possible to triangulate spatial data derived from remote sensing and GIS with empirical observations and local knowledge. To complement these observations, an exploratory survey was conducted with fifteen households along the main flow path to document the 2023 flood event. The survey focused on four themes: peak water heights inside and outside houses, frequency of past events, extent of damages, and perceived drivers of flooding. Qualitative data were analysed manually to identify recurring elements in respondents' statements. This survey aimed not at statistical representativeness, but at reconstructing flood characteristics through local knowledge.

The methodology was further enhanced by the use of a high-resolution satellite image from ALSAT-2, dated 2017 and obtained via the Algerian Space Agency (ASAL). This imagery made it possible to identify areas previously affected by flooding that correspond closely to the zones impacted during the June 2023 flood event. This spatial overlap supports the hypothesis of recurring extreme hydrological phenomena within the micro-watershed, despite the lack of long-term hydroclimatic data.

The integration of this satellite data strengthens the overall analytical framework by helping to locate areas that are frequently affected by flooding—an essential step in indirectly validating the watershed's hydrodynamic behavior.

Morphometric Analysis Method
Morphometric analysis constitutes a fundamental step in assessing the hydrological behavior of a watershed (Hamad, 2020), particularly in urban environments where dense development and soil impermeability intensify runoff processes. In the absence of continuous hydrometric data, morphometric analysis serves as a valuable proxy for understanding the watershed's response to extreme rainfall events (Garzon et al., 2023). This method enables a quantitative characterization of the basin's geometry, topography, and drainage network organization in order to identify the structural factors that influence surface runoff generation and concentration (Strahler, 1964; Horton, 1945).

Among the core hydrological parameters, watershed area is one of the most critical, as it directly determines the volume of surface water generated during a rainfall event. Under equal precipitation conditions, a larger drainage area implies a higher potential for runoff generation. This relationship is explicitly incorporated into the Rational Method, which is widely used to estimate peak discharge in small catchments, and it is a foundational component of various hydrological design methods applied to small basins (MFFP, 2018).

In this study, the watershed area was calculated using a 30-meter resolution Digital Elevation Model (DEM), employing ArcGIS Hydrology tools and following the method developed by Jenson and Domingue (1988). The catchment was delineated from the identified outlet by applying the *fill*, *flow direction*, and *flow accumulation* procedures.

In parallel with watershed delineation, several morphometric indices were calculated to characterize the basin's physical attributes. These parameters describe the basin's size, shape, topography, and the structure of its drainage network. They were derived from a 30-meter resolution DEM and a 1:50,000 scale topographic map.

The indices selected for this study are based on classical and widely accepted methodologies developed by Gravelius (1914), Horton (1945), Strahler (1957), among others. These indices are extensively used in contemporary scientific literature, particularly for evaluating watershed hydrological behavior (Shekar & Mathew, 2024). Tables 1a and1b presents the key morphometric indices employed, along with their respective formulas.

Table 1a. Overview of the main geometric morphometric indices used.

	Index	Formula	Unit	Value	Reference
Geometric Parameters	Area of watershed	A	($km^{2)}$	24.83	Horton (1945)
	Perimeter of watershed	P	(Km)	25.54	
	Gravelius Compactness Index (KG)	$k_G = \frac{P}{2\sqrt{\pi A}} = 0.28 \times \frac{P}{\sqrt{A}}$		1.45	Gravelius (1914)
	Length/Width of Equivalent Rectangle (Lr / lr)	$Lr = \frac{KG\sqrt{S}}{1,12} \times \left[1 + \sqrt{1 - \left(\frac{1,12}{G}\right)^2}\right]$ $lr = \frac{KG\sqrt{S}}{1,12} \times \left[1 - \sqrt{1 - \left(\frac{1,12}{G}\right)^2}\right]$	(Km)	10.56 2.35	Benzougagh (2019)

Table 1b. Overview of the main topographic and hydrographic morphometric indices used.

	Index	Formula	Unit	Value	Reference
Topographic	Total Elevation Range (Dg)	$Dg = H5\% = H95\%$	(m)	354	Benzougagh (2019)
	Minimum height	Hmax	(m)	1104	
	Maximum height	Hmin	(m)	750	

	Overall Slope Index (Ipg)	$Ipg = \frac{D_g}{Lr}$		0.032	
Hydrographic Parameters	Drainage Density (Dd)	$Dd = \frac{\sum_{i=1}^{n} L_i}{s}$	(km/km^2)	1.41	Horton (1945)
	Time of Concentration (Tc)	$Tc = \frac{4\sqrt{s} + 1{,}5Lt}{0{,}8\sqrt{H}}$	(heures)	0.126h≈7.6min	Benzougagh (2019)
	Torrentiality Coefficient (Ct)	$Ct = Dd \times Fcl = Dd$		0.85	Mashauri (2023)

Morphodynamic Analysis Method

In ungauged watersheds—where no instrumental hydrological data (e.g., streamflow, water levels, or rainfall records) are available—post-flood morphodynamic analysis offers a valuable alternative for understanding surface flow dynamics. This method relies on the direct observation of the physical traces left by flood events, as well as the interpretation of runoff trajectories based on visual indicators and local testimonies. According to Alam and Ahmed (2020), when combined with topographic and spatial readings, morphodynamic observations can robustly reconstruct hydrological events—even in the absence of quantitative data. This approach is particularly well-suited to urban areas in developing contexts, where hazards are often underestimated due to the lack of instrumentation.

In the case of the Aïn M'lila watershed, the morphodynamic approach was implemented through a series of field observations conducted in the most severely affected zones. Key indicators included: submersion marks on walls and infrastructure (mud stains, waterlines), zones of concentrated erosion (at slope bases, along road edges, or on canalized banks), and sediment deposits (accumulations of gravel, ridges of fine materials, floating debris). These indicators allowed for the identification of runoff concentration zones and the localization of morphological impact points.

In addition to these observations, a participatory survey was carried out with local residents and shopkeepers. The semi-structured interviews helped validate hypotheses regarding water flow paths, clarify critical moments during the flood event (e.g., rate of water rise, duration of inundation), and provide insight into the flood's socio-spatial impacts (property damage, traffic disruptions, water intrusion into homes).

This methodological approach—rooted in the triangulation of visible flood traces, local perceptions, and fine-scale spatial interpretation—compensates for the lack of hydrological measurement and offers a meaningful understanding of runoff processes in uninstrumented urban environments. The integration of morphometric data, morphodynamic indicators, and GIS-based cartographic outputs enables a comprehensive interpretation of the ungauged micro-watershed's behavior during the flood event.

In the morphodynamic section, our observations drew on the concepts and examples set out by Bravard and Petts (2005), whose work offers clear, detailed insights into channel dynamics, the transfer of sediment during floods, and the identification of key geomorphic indicators — notably bank erosion, depositional forms, and channel adjustments.

Results and Discussion

The results of the morphometric and morphodynamic analyses provide a detailed reading of runoff processes within the watershed and allow for the identification of hydro-

geomorphological susceptibility zones associated with the recent flood event. In a context characterized by the absence of instrumental hydrological data, the use of a Digital Elevation Model (DEM) enabled the generation of several key thematic maps, including slope maps, hypsometric (elevation) maps, and drainage network maps. These geospatial outputs form an essential analytical foundation for interpreting the hydrological and morphodynamic functioning of the basin.

This section presents a structured account of the main findings from spatial modeling, field observations on erosion dynamics and post-flood sediment deposits, and qualitative insights drawn from testimonies of residents directly affected by the event.

Topographic Interpretation of the Basin: Relief, Slopes, and Drainage Dynamics

As shown in Figure 3**,** the studied micro-watershed displays a pronounced altitudinal structure, with a gradual decrease in elevation from upstream to downstream. The highest point, located in the southwest, reaches 1,104 meters, while the outlet in the northeast lies at 757 meters—yielding a total elevation drop of 347 meters. Given the basin's modest area of 24.83 km², this altitudinal variation reflects a markedly contrasted topographic configuration. The spatial distribution of elevation suggests a structured gravitational runoff pattern oriented predominantly from the southwest to the northeast, which promotes rapid surface water concentration.

The slope map reveals a concentration of steep slopes (ranging from 9% to 40%) in the southwestern upstream section of the basin. This zone accounts for approximately 20% of the total basin area, while the remaining 80% is characterized by low slopes (less than 3%), mainly located in the midstream and downstream sectors (Figure 4). These lower-gradient areas—when combined with the presence of impervious surfaces in the downstream zones—facilitate rapid surface runoff, reduced infiltration, and a very short hydrological response time (Lei et al., 2020).

The dominant flow direction aligns with the basin's altitudinal gradient, running from the southwest to the northeast, consistent with the natural drainage pattern. In this context, the gently sloped downstream areas—particularly within the densely urbanized sections of old Aïn M'lila—serve as preferential zones for flow accumulation and water pooling, thereby increasing the risk of localized flooding.

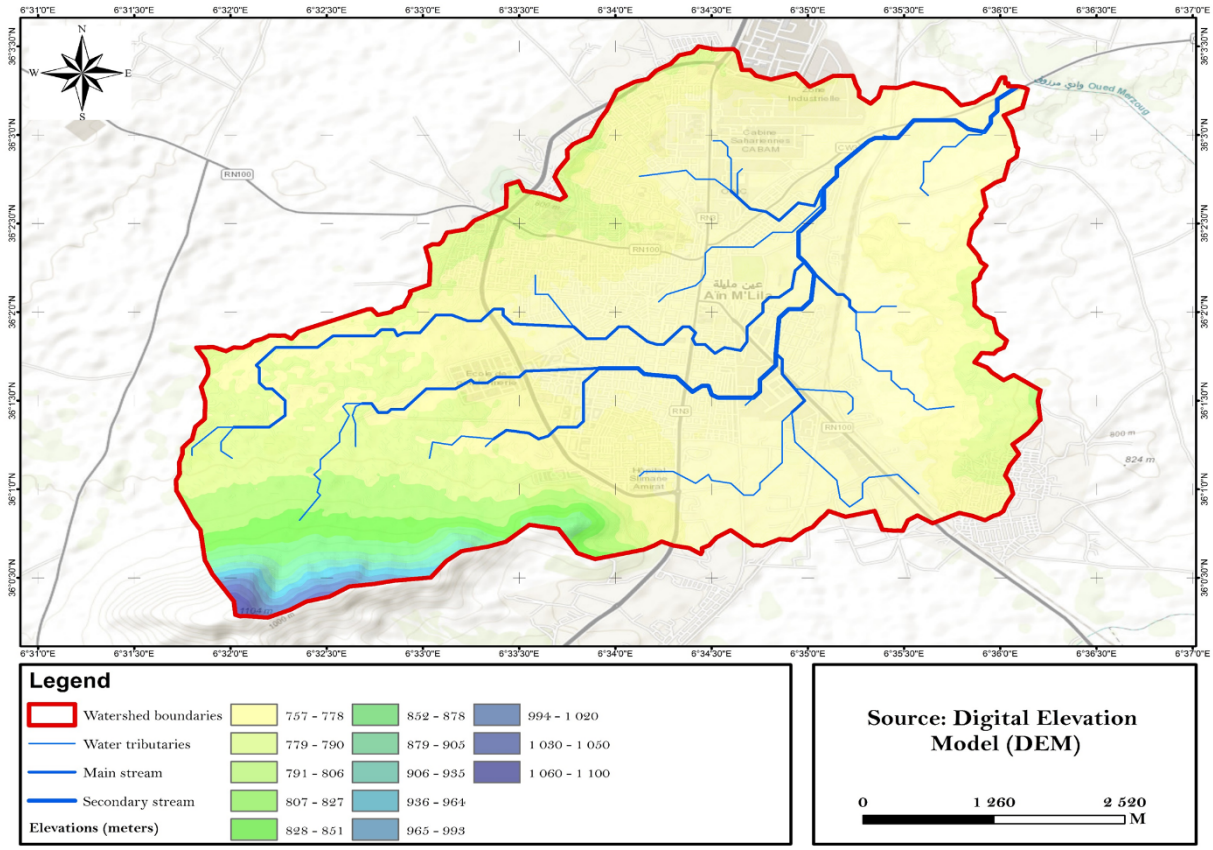

Figure 3. Altitudinal distribution of the studied micro-watershed

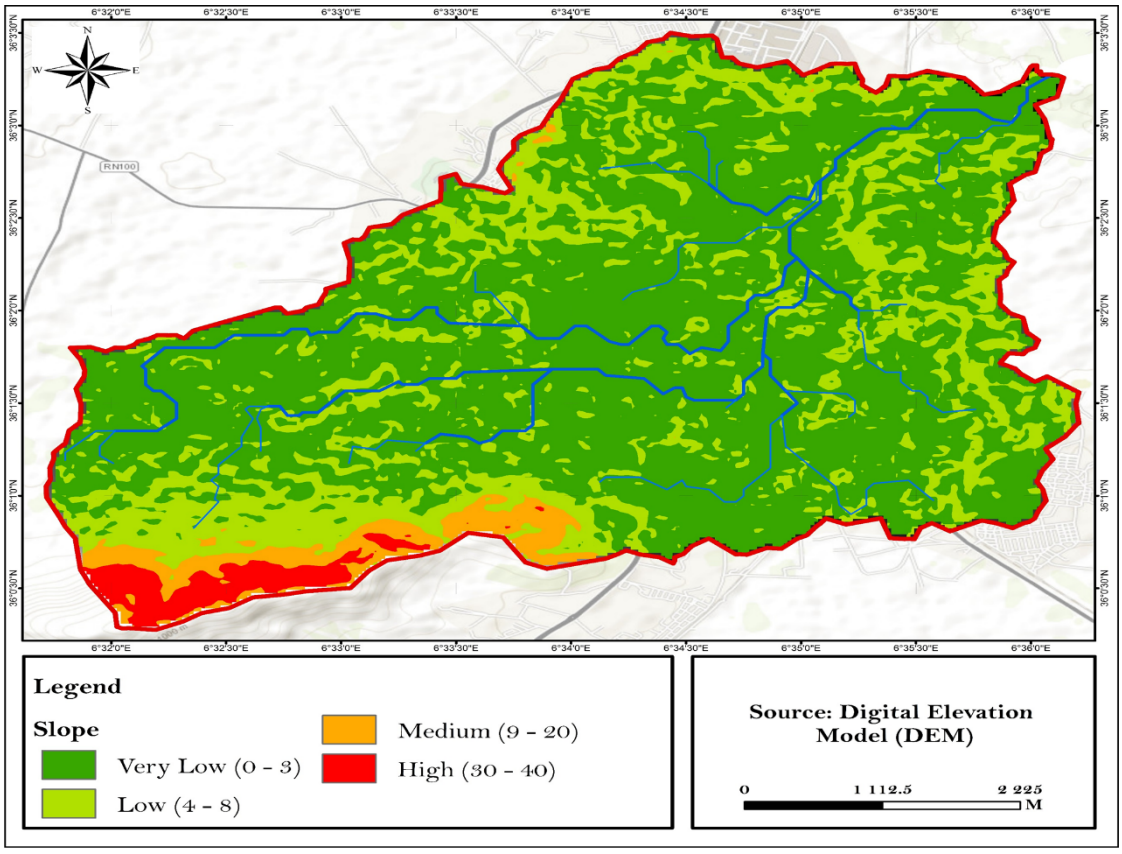

Figure 4. Slope distribution within the studied micro-watershed

Morphometric Interpretation of the Micro-Watershed

The morphometric analysis of the studied micro-watershed is based on a combined evaluation of geometric, topographic, and hydrographic parameters (Tables 1a and 1b). The computed geometric indicators—including area, perimeter, Gravelius compactness index, and equivalent length and width—point to a predisposition for hydrological sensitivity to rainfall inputs.

For example, when the compactness index is greater than 1.12, it indicates that the catchment has an elongated shape (here Kg = 1.45). In theory, this type of shape leads to a slower concentration of runoff: the water takes longer to reach the outlet, resulting in a more gradual rise in floodwaters (Strahler, 1957). This relationship is consistent with flood hydrograph theory and shape-related morphometric controls. In general, elongated catchments, characterized by low shape indices, produce hydrographs spread out over time and relatively moderate flood peaks (Horton, 1945).

However, in the case of the studied basin, this morphometric organization does not result in a slow hydrological response. Despite its elongated shape (Kg = 1.45), the basin exhibits a rapid reaction to rainfall events. According to Strahler (1957) and Horton (1945), a drainage density greater than 1 km/km² indicates a well-developed hydrographic network, promoting rapid concentration and strong synchronization of flows. This configuration leads to a sharp rise in the hydrograph and a significant increase in peak discharge. In this context, the combined effect of a high drainage density and a very short time of concentration directly controls the scaling of peak flow at the outlet, overriding the moderating influence of basin elongation. The estimated time of concentration (Tc = 0.126 h, or approximately 7.6 minutes) thus confirms the occurrence of an early flood peak, appearing in the very first minutes following the rainfall event. The high drainage density (Dd = 1.41 km/km²) highlights a morphology particularly conducive to rapid water concentration and a high potential for flash floods, which helps to explain, at least in part, the flooding observed in the studied basin.

The analysis of topographic parameters provides additional insight into the basin's hydrological behavior. As shown in Table 1, the overall slope index reaches 3.2%, a value often cited (Strahler, 1957) as a limiting factor for flow concentration. However, the significant elevation difference of 354 meters indicates a varied topography that may generate locally elevated runoff velocities. This heterogeneity is confirmed by the spatial analysis of slope and elevation patterns (Figures 3 and 4).

The morphological interpretation is corroborated by a torrentiality coefficient of 0.85 (Table 1b). This coefficient reflects the basin's capacity to generate rapid, concentrated runoff during intense rainfall events, and values exceeding 0.7 are commonly associated with high torrential behavior. Consequently, the Ct value obtained indicates pronounced torrential dynamics and a strong hydrological reactivity of the watershed. When combined with the very short time of concentration (Tc = 0.126 h) and steep upstream slopes, this high torrentiality enhances runoff velocities, limits infiltration, and further amplifies peak discharge. These factors collectively increase the watershed's susceptibility to fast, high-magnitude flood responses and thus elevate its flood hazard potential.

When compared with other Mediterranean and semi-arid catchments, the rapid hydrological response observed in the study basin is consistent with similar findings. Morphometric analyses in the Wadi Easal Basin in Jordan (Obeidat et al., 2021) and the Oued Adoudou Basin in Morocco (Nait-Si et al., 2025) show that steep slopes, high relief, and dense drainage networks favor rapid runoff generation and high flood susceptibility. These studies support the interpretation of the present results within the broader context of Mediterranean and semi-arid environments.

Morphodynamic Response of the Watershed to the June 2023 Flood: Effects at the Basin and Urban Scales in Aïn M'lila

In the absence of monitoring stations or detailed hydrological data, direct field observation becomes an essential tool for understanding the dynamics of the June 2023 flood. Visible signs of erosion, sediment deposition, overflow, and gully formation—recorded during field surveys—provide valuable insights into the actual behavior of the watershed and the downstream urban runoff.

Visual analysis, supported by targeted photographic documentation, made it possible to reconstruct the flow paths and identify the sectors most exposed to hydro-geomorphological hazards.

Upstream Zone: Initial Flow Concentration

In the upstream portion of the basin, topographic configuration plays a decisive role in triggering surface runoff. During the June 2023 flood event, field observations revealed evidence of linear erosion, gully formation, and sediment accumulation in steep slope areas and along unpaved pathways. These features indicate early-stage flow concentration zones, where rainwater rapidly converged to form channelized flows.

Figure 5 illustrates two types of concentrated erosion forms observed at the headwaters of the basin. These features occur in areas characterized by steep gradients, sparse vegetation cover, and clearly visible water pathways—marking the onset of concentrated surface flow toward the downstream zones.

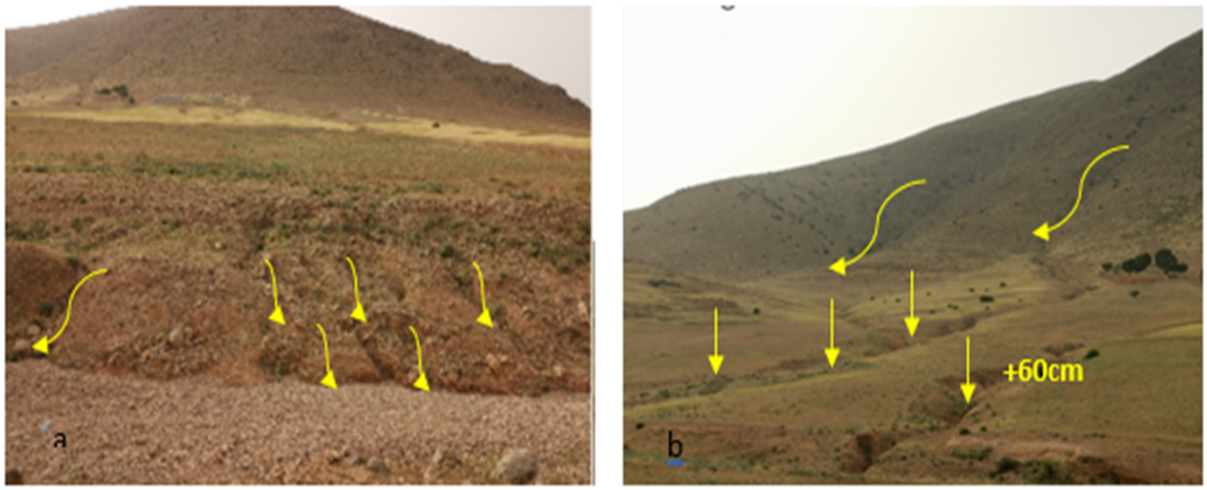

Figure 5. Signs of concentrated runoff on sloped terrain in the upstream zone of the watershed.
(a) Rill erosion caused by concentrated rainfall runoff on bare soil.
(b) Gully formation on an unvegetated slope, indicating active erosion processes during the June 2023 flood.

Intermediate Flow Path: Runoff Dynamics and Nature of Sediment Deposits

In the intermediate zone of the basin, flow paths were reconstructed through the analysis of sediment deposits left in the aftermath of the flood. These deposits—characterized by their

grain size, thickness, and spatial distribution—enabled the tracing of runoff trajectories. Rills measured between 1.5 and 4 m in length and 0.1–0.3 m in depth, providing quantitative markers of concentrated flow paths. The sediment patterns reflect local variations in flow energy, indicating zones of intense concentration, decantation, or overflow.

The observed deposits exhibited clear granulometric sorting, with coarse materials (boulders and gravel, 50–200 mm in diameter) located within active channels and finer silts (0.05–0.2 mm) along channel banks and in adjacent agricultural plots. Estimated sediment volumes ranged from 0.5 to 2 m³ per linear meter of channel, highlighting the considerable material transport during the flood.

This spatial distribution mirrors the underlying runoff dynamics: linear and uniform deposits indicate concentrated flow and high transport capacity, while diffuse and irregular deposits mark overflow areas and zones where flow energy gradually dissipated (Figure 6).

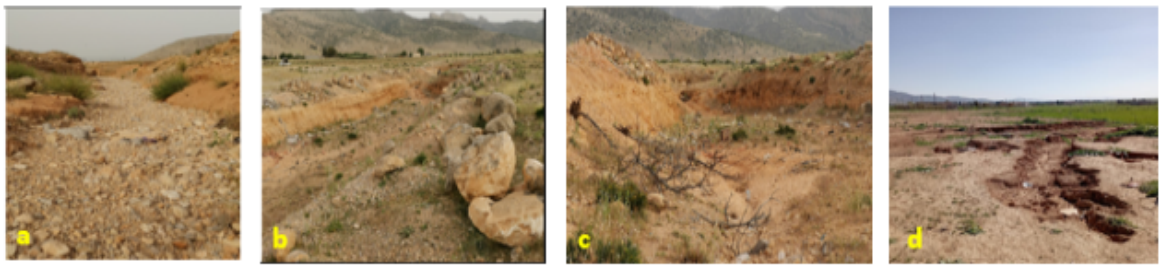

Figure 6. Evidence of post-flood hydro-sedimentary dynamics in the intermediate zone of the watershed. (a, b) Main transport channel with coarse deposits (gravel and boulders), indicating strong post-flood flow concentration. (c) Branches deposited in the riverbed following the flood. (d) Erosion rills (20 to 50 cm deep) formed on an agricultural plot, reflecting localized overflow and temporary concentration of hydrodynamic energy.

In specific areas of the basin, particularly near flow convergence zones, very thick sediment deposits—ranging from 1.5 to 3 m in thickness—were observed. These deposits were composed of coarse materials such as boulders, cobbles, and gravel. Their presence indicates that the flood event was not merely a case of superficial water runoff; rather, it involved highly sediment-laden flows.

Downstream from these zones of hydrodynamic concentration, homogeneous silty deposits mark a post-flood decantation phase, consistent with classical models of sedimentation under low-energy conditions. Approximately 15–20 % of the watershed area exceeded critical slope thresholds (15–25 %), contributing to rapid runoff concentration and sediment transport. The uniform grain size and spatial distribution of these deposits reflect a gradual dissipation of flow energy—a phenomenon well-documented in fluvial systems subject to rapid flood events. This type of hydrodynamic behavior is extensively described in the work of Bravard (2000).

Downstream Zone: Limitations of Hydraulic Infrastructure and Vulnerability of Built Systems

Downstream of the hydrodynamic concentration zones, homogeneous silty deposits provide evidence of a post-flood decantation phase, in line with classical sedimentation models under low-energy flow regimes. The uniform grain size and spatial spread of these deposits reflect

the progressive dissipation of flow energy—a phenomenon well documented in fluvial systems experiencing rapid flood events (Bravard, 2000).

This hydrodynamic slowdown is further confirmed by field observations, including the formation of stagnant water ponds—either clear or rich in algal blooms—within agricultural plots and anthropogenic depressions. These water bodies, resulting directly from the flood, reflect the inability of the flow to fully evacuate residual water, indicating both weak topographic constraints and insufficient flow energy for effective drainage (Figure 7).

Figure 7. Post-flood stagnant water in the downstream zone: (a, b) Ponds formed in low-lying agricultural land. (c) Stagnant water in an anthropogenic depression within an urbanized area.

The hydraulic infrastructure within the valley exhibits significant structural weaknesses in the face of extreme flood events, primarily due to design approaches that do not align with the actual morphometric and hydrological characteristics of the basin. These structures become quickly obstructed by transported debris, drastically reducing their operational capacity. Meanwhile, rigid linings and reinforcements fail under hydraulic overload, posing risks to the stability of roadways and adjacent infrastructure.

The drainage network is heavily impaired by sediment deposits and a lack of maintenance. Major transport corridors—such as the railway and National Road RN3—create topographic discontinuities that obstruct natural water flow, resulting in localized accumulation zones. Furthermore, the main stormwater drainage channel is under-designed both in slope and depth, severely limiting its functionality during high-flow periods (Figure 8).

Figure 8. Malfunctioning of the urban drainage system observed in the field: (a) Heavily loaded discharge canal, impairing proper flow. (b) Sewer blocked by solid waste, observed in a residential neighborhood. (c) Drainage structure clogged with poorly sorted coarse sediment deposits (silt, gravel), hindering flow and promoting overflow.

The drainage network suffers from poor maintenance, with frequent obstructions caused by debris and silty deposits. Both the railway line and National Road RN3 create artificial topographic barriers that trap water and exacerbate local accumulation. Even the main stormwater drainage canal—despite its 2000 mm diameter—has an insufficient slope, which severely compromises its evacuation capacity during flood events (Figure 9).

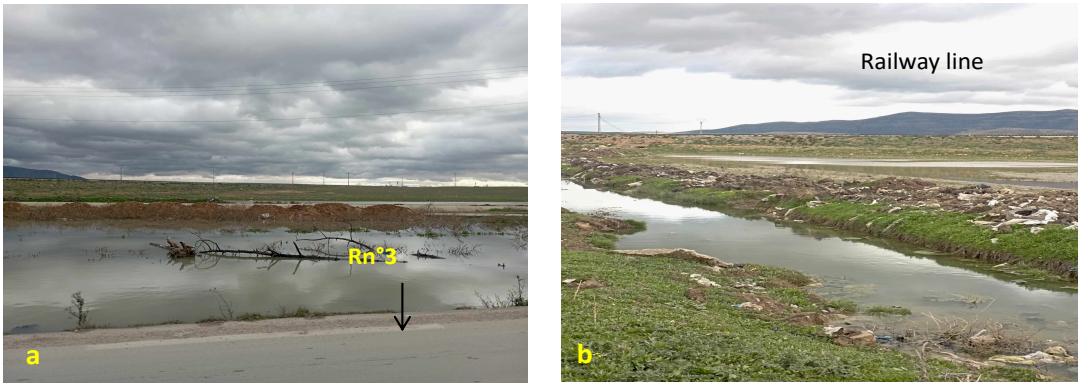

Figure 9. Water accumulation upstream of the railway line acting as a topographic barrier: (a) Flooding of National Road RN3. (b) Accumulation of rainwater upstream of the railway due to the absence of adequate hydraulic crossings.

To enhance understanding of sediment dynamics within the watershed, a sediment transport map was developed (Figure 10) that delineates dominant flow pathways across the upper, middle, and lower sectors of the basin. This map identifies zones of preferential erosion, sediment transfer, and deposition, thereby establishing a coherent linkage between basin-scale morphodynamic processes and the localized impacts documented during flood events.

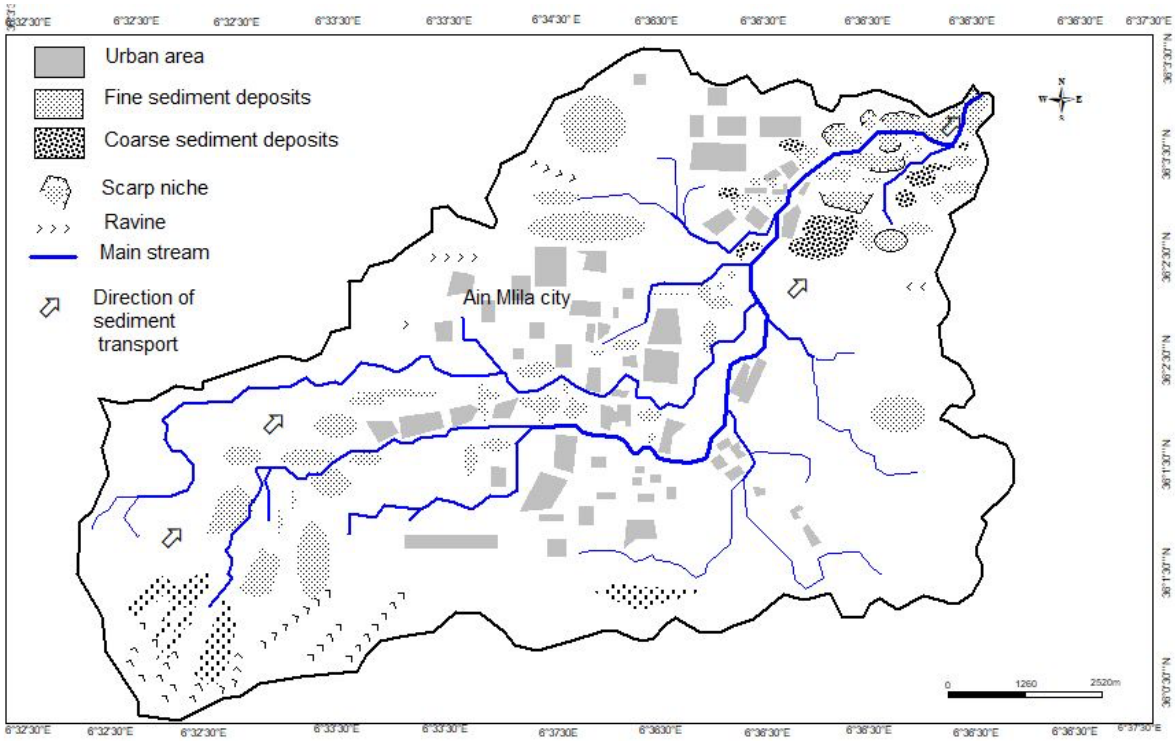

Figure 10. Spatial Distribution of Sediment Transport in the Watershed

In response to these observations, measurements were taken on the exterior walls of several homes located in low-lying areas along the watercourse, recording floodwater marks to estimate the maximum height reached by the waters. This assessment was supplemented by the analysis of photographs captured during the event, offering direct visual evidence of the flood's extent and severity (Figure 12). In addition, conversations with local residents helped reveal spontaneous forms of adaptation in the face of recurrent risk: raising door thresholds, installing gates or barriers, modifying building façades, and constructing small staircases to prevent water intrusion into living spaces. These resident-led interventions reflect both the recurring nature of flooding in the area and the glaring absence of a formal risk management strategy—even in recently built urban neighborhoods (Figure 11).

Figure 11. Effects of the June 2023 flood on buildings and residents' individual adaptations: (a, b) Flood marks visible on the walls of a dwelling (June 2023). (c) Raised doorway threshold installed to limit water intrusion.

Figure 12. Submersion of residential neighborhoods during the June 2023 flood: (a, b) Newly urbanized collective residential area. (c) Single-family home in an older neighborhood, inundated by floodwaters.

To deepen the morphodynamic analysis, a spatial verification was conducted using a high-resolution satellite image (ALSAT-2, 2017), provided by the Algerian Space Agency. This image highlights areas that have historically been affected by flooding within the study region.

By overlaying the flood zones identified in 2017 with the watershed boundary mapped on Google Earth imagery and its associated hydrographic network, it was observed that all sites impacted by the June 2023 flood are located within the same basin. This spatial coincidence reinforces the hypothesis of recurring extreme hydrological events, particularly

in the lower reaches of the valley (Figure 13). This integration of satellite data, cartographic outputs, and field observations compensates for the absence of precise hydroclimatic records by offering a spatial validation of flood risk. It also underscores the necessity of adopting a systemic interpretation of the watershed, where any morphological disruption or change in land use can amplify the impacts of future flood events.

Nevertheless, several sources of uncertainty and methodological limitation must be acknowledged. The use of a 30 m resolution DEM may attenuate fine-scale topographic variability, thereby influencing the accuracy of slope estimates, flow-path delineation, and the representation of micro-channel features. In the absence of direct hydrological measurements, analyses in this ungauged basin necessarily rely on indirect inferences of runoff and flow behavior. Moreover, the visual identification of flood traces and depositional forms involves an element of subjectivity, and some topographic or land-use datasets may not fully capture cur-rent surface conditions. The analysis is also grounded primarily in a single documented flood event, which constrains the extent to which the findings can be generalized to other hydrological scenarios. Despite these limitations, the integrative framework that combines morphometric analysis, targeted field observations, and GIS-based interpretation yields robust and informative insights into the basin's morphodynamic functioning.

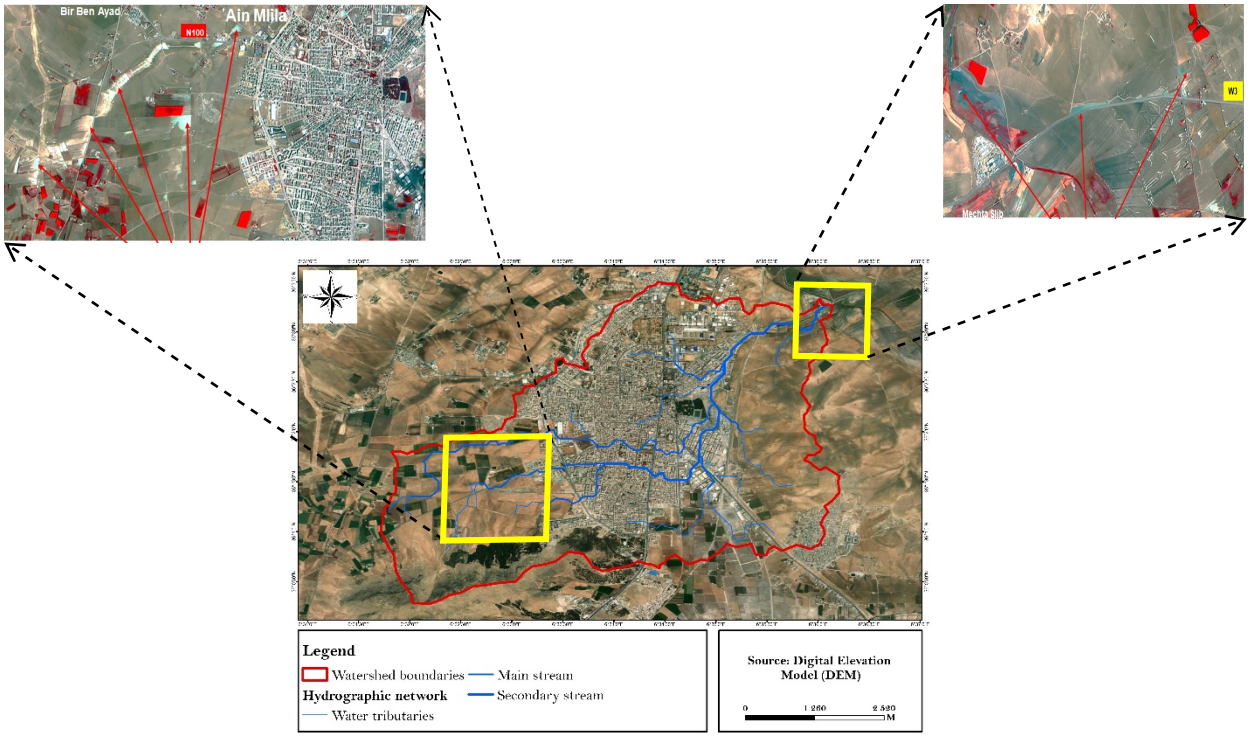

Figure 13. Identification of flood-prone areas within the studied watershed based on an ALSAT-2A satellite image with 2.5 m resolution, dated June 3, 2017.

Conclusion

This study elucidates the hydrological behavior of an ungauged micro-watershed responsible for localized flooding in Aïn M'lila during the June 2023 event. By integrating morphometric analysis, direct field-based observation of morphodynamic responses, and the cross-analysis of slope and hydrographic maps, the research provides refined insights into runoff processes and spatial vulnerability. It demonstrates that small, frequently overlooked watersheds can exert a disproportionate influence on the occurrence and severity of localized flood events.

In the absence of direct hydrological monitoring, the combined use of a Digital Elevation Model (DEM), slope analysis, and morphometric indicators proved critical for delineating the watershed, characterizing its topographic controls, and identifying zones susceptible to runoff concentration. The integration of these datasets with field evidence enabled the identification of sediment accumulation areas, overflow signatures, active erosion zones, and ephemeral flow pathways. In particular, neighborhoods such as Rezaigui were identified as highly vulnerable due to their downstream position relative to steep upstream slopes and their location within a diffuse hydrographic network, where rapid runoff concentration—enhanced by re-current convective rainfall—resulted in localized yet substantial damage.

These findings are consistent with assessments conducted by the Algerian Space Agency (ASAL), which, following the July 2017 flood, had already classified the same sectors as highly exposed using high-resolution ALSAT-2 satellite imagery. The recurrence of flooding in these areas underscores their pronounced vulnerability and highlights the urgency of integrating them into targeted and sustained flood risk prevention strategies.

From an applied perspective, the results emphasize the necessity for regular maintenance of urban drainage networks, the explicit consideration of sediment transport processes in land-use and urban planning, and the implementation of localized mitigation measures, such as retention basins or flow-attenuation structures. In addition, early warning systems adapted to the scale of micro-watersheds could substantially reduce exposure and damage in these high-risk zones.

More broadly, this study underscores the scientific and operational value of coupling spatial analyses with empirical field observations in small, ungauged watersheds. Future research should prioritize the deployment of low-cost hydrological monitoring devices to generate continuous runoff and sediment datasets, thereby supporting more robust risk assessments and the development of effective, integrated watershed management strategies.

Acknowledgements

The authors gratefully acknowledge Dr. Benhamlaoui.A, for his assistance with the English language editing of the manuscript and Mr A. Bouchachoua for his support during the fieldwork.

References

Achite, M., Katipoğlu, O. M., Jehanzaib, M., Elshaboury, N., Kartal, V., & Ali, S. (2023). Hydrological drought prediction based on hybrid extreme learning machine: Wadi Mina Basin Case Study, Algeria. *Atmosphere*, *14*(9), 1447. https://doi.org/10.3390/atmos14091447

Alam, A., Ahmed, B., & Sammonds, P. (2021). Flash flood susceptibility assessment using the parameters of drainage basin morphometry in SE Bangladesh. *Quaternary International, 575*, 295–307. https://doi.org/10.1016/j.quaint.2020.04.047

Benzougagh, B., Dridri, A., Boudad, L., Sdkaoui, D., & Baamar, B. (2019). Apport des SIG et télédétection pour l'évaluation des caractéristiques physiques du bassin versant d'oued Inaouene (Nord-Est Maroc) et leurs utilités dans le domaine de la gestion des risques naturels. *American Journal of Innovative Research and Applied Sciences, 8*(4), 120–130.

Bouchachou, A. (2023). *Morphodynamic reading of hydrological risks in small urban catchments: The case of Ain M'lila (Algeria)* (Master's thesis, University of Larbi Ben M'hidi, Oum El Bouaghi).

Bravard, J. P., & Petit, F. (2000). *Les cours d'eau : Dynamique du système fluvial*. Collection U.

Elahcene, O., Terfous, A., Remini, B., Ghenaim, A., & Poulet, J. B. (2013). Etude de la dynamique sédimentaire dans le bassin versant de l'Oued Bellah (Algérie). *Hydrological Sciences Journal*, *58*(1), 224–236. 02626667.2012.742530/10.1080

Garzon, L. F. L., Johnson, M. F., Mount, N., & Gomez, H. (2023). Exploring the effects of catchment morphometry on overland flow response to extreme rainfall using a 2D hydraulic-hydrological model (IBER). *Journal of Hydrology, 627*, 130405. https://doi.org/10.1016/j.jhydrol.2023.130405

Ghaleno, M. R. D., Meshram, S. G., & Alvandi, E. (2020). Pragmatic approach for prioritization of flood and sedimentation hazard potential of watersheds. *Soft Computing, 24*(20), 15701–15714. https://doi.org/10.1007/s00500-020-04899-4

Gravelius, H. (1914). *Grundriß der gesamten Gewässerkunde. Band 1: Flußkunde [Compendium of hydrology]*. Göschen.

Hamad, R. (2020). Multiple morphometric characterization and analysis of Malakan valley drainage basin using GIS and remote sensing, Kurdistan Region, Iraq. *American Journal of Water Resources, 8*(1), 38–47. 10.12691/ajwr-8-1-5

Horton, R. E. (1945). Erosional development of streams and their drainage density: A hydrophysical approach to quantitative geomorphology. *Geological Society of America Bulletin, 56*, 275–370.

IPCC. (2021). Chapter 8: Water cycle changes. In *Climate change 2021: The physical science basis. Contribution of Working Group I to the Sixth Assessment Report of the Intergovernmental Panel on Climate Change*. Cambridge University Press. https://www.ipcc.ch/report/ar6/wg1/chapter/chapter-8/

Jakubínský, J., Bácová, R., Svobodová, E., Kubíček, P., & Herber, V. (2014). Small watershed management as a tool of flood risk prevention. *Proceedings of the International Association of Hydrological Sciences*, *364*, 243–248. https://doi.org/10.5194/PIAHS-364-243-2014

Jenson, S. K., & Domingue, J. O. (1988). Extracting topographic structure from digital elevation data for geographic information system analysis. *Photogrammetric Engineering and RemoteSensing, 54*(11), 1593–1600.

Jourgholami, M., Karami, S., Tavankar, F., Lo Monaco, A., & Picchio, R. (2020). Effects of slope gradient on runoff and sediment yield on machine-induced compacted soil in temperate forests. *Forests, 12*(1), 49. https://doi.org/10.3390/f12010049

Lei, W., Dong, H., Chen, P., Lv, H., Fan, L., & Mei, G. (2020). Study on runoff and infiltration for expansive soil slopes in simulated rainfall. *Water, 12*(1), 222. https://doi.org/10.3390/w12010222

Mashauri, F., Mbuluyo, M., & Nkongolo, N. (2023). Influence des paramètres hydro-morphométriques sur l'écoulement des eaux des sous-bassins versants de la Tshopo, République Démocratique du Congo. *Revue Internationale de Géomatique, 32*, 79–98. https://doi.org/10.32604/RIG.2023.044124

Meddi, M., Talia, A., & Martin, C. (2009). Évolution récente des conditions climatiques et des écoulements sur le bassin versant de la Macta (Nord-Ouest de l'Algérie). *Physio-Géo. Géographie physique et environnement*, *3*, 61–84.

Merheb, M., Moussa, R., Abdallah, C., Colin, F., Perrin, C., & Baghdadi, N. (2016). Hydrological response characteristics of Mediterranean catchments at different time scales: A meta-analysis. *Hydrological Sciences Journal, 61*(14), 2520–2539. https://doi.org/10.1080/02626667.2016.1140174

Ministère des Forêts, de la Faune et des Parcs (MFFP), Québec. (2018). *Guide de réalisation d'aménagements durables en forêt privée – Annexe 6 : Méthodes de calcul des débits de pointe*. https://mffp.gouv.qc.ca

Nait-Si, H., Nmiss, M. H., Benbih, M., Boukdoun, A., & Ouammou, A. (2025). Impact des caractéristiques hydro-morphométriques sur la réponse hydrologique du bassin versant de l'oued Adoudou (Anti-Atlas occidental, Maroc) [Impact of hydro-morphometric characteristics on the hydrological response of the Oued Adoudou watershed (Western Anti-Atlas, Morocco)]. *Revista de Estudios Andaluces, 50*, 185–217. https://doi.org/10.12795/rea.2025.i50.09

Obeidat, M., Awawdeh, M., & Al-Hantouli, F. (2021). Morphometric analysis and prioritisation of watersheds for flood risk management in Wadi Easal Basin (WEB), Jordan, using geospatial technologies. *Journal of Flood Risk Management, 14*(2), e12711. https://doi.org/10.1111/jfr3.12711

Özcan, Z., Trinh, T., Kavvas, M. L., & Alp, E. (2025). Assessment of climate change for predicting water–energy–food–ecosystem nexus vulnerability in a semi-arid basin. *Journal of Water and Climate Change, 16*(2), 712–735. https://doi.org/10.2166/wcc.2024.703

Seethapathi, P. V., Dutta, D., & Kumar, R. S. (Eds.). (2008). *Hydrology of small watersheds*. TERI Press.

Shekar, P. R., & Mathew, A. (2024). Morphometric analysis of watersheds: A comprehensive review of data sources, quality, and geospatial techniques. *WatershedEcology and the Environment*, *6*, 13–25. https://doi.org/10.1016/j.wsee.2023.12.001

Strahler, A. N. (1957). Quantitative analysis of watershed geomorphology. *Transactions of the American Geophysical Union, 38*(6), 913–920. https://doi.org/10.1029/TR038i006p00913

Strahler, A. N. (1964). Quantitative geomorphology of drainage basins and channel networks. In V. T. Chow (Ed.), *Handbook of applied hydrology* (pp. 439–476). McGraw-Hill.

Topography Platform. (2023). *Données MNT 30m*. https://www.topography.com

Tramblay, Y., & Somot, S. (2018). Future evolution of extreme precipitation in the Mediterranean. *Climatic Change*, *151*(2), 289-302. https://doi.org/10.1007/s10584-018-2300-5

Vaze, J., & Teng, J. (2007). Impact of DEM resolution on topographic indices and hydrological modelling results. In *MODSIM 2007 International Congress on Modelling and Simulation*.

World Bank. (2020). *Adaptation to climate change in the Middle East and North Africa (MENA) region*. https://www.worldbank.org/en/topic/climatechange/publication/adaptation-to-climate-change-in-mena

INTERNATIONAL SCIENTIFIC JOURNAL | GEOGRAPHICA PANNONICA

Elona Pojani, Xhoana Hudhra, Dorina Pojani, Henrik Hassel
Geographica Pannonica | Volume 29, Issue 4, 322-337

Disaster Risk Perception and Communication in Flood-prone Areas in Albania: A Comparison of Urban and Rural Settings

Elona Pojani[A], Xhoana Hudhra[A], Dorina Pojani[B*], Henrik Hassel[C]

[A] Faculty of Economics, University of Tirana, Rruga Arben Broci 1 1001, Tiranë, Albania. ORCID EP: 0000-0001-9854-2382
[B] School of Architecture, Design and Planning, The University of Queensland, Level 3, Room 306, Zelman Cowen Building (51), St Lucia, Qld 4072 Australia. ORCID DP: 0000-0002-2018-6338
[C] Division of Risk Management and Societal Safety, Lund University, Klas Anshelms väg 14, 22363 Lund, Sweden. ORCID HH: 0000-0002-4178-7634

Received: July 10, 2025| Revised: December 18, 2025| Accepted: December 23, 2025

doi: 10.5937/gp29-60075

Abstract

This study examines disaster risk perception and communication in Albania, focusing on two districts in the cities of Tirana and Fier and the villages of Novosela and Dajç, all affected by severe flooding in recent years. The research highlights how dimensions of national culture - particularly fatalism and attachment to home and hearth - interact with contextual, psychological, and demographic characteristics to shape flood risk perceptions. Quantitative analysis using surveys (N=104) and ORL regression models shows that disaster risk tolerance is influenced by location, household income, and prior exposure to natural disasters. Urban residents are less tolerant of risk, while higher-income individuals and those with previous disaster experience show greater tolerance. Qualitative interviews reveal that city dwellers often perceive floods as inevitable, while rural participants emphasize communal coping and local knowledge.

Keywords: disaster risk perception; disaster risk communication; floods; Albania; rural areas; urban areas

JEL classification codes

Q54 Climate • Natural Disasters and Their Management • Global Warming
R14 Land Use Patterns
I31 General Welfare, Well-Being
D81 Criteria for Decision-Making under Risk and Uncertainty

[*] Corresponding author: Dorina Pojani; e-mail: d.pojani@uq.edu.au

Introduction

Natural hazards, including floods, earthquakes, volcanic eruptions, wildfires, droughts, landslides, and various types of storms, are globally becoming more frequent, intense, and diverse (Xu & Lin, 2025). With greater human exposure and social vulnerabilities, disasters risk - "the potential loss of life, injury, or destroyed or damaged assets which could occur to a system, society or a community in a specific period of time" (UNDRR, 2017:10) - is increasing.

Flood risk is rising across the Global South and the Global North, driven by anthropogenic climate change and human activities (Shamsudduha, 2025; Vojtek & Vojteková, 2016; Halecki & Młyński, 2025). In Central Europe, the 2021 floods caused more than 200 fatalities and over USD 54 billion in economic losses (Fang et al., 2025). Regional characteristics strongly shape expected impacts (Fang et al., 2025), and the Balkan region is no exception (Sabljić et al., 2023).

On a global scale, Albania faces some of the most severe economic consequences from natural disasters. By the late 2000s, the country experienced average annual losses amounting to about 2.5% of its GDP (World Bank, 2009). Between 1995 and 2015, an average of 30,000 people were affected by natural disasters each year, with over 95% of Albanian municipalities experiencing at least one disaster during this period (World Bank, 2020). These figures are substantial, considering the country's small population of less than 3 million.

Floods have become a major problem in built areas near rivers and along the coast (Zaimi & Jaupaj, 2020; Lushaj, 2016). Yet, Albania lacks a comprehensive system for long-term disaster monitoring. Risk assessment often boils down to mere risk tabulation, lacking a thorough analysis of different disaster scenarios and levels of exposure for local populations and assets (Duro, 2015). Few individuals have disaster insurance, and public compensation is limited to covering only 40% of losses (Grabova & Mesiti, 2018; Sharku & Koçi, 2017).

Disaster risk perception, defined as the psychological processes of "collecting, selecting, and interpreting signals about uncertain impacts of events, activities, or technologies" (Wachinger et al., 2013:1049), plays a key role in society´s response to disaster risks. People's risk attitudes, perceptions, information, and preparedness have previously been studied in the context of floods (Heitz et al., 2009; Plapp & Werner, 2006; Plattner et al., 2006; Terpstra, 2009), whereas research concerning other types of natural disasters is limited. The existing literature suggests that risk perceptions depend on the (1) *type of risk*, (2) *socio-demographic characteristics*, (3) *personality and cognition*, and (4) *access to risk-related information* (Renn, 2008; Heitz et al., 2009; Wachinger et al. 2013). We add another factor to this list: *(5) national culture*. Some studies have hinted at this aspect by highlighting the role of trust in authorities and people's voluntary involvement in post-disaster recovery efforts (Miceli et al., 2008; Armaş, 2007; Baan & Klijn, 2004). However, national culture is yet to be unpacked in the disaster risk literature.

Public authorities can and should make an effort to manage risks effectively – cultural and demographic barriers notwithstanding. It is the task of authorities to devise disaster response strategies and share those with individuals, workplaces, and communities (Miceli et al., 2008). To be successful, these strategies must account for the risk perception in the population, which can be measured through surveys, interviews, and/or public forums (Morgan et al., 2001). Where disaster response strategies undermine the interests of particular stakeholders, conflict resolution sessions may be necessary (Renn, 2008). In combination, these iterative processes are known as 'risk communication' (Rohrmann, 2000). Indirectly, the success of risk communication strategies also depends on the national culture.

This study examines disaster risk perception and communication in Albania, focusing on two cities (Tirana and Fier) and two villages (Dajç and Novosela) that have been severely affected by floods in recent years. Based on primary survey data and field observations, we provide insights that will assist local risk management agencies in developing effective strategies to prepare for, and respond to, flood events. This research is crucial because risk perceptions and the effectiveness of risk communication are known to vary based on time and context (Marshall, 2020), making it unlikely that findings from other regions will fully apply to Albania.

Beyond its local relevance, this study contributes to the broader theory by:

(a) Highlighting the role of national culture in disaster risk perception and communication, alongside contextual, psychological, and demographic factors. Albanian culture is often described as having a fatalistic streak, with people more inclined to trust in fate than to plan for the long term. This may be linked to Islamic concepts of predestination and acceptance in the face of adversity, as well as to patterns of learned helplessness developed during decades of communist dictatorship and the turbulent post-communist period. While fatalism has not yet been systematically examined in the context of natural hazards in Albania, a study in neighbouring North Macedonia suggests its presence in the broader region (Sickmiller, 2007). Another relevant cultural trait is the strong attachment to home and hearth. This stems from the country's deeply rooted rural traditions and agrarian past. A culture centred on family ties and close-knit communities has persisted even as Albania has urbanized in recent decades, and homeownership rates are among the highest in Europe (Instat, 2021).

(b) Distinguishing between urban and rural areas. While rural areas have been the focus of extensive research, there is a notable gap in the literature on natural disaster risk management in urban areas; in the Western Balkans, studies are virtually nil. In this region, urban living has been the aspiration whereas rural areas were traditionally considered as the epicentre of backwardness. But is this true when it comes to coping with disasters?

The rest of the article presents the case study settings, the methodological approach, and the empirical findings.

Case studies

We have studied four flood prone areas along Albania's western lowlands, which border the Adriatic and Ionian Seas (Figure 1). Two areas, Tirana and Fier, are urban, and two others, Dajç and Novosela, are rural. Housing in all four areas is mostly single-family. Tirana and Fier are large cities; therefore, two districts near their rivers (Tirana River and Gjanica River respectively) were selected as case studies. Those districts have about 1000 – 1500 people. The Tirana case study houses impoverished people, including many Romani minorities, living in informally built housing whereas the Fier case study comprises more middle-class residents. Dajçi is a scenic village of about 2,000 inhabitants, located on the banks of Buna River, near the city of Shkodra. Novosela is an agricultural village of about 8,200 people along the Vjosa River (for Census data, see Instat, 2021).

Figure 1. Location of case studies
Map source: d-maps (https://d-maps.com/m/europa/albanie/albanie13.gif), modified by authors

All four cases have experienced flooding at different times. Flood events have been increasing, partly due to climate change and partly owing to the poor management of river flows (Deda et al., 2025). For example, Novosela has been struggling with floods since the construction of the Fier-Vlora highway, which has hindered the normal flow of the Vjosa River (*OraNews*, 1 February 2015). Gjanica's riverbed has deteriorated due to construction waste being illegally tossed in the water (*Top Channel*, 12 October 2015).

Data and Methods

This study was based on a face-to-face survey of people affected by floods in the four areas. The sample size was 104 (Tirana: 30; Fier: 20; Dajç: 32; Novosela: 22). Participants were recruited via convenience sampling. While this sample is not large and convenience sampling has its drawbacks, it must be noted that it was excessively difficult to recruit participants, considering the anxiety and even trauma caused by flooding or the prospect of flooding. Individuals who have experienced natural disasters are understandably reluctant to participate in research studies due to the emotional burden of revisiting distressing events (Patton, 2014).

Furthermore, the nature of our research population (a 'specialised' group scattered around Albania) necessitated a smaller sample size. While their frequency is increasing, disaster-related experiences are not an everyday occurrence, making large-scale recruitment impractical (see Patton, 2014). However, our sample yielded valuable insights that can

enhance both academic knowledge and policy development. To address the limitations of a smaller sample, we triangulated the survey data with qualitative interviews and site observations.

The survey sample was balanced in terms of gender, and most respondents were married and middle aged. Households were relatively large, suggesting that many respondents lived in extended families. Urban residents were generally poorer and less educated than those in rural areas, which suggests that in larger cities the most impoverished and socially disadvantaged individuals are often the ones who end up living in less desirable, disaster-prone areas along riverbanks. (This contrasts with wealthier cities in Europe, where the prime residential areas are often located near water.) Although many rural respondents reported lacking formal employment, the reality is that they are usually engaged in family farming (Table 1).

Table 1. Sample characteristics (N=104)

Location		**Rural**	**Urban**	**Total**
Respondents		54	50	104
Gender (%)	F	19	33	52
	M	19	33	52
Age	Mean	47	47	94
Education (%)	Primary	48	61	109
	Secondary	46	24	70
	Tertiary	6	14	20
Monthly household income* (%)	≤300	35	68	103
	301-500	37	16	53
	501-900	26	16	42
Household size	Mean	4.9	4.7	9.6
Marital status (%)	Not married	16	12	28
	Married	84	88	172
Employment (%)	Employed	100	84	184
	Unemployed	84	16	100

**Reported in Euro. 1 Euro = 100 Albanian Lek*

The survey questionnaire was in five parts. The first part collected demographic data at the individual or household level while the second part focused on the amenities of the participant's home. (Note that our research populations are traditional and conservative, understanding gender in binary terms; our research questions reflect local norms.) The third and fourth parts consisted of a series of Likert scale questions related to disaster risk perceptions and attitudes and the level of risk communication and preparedness. The fifth part included a series of open-ended questions related to risk perception and communication, the answers to which were treated as qualitative data and were subjected to content analysis. This helped provide nuance and depth to the findings. In addition, researchers took field notes - for example, on the type and quality of local housing and the level of community interactions.

The quantitative data were used to compute descriptive statistics (see later) and to fit two ordinary least squares (OLS) regression models. In both models, the dependent variable was a construct called 'disaster risk tolerance' which was calculated as the average of the responses to a series of Likert scale questions listed in Table 2. This variable was logarithmically transformed so that the model computed relative changes rather than absolute

changes in disaster risk tolerance. In a simpler model, we looked at urban and rural differences in 'disaster risk tolerance' while controlling for other socio-demographic factors.

Table 2. The 'disaster risk tolerance' construct (dependent variable)

Question	Mean*	SD
1-4 Likert scale (government responsibility)		
The government must keep financially assisting families affected by floods	3.88	0.34
People who choose to live in flood-prone areas should have to pay for damages	1.53	1.18
The government should ban construction in flood-prone areas	2.5	1.96
The government should strengthen building codes in flood-prone areas	2.61	2.01
The government should require homeowners to purchase flood insurance	2.05	1.92
The government should levy an earmarked flood tax	1.90	1.86
Residents in flood-prone area are responsible for maintaining drainage canals	2.01	1.85
1-5 Likert scale (individual responsibility)		
One must accept that everything in life carries some risk	4.01	1.17
My/my family's life is in God's hands	4.08	1.19
Government measures to mitigate flood damage are adequate	4.25	1.22
Flood damage can be minimized if everyone takes prevention measures	3.5	1.39
Individual measures to reduce flood damage make no difference	2.95	1.57
I want to learn more about how to prepare for natural disasters	3.14	1.81

**Lower figures indicate disagreement and higher figures indicate agreement*
A 1-4 Likert scale was used in one section of the questionnaire and a 1-5 scale in another, reflecting the fact that different sections were adapted from previous studies (Ogston, 2006; Miceli et al., 2008).

In a more complex model, the independent variables sought to capture five the facets listed at the outset:

1) *Type of risk*. People who live on the seafront or in proximity to rivers may fear floods whereas those who live in arid and isolated towns may be apprehensive about fires (Heitz et al., 2009). We only considered floods in this study, upon confirming with the survey respondents that this was indeed the most serious concern in their area (Figure 2). Therefore, no variable was included.
2) *Socio-demographic profile*. Characteristics such as age, education, income, homeownership status, employment status, and family size are known to affect risk perception (Heitz et al., 2009). We considered these in addition to marital status, family size, and, importantly, location (binary: urban vs rural).
3) *Personality and cognition.* We considered exposure to natural disasters, measured as the number of times people have experienced natural disasters, including floods, in their areas. More than half of the respondents reported regular occurrences of heavy snow, windstorms, landslides, hail, and earthquakes, and more than two thirds have dealt with the aftermath of floods.
4) *Information about risk*. This was measured through a binary question asking if participants had ever been aware of any flood warning (from the government or other sources).
5) *National culture*. Given the broad scope of this construct, we limited the analysis to two aspects: (a) 'fatalistic mindset', with people regarding floods as god's will (0=otherwise); and (b) 'attachment to home and hearth', with people stating that they would never leave their area, despite it being prone to flooding (0=otherwise).

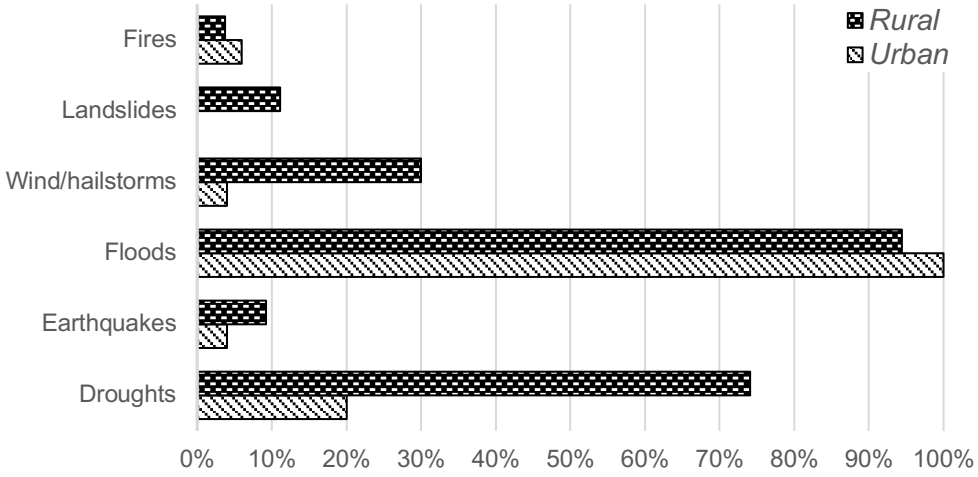

Figure 2. Responses to question: 'What is the most serious natural disaster affecting your area'?

Results and Discussion

Disaster risk perception

Descriptive statistics

We considered two aspects, contrasting urban and rural settings: (1) attitudes towards government responsibility; (2) attitudes towards individual responsibility. Figures 3 and 4 show that people had high expectations of the government, particularly around financial support in case of floods.

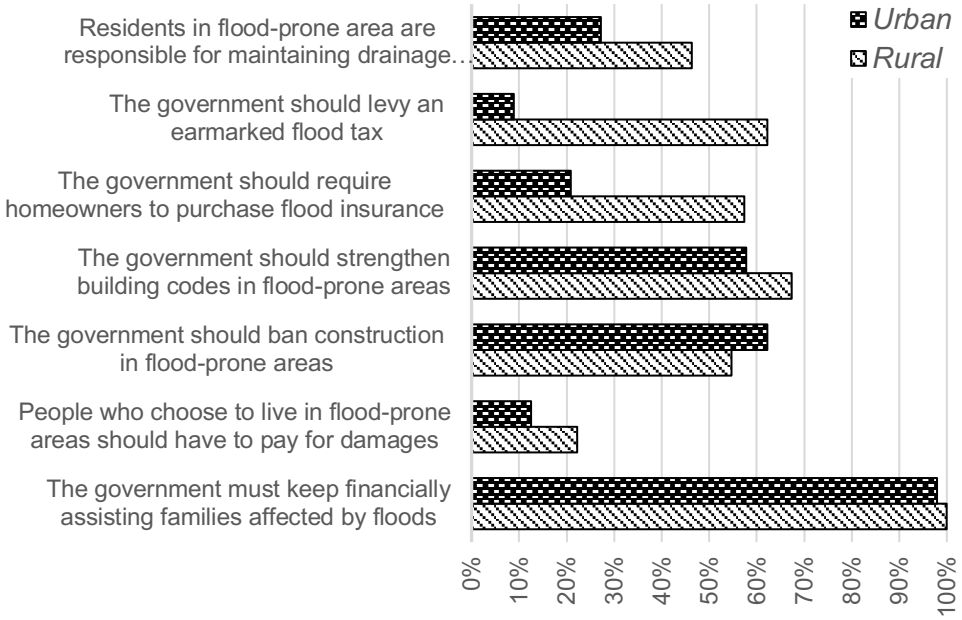

Figure 3. Attitudes toward government responsibility

More than half of all respondents in both urban and rural areas agreed that the planning sector has a large role to play in strengthening building codes, and even banning new construction in flood-prone zones. However, urbanites were more passive and fatalistic whereas rural dwellers were more willing to contribute to mitigating flood damage by paying earmarked taxes and insurance premiums. This suggested a longer-term orientation in rural areas, where communities are more consolidated, homeownership is virtually universal, and people are less likely to move.

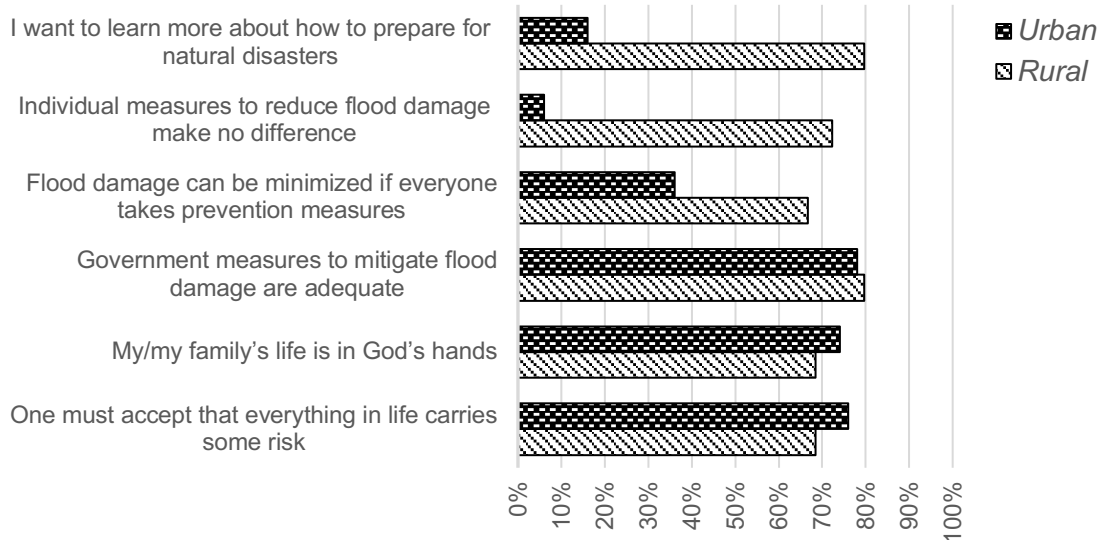

Figure 4. Attitudes toward individual responsibility

Regression analysis

The results of the first model are shown in Table 3. This model explained approximately 48% of the variability in disaster risk tolerance. Three independent variables were statistically significant: location, monthly household income, and exposure to natural disasters. Individuals residing in urban areas were less tolerant of disaster risks, likely due to lower incomes and greater perceived vulnerability. In line with the literature (Wang et al., 2022; Yildiz et al., 2024), higher income people had a higher disaster risk tolerance, probably because they feel more financially secure and able to cope with the aftermath of disasters. They can also afford better housing, insurance, and recovery resources, thus reducing their vulnerability (Perić & Cvetković, 2019; Xu et al., 2019; Yin et al., 2021).

Lastly, individuals with prior exposure to natural disasters exhibit higher risk tolerance, potentially due to developed resilience or coping mechanisms, or because they become nonchalant, reasoning that a disaster is unlikely to strike the same place twice (Heitz et al., 2009). This aligns with existing research showing that personal experiences shape individuals' estimates of the frequency and consequences of disasters (Morgan et al., 2001). However, responses to prior exposure vary: while some individuals become indifferent, others develop heightened anxiety about future disasters (Onuma et al., 2017; Baan & Klijn, 2004; Udwin et al., 2000). These variations reflect differences in personality and cognition, which may lead to risk perceptions that diverge significantly from expert assessments and, consequently, to behaviours and resource allocation decisions that are irrational or inconsistent with recommended measures (Slovic, 1992; Rundmo, 1996; Becker et al., 2014; Ardaya et al., 2017). Moreover, exposure to natural disasters interacts with the availability and credibility of risk information: even experienced populations may lack comprehensive knowledge or doubt the reliability of information from authorities and experts, further shaping their risk perceptions and responses (UNISDR, 2015).

Table 3. Model 1 results (N=104)

Variable	Coefficient	Std. Error	t-statistic	p-value
Dependent variable: Disaster risk tolerance				
Independent variables				
Socio-demographic profile				
Location (rural / urban)	-0.438850	0.130114	-3.372041	0.0011***
Gender	0.057915	0.102884	0.562912	0.5750
Education	0.009072	0.115829	0.080579	0.9360
Monthly household income	0.180343	0.077571	2.324888	0.0225***
Household size	-0.017814	0.039120	-0.455365	0.6500
Marital status	0.079030	0.067203	1.175983	0.2430
Employment	0.085968	0.153077	0.561600	0.5759
Personality and cognition				
Exposure to natural disasters	0.059177	0.027110	2.182836	0.0319***
Information about risk				
Awareness of flood warnings	0.097786	0.124749	0.783862	0.4354
National culture				
Fatalistic mindset	0.144300	0.132784	1.086726	0.2803
Attachment to home and hearth	0.067567	0.115264	0.586198	0.5593
Constant (C)	*2.063140*	*0.351463*	*5.870149*	*0.0000****
R-squared: 0.48 (moderate power)				
Adjusted R-squared: 0.411098 (reasonable fit)				
SE of regression: 0.451231				
Log likelihood: -52.78623				
*F-statistic: 6.965382****				
Prob(F-statistic): 0.000000 (overall model is statistically significant)				
Mean dependent variable: 2.861404				
SD dependent variable: 0.588000				
Akaike info criterion: 1.363921				
Schwarz criterion: 1.686516				
Hannan-Quinn criterion: 1.494273				
Durbin-Watson statistic: 1.720515				
**p<0.2 **p<0.1 ***p<0.05 ****p<0.01*				

Previous research has shown that parents and homeowners tend to be more concerned about loss of life, health, or property; however, in this study, these variables were not statistically significant. Research also suggests that women are generally more sensitive to disaster risk, due to financial constraints and/or socialization (Slovic, 1992; Wachinger et al., 2013; Mızrak et al., 2021; Cuesta et al., 2022); however, this variable was not included in our analysis.

The second, simpler model (Table 4) was applied to reassess the role of socio-demographic variables, particularly rural vs urban location. This model explained approximately 46% of the variability in disaster risk tolerance. Location, age, and income were found to be significant predictors of risk tolerance. As before, urban residents were less tolerant of disaster risks, while higher-income individuals were more tolerant. Additionally,

risk tolerance tended to increase with age, possibly due to greater financial security over time. Other studies have found age to be associated with a lower likelihood of participating in capacity-building and educational activities, which in turn increases vulnerability, limits the adoption of coping strategies, and heightens the risk of livelihood loss during flood events (Savari et al., 2025). Education and marital status, however, were not statistically significant.

Table 4. Model 2 results (N=104)

Variable	Coefficient	Std. Error	t-statistic	p-value
Dependent variable: Disaster risk tolerance				
Independent variables				
Location (rural / urban)	-0.511885	0.097851	-5.23181	0.0000****
Age	0.111113	0.004095	2.14159	0.0080***
Monthly household income	0.176439	0.072015	2.450028	0.0162***
Education	0.121427	0.090813	1.337112	0.1846*
Marital status	0.079466	0.056652	1.402709	0.1641*
Constant (C)	2.012567	0.254891	7.89510	0.0000****
R-squared: 0.4641 (moderate power)				
Adjusted R-squared: 0.434326 (reasonable fit)				
SE of regression: 0.443161				
Log likelihood: -54.99333				
F-statistic: 15.58825****				
Prob(F-statistic): 0.000000 (overall model is statistically significant)				
Mean dependent variable: 2.861404				
SD dependent variable: 0.588000				
Akaike info criterion: 1.270694				
Schwarz criterion: 1.430966				
Hannan-Quinn criterion: 1.335479				
Durbin-Watson statistic: 1.705257				
**p<0.2 **p<0.1 ***p<0.05 ****p<0.01*				

Disaster risk communication

The qualitative portion of this research revealed that disaster risk communication was quite poor in all four case studies, with little difference between urban and rural areas. Typically, residents reported that they had received flood warnings only a couple of days before the event, which, according to them, allowed very little time for evacuation. An alarmingly low rate of residents (18% in villages and 8% in cities) had received training on how to cope with natural disaster situations. Nonetheless, many residents (48% in villages and 54% in cities) were aware that emergency management committees existed in their district, which could be consulted if necessary.

Prior research has similarly highlighted that, in Albania the concept of 'early warning' is typically limited to signalling an imminent disaster or accident whereas individuals tend to rely on hearsay from friends and relatives, instead of seeking reliable information from public authorities (Duro, 2015). Given a general attitude of distrust and disrespect for authorities, it is unclear whether earlier warnings and more trainings would have been effective. Similar communication gaps between authorities and local communities have been observed in other contexts, such as Pakistan, where delayed information from authorities has prevented people from taking precautionary measures to avoid the negative consequences of floods (Iqbal & Nazir, 2023). Furthermore, even when governments issue timely recommendations to

evacuate or stay put, citizens may choose not to follow the advice due to limited financial means, lack of safe shelter, or fear of burglary (Auliagisni et al., 2022).

In Albania, despite the risks, only few residents planned on moving. This speaks to a level of cultural attachment to home and hearth (which, however, was not statistically significant in the quantitative model). Some - especially youth in the two rural areas, and the most impoverished residents in Tirana - wanted to move but felt that they had nowhere to go. Many people had been aware of the risk before purchasing or building their house, but they had accepted the risk because, due to weak finances, their options had been quite limited. The same pattern is observed in other studies. For example, in Pakistan, Iqbal & Nazir (2023) found that residents often relocated temporarily but tend to return, likely because they depend on the area for their livelihoods. This speaks to a short-term cultural orientation among people who face little choice and many unsurmountable financial barriers in terms of access to adequate housing. Given their circumstances, people had framed their choice in fatalistic terms: "if it's meant to happen, it will happen." This attitude was expected, given the Albanian cultural context of prevailing fatalism, mentioned earlier.

Novosela was an exception: floods had not been common here before the construction of the Fier-Vlora highway, which disrupted the flow of the Vjosa River. As a result, residents were upset about being unexpectedly exposed to natural disasters due to a public planning intervention. Attachment to home and hearth was stronger in Novosela and Fier (both considered as part of southern Albania).

Despite (or perhaps because of) poor disaster risk communication, respondents were very anxious about the potential impact of floods. They worried about personal safety as well as damage to their houses and home appliances. In rural areas with more space and flexibility in terms of construction, some residents (53% in Dajç and 18% in Novosela) had built their houses on stilts to protect from flooding. In addition, 35% of rural respondents had secured the foundations of their houses. In urban areas, houses were usually built at ground level, and due to the type of construction (brick and concrete) could not be raised later. Only 16% of urban respondents had reinforced their home foundations.

With floods becoming more frequent, households had started to develop rudimentary emergency plans. In rural areas 53% of rural respondents had a plan, compared to only 34% of urban respondents. This disparity may reflect a greater sense of self-reliance in rural areas, with residents more accustomed to preparing for emergencies independently due to less immediate access to public services. Plans were always at the family rather than the community level. This is in line with an aspect of the national culture - lack of collaboration and volunteerism - discussed earlier. Tirana and Fier residents appeared to be the least prepared, which went against expectations of urban areas being more advanced and able to cope with disasters.

Typically, household emergency plans involved the steps needed to evacuate their area more efficiently. People had come to realise that, in some cases, evacuation might not be possible, and therefore kept some food and supplies in storage in case they became trapped. Specifically, 26% of all respondents had set aside some emergency supplies. Other studies have shown that emergency stockpiling may be linked to prior experiences of flood events (Auliagisni et al., 2022), highlighting the importance of risk awareness and knowledge for an effective response.

In all cases, a large majority of residents (61% in rural areas and 80% in urban areas) did not have sufficient savings to cover any losses. Consistent with previous findings (Grabova & Mesiti, 2018), very few people had property or life insurance - 12% in rural areas and 6% in urban areas. Additionally, not many were aware that public compensation is capped at 40% of the cost of losses. Overall, urban residents appeared to have less financial

capacity than rural dwellers, despite wealth being concentrated in cities in Albania. This finding is likely due to the fact that, in cities, it is often the most impoverished and socially disadvantaged individuals who end up living in less desirable, disaster-prone areas, making them more financially vulnerable when disasters occur. Also, the cost of living is higher in cities.

Conclusion

This study emphasises the role of national culture - particularly dimensions such as fatalism and attachment to home and hearth - in shaping disaster risk perception and communication, alongside various contextual, psychological, and demographic factors. It differentiates between urban and rural areas, demonstrating that, in Albania at least, urban residents are less prepared and more vulnerable to flooding than those in rural areas. The findings further underscore that socio-cultural factors are critical in understanding disaster impacts, suggesting that disaster management efforts should not focus solely on the physical aspects of disasters and hazards (Mercer et al., 2012).

The Western approach to natural disaster management assumes stable government, economic strength, and a population receptive to early warning systems (Sickmiller, 2007). Since Albania does not fully meet these criteria, disaster preparedness must be community-based, relying on social capital in addition to addressing physical vulnerabilities. Only through a community-centred approach that emphasizes education, trust, and social cohesion, rather than strict regulation and enforcement, can Albanian cities and villages build resilience to natural disasters (see Sickmiller, 2007). However, given the small sample size, this study should be considered exploratory. Further research with larger samples and additional locations is needed to confirm and extend these findings and policy recommendations.

Acknowledgements

This study received financial support from the European Commission, ERASMUS+ Programme (Knowledge FOr Resilient soCiEty, Project no 573942-EPP-1-2016-1-RS-EPPKA2-CBHE-JP). The authors thank the students at the University of Tirana who helped collect data for this study.

References

Armaş, I. (2008). Social vulnerability and seismic risk perception. Case study: the historic center of the Bucharest Municipality/Romania. *Natural Hazards*, *47*(3), 397–410. https://doi.org/10.1007/s11069-008-9229-3

Auliagisni, W., Wilkinson, S., & Elkharboutly, M. (2022). Learning from Floods—How a Community Develops Future Resilience. *Water*, *14*(20), 3238. https://doi.org/10.3390/w14203238

Baan, P. J. A., & Klijn, F. (2004). Flood risk perception and implications for flood risk management in the Netherlands. *International Journal of River Basin Management*, *2*(2), 113–122. https://doi.org/10.1080/15715124.2004.9635226

Becker, G., Aerts, J. C. J. H., & Huitema, D. (2013). Influence of flood risk perception and other factors on risk-reducing behaviour: a survey of municipalities along the Rhine. *Journal of Flood Risk Management*, *7*(1), 16–30. https://doi.org/10.1111/jfr3.12025

Bustillos Ardaya, A., Evers, M., & Ribbe, L. (2017). What influences disaster risk perception? Intervention measures, flood and landslide risk perception of the population living in flood risk areas in Rio de Janeiro state, Brazil. *International Journal of Disaster Risk Reduction*, *25*, 227–237. https://doi.org/10.1016/j.ijdrr.2017.09.006

Cuesta, A., Alvear, D., Carnevale, A., & Amon, F. (2022). Gender and public perception of disasters: A multiple hazards exploratory study of EU citizens. *SSRN Electronic Journal*. https://doi.org/10.2139/ssrn.4019363

Deda, M., Ndini, M., & Lata, L. (2025). Climate variability and its impact on flood risk in the Vjosa River basin: An analysis of precipitation trends and vulnerability. In *20th Annual System of Systems Engineering Conference*, Tirana, Albania, 8–11 June.

Duro, F. (2015). *Menaxhimi i emergjencave civile në Shqipëri [Management of civil emergencies in Albania]*. Institute for Democracy and Mediation; Centre for European and Security Issues.

Fang, B., Rakovec, O., Bevacqua, E., Kumar, R., & Zscheischler, J. (2025). Diverging trends in large floods across Europe in a warming climate. *Communications Earth & Environment*, *6*(1). https://doi.org/10.1038/s43247-025-02734-y

Grabova, P., & Mesiti, E. (2018). *Insurance as a means for financial resilience: The case of business sector in Albania*. In Proceedings of the 1st International Symposium: Students for Resilient Society (S-FORCE) (Novi Sad, September 28–29).

Halecki, W., & Młyński, D. (2025). Urban flood dilemmas: How European cities growth shapes flood risk and resilience strategies? *Journal of Environmental Management*, *374*, 124161. https://doi.org/10.1016/j.jenvman.2025.124161

Heitz, C., Spaeter, S., Auzet, A.-V., & Glatron, S. (2009). Local stakeholders' perception of muddy flood risk and implications for management approaches: A case study in Alsace (France). *Land Use Policy*, *26*(2), 443–451. https://doi.org/10.1016/j.landusepol.2008.05.008

Instat. (2021). *Statistical database*. https://databaza.instat.gov.al:8083/pxweb/sq/DST/ Retrieved November 28, 2025

Iqbal, A., & Nazir, H. (2023). Community perceptions of flood risks and their attributes: A case study of rural communities of Khipro, District Sanghar, Pakistan. *Urban Climate*, *52*, 101715. https://doi.org/10.1016/j.uclim.2023.101715

Lushaj, B. (2016). *The transboundary waters of rivers, lakes, groundwater, flood risk assessment and the measures for flood mitigation in Albania*. Paper presented at the Environmental Impact Assessment Centre workshop "Flood risk assessment and the measures for flood mitigation in Albania", Tirana, January 29.

Marshall, T.M. (2020). Risk perception and safety culture: Tools for improving the implementation of disaster risk reduction strategies. *International Journal of Disaster Risk Reduction*, *47*, 101557. https://doi.org/10.1016/j.ijdrr.2020.101557

Mercer, J., Gaillard, J. C., Crowley, K., Shannon, R., Alexander, B., Day, S., & Becker, J. (2016). Culture and disaster risk reduction: Lessons and opportunities. In Fearnley, C., Wilkinson, E., Tillyard, C. Edwards, S. (eds.), *Natural Hazards and Disaster Risk Reduction*, pp. 4–25. London: Routledge.

Miceli, R., Sotgiu, I., & Settanni, M. (2008). Disaster preparedness and perception of flood risk: A study in an alpine valley in Italy. *Journal of Environmental Psychology*, *28*(2), 164–173. https://doi.org/10.1016/j.jenvp.2007.10.006

Mızrak, S., Özdemir, A., & Aslan, R. (2021). Adaptation of hurricane risk perception scale to earthquake risk perception and determining the factors affecting women's earthquake risk perception. *Natural Hazards*, *109*, 2241–2259. https://doi.org/10.1007/s11069-021-04918-z

Morgan, M., Fischhoff, B., Bostrom, A., & Atman, C. (2001). *Risk Communication: A Mental Models Approach*. Cambridge, UK: Cambridge University Press.

Ogston, D. J. (2006). *Perception of natural hazard risk and preparedness: a case study of St. Jean Baptiste, Manitoba*. Master's thesis, University of Manitoba, Winnipeg, Canada.

Onuma, H., Shin, K. J., & Managi, S. (2017). Household preparedness for natural disasters: Impact of disaster experience and implications for future disaster risks in Japan. *International Journal of Disaster Risk Reduction*, *21*, 148–158. https://doi.org/10.1016/j.ijdrr.2016.11.004

Patton, M.Q. (2014). *Qualitative Research & Evaluation Methods: Integrating Theory and Practice.* Thousand Oaks, Ca: Sage.

Perić, J., & Cvetković, V. M. (2019). Demographic, Socio-Economic and Phycological Perspective of Risk Perception from Disasters Caused by Floods: Case Study Belgrade. *International Journal of Disaster Risk Management*, *1*(2), 31–43. https://doi.org/10.18485/ijdrm.2019.1.2.3

Plapp, T., & Werner, U. (2006). Understanding Risk Perception from Natural Hazards. Examples from Germany. In Ammann, W., Dannenmann, S., Vulliet, L. (eds.), *RISK21: Coping with Risks due to Natural Hazards in the 21st Century*, pp. 111-118. London: Routledge.

Plattner, Th., Plapp, T., & Hebel, B. (2006). Integrating public risk perception into formal natural hazard risk assessment. *Natural Hazards and Earth System Science*, *6*(3), 471–483. https://doi.org/10.5194/nhess-6-471-2006

Renn, O. (2008). *Risk Governance. Coping with Uncertainty in a Complex World.* London: Routledge.

Rohrmann, R. (2000). A socio-psychological model for analyzing risk communication processes. *The Australasian Journal of Disaster and Trauma Studies* 2. https://www.massey.ac.nz/~trauma/issues/2000-2/rohrmann.htm

Rundmo, T. (1996). Associations between risk perception and safety. *Safety Science*, *24*(3), 197–209. https://doi.org/10.1016/s0925-7535(97)00038-6

Sabljić, L., Pavić, D., Savić, S., & Bajić, D. (2023). Extreme precipitations and their influence on the river flood hazards: A case study of the Sana River Basin in Bosnia and Herzegovina. *Geographica Pannonica 27*(3), 184–198. https://doi.org/10.5937/gp27-45600

Savari, M., Jafari, A., & Sheheytavi, A. (2025). Determining factors affecting flood risk perception among local communities in Iran. *Scientific Reports*, *15*(1). https://doi.org/10.1038/s41598-025-88673-2

Shamsudduha, M. (2025). Redefining flood hazard and addressing emerging risks in an era of extremes. *Npj Natural Hazards.*, *2*(1). https://doi.org/10.1038/s44304-025-00082-7

Sharku, G., & Koçi, D. (2017). *Insurance Availability For Disasters Risk Management In Albania*. Paper presented at the 1st International Symposium: Students for Resilient Society (S-FORCE), Novi Sad, September 28-29.

Sickmiller, A. (2007). *Social vulnerability to natural disasters: A study of Skopje, Macedonia*. Master's thesis, University of Cincinnati, Cincinnati, Oh, USA.

Slovic, P. (1992). Perception of risk: Reflections on the psychometric paradigm. In Krimsky, D., Golding, D. (eds.), *Social Theories of Risk*, pp. 117-152. New York: Praeger.

Terpstra, T. (2009). *Flood preparedness: thoughts, feelings and intentions of the Dutch public*. PhD thesis, University of Twente, Enschede, The Netherlands.

Udwin, O., Boyle, S., Yule, W., Bolton, D., & O'Ryan, D. (2000). Risk Factors for Long-term Psychological Effects of a Disaster Experienced in Adolescence: Predictors of Post Traumatic Stress Disorder. *Journal of Child Psychology and Psychiatry*, *41*(8), 969–979. https://doi.org/10.1111/1469-7610.00685

UNISDR (United Nations Office for Disaster Risk Reduction). (2017). *National disaster risk assessment: Words into action guidelines governance system, methodologies, and use of results*. Report, Geneva, Switzerland.

UNISDR (United Nations Office for Disaster Risk Reduction). (2009). *UNISDR Terminology on disaster risk reduction*. Report, Geneva, Switzerland.

UNISDR (United Nations Office for Disaster Risk Reduction). (2015). *Global assessment report*. Report, Geneva, Switzerland.

Vojtek, M., & Vojteková, J. (2016). Flood hazard and flood risk assessment at the local spatial scale: A case study. *Geomatics, Natural Hazards and Risk*, *7*(6), 1973–1992.

Wachinger, G., Renn, O., Begg, C., & Kuhlicke, C. (2013). The risk perception paradox: Implications for governance and communication of natural hazards. *Risk Analysis 33*(6), 1049–1065.

Wang, X., Peng, L., Huang, K., & Deng, W. (2022). Identifying the influence of disaster education on the risk perception of rural residents in geohazard-prone areas: A propensity score-matched study. *International Journal of Disaster Risk Reduction 71*, 102795. https://doi.org/10.1016/j.ijdrr.2022.102795

World Bank. (2020). *Disaster risk finance diagnostic*: Albania. Report, Tirana, Albania.

World Bank. (2009). *Albania's climate vulnerability*. Report, Tirana, Albania.

Xu, C., & Lin, N. (2025). Building a global forum for natural hazard science. *Npj Natural Hazards*, *2*(1). https://doi.org/10.1038/s44304-025-00130-2

Xu, D., Yong, Z., Deng, X., Liu, Y., Huang, K., Zhou, W., & Ma, Z. (2019). Financial Preparation, Disaster Experience, and Disaster Risk Perception of Rural Households in Earthquake-Stricken Areas: Evidence From the Wenchuan and Lushan Earthquakes in China's Sichuan Province. *International Journal of Environmental Research and Public Health*, *16*(18), 3345. https://doi.org/10.3390/ijerph16183345

Yildiz, A., Dickinson, J., Priego-Hernández, J., Teeuw, R., & Shaw, R. (2024). Effects of disaster education on children's risk perception and preparedness: A quasi-experimental longitudinal study. *The Geographical Journal 190*(2), e12556. https://doi.org/10.1111/geoj.12556

Yin, Q., Ntim-Amo, G., Ran, R., Xu, D., Ansah, S., Hu, J., & Tang, H. (2021). Flood Disaster Risk Perception and Urban Households' Flood Disaster Preparedness: The Case of Accra Metropolis in Ghana. *Water*, *13*(17), 2328. https://doi.org/10.3390/w13172328

Zaimi, K., & Jaupaj, O. (2020). Flood forecasting in the western lowland of Albania with application of the hydrological modeling. *Journal of International Environmental Application and Science 15*(4), 216-223.

INTERNATIONAL SCIENTIFIC JOURNAL | GEOGRAPHICA PANNONICA

Effective Street Geometry and Shading Strategies for Pedestrian Thermal Comfort: A Scenario Based Simulation Approach

Shivanjali Mohite[A*]

[A] Visvesvaraya National Institute of Technology, Nagpur, India;
ORCID: 0009-0009-8349-3982

Received November 20, 2025| Revised: January 10, 2026| Accepted: January 13, 2026

doi: 10.5937/gp29-62910

Abstract

The development of urban heat issues poses significant challenges for pedestrians in tropical cities, necessitating climate-responsive street design. This study employs a scenario-based simulation approach to determine optimal combinations of street geometry and shading strategies that enhance Pedestrian Thermal Comfort (PTC). Using ENVI-met, this study simulated 90 scenarios by combining geometric variables, such as aspect ratio (AR), building typology (BT), and street orientation, with five shading strategies in Nagpur City, India. The modified Physiological Equivalent Temperature (mPET) index was calculated for each scenario using a pre-trained machine learning model. Results quantified that canopy shading was the most effective strategy, reducing mPET by up to 7°C in E-W streets. The effective street geometric combination was a N-S oriented street with a deep AR and linear BT, which consistently achieved the lowest mPET values (33.1–35.8°C). The study concludes with a rating matrix that guides the integration of shading design with street geometry to achieve thermally resilient streets.

Keywords: Pedestrian Thermal Comfort; Urban Street Geometry; ENVI-met; Machine Learning; Microclimate

Introduction

Urban areas worldwide are experiencing profound transformations in their thermal environments, driven by the dual forces of climate change and rapid urbanization. The Intergovernmental Panel on Climate Change (IPCC) has emphasized the increase in vulnerability of tropical and subtropical regions to the impacts of climate change, projecting a scenario where these areas face notable seasonal and annual temperature variations compared to mid-latitudes (IPCC, 2022). This susceptibility arises from the narrow environmental tolerances inherent to tropical ecosystems (Marcotullio et al., 2021). Within these regions, the indicator of climate change is increasingly evident through the intensification of the Urban Heat Islands (UHI) effect, where urban areas are significantly warmer than surrounding rural areas and the frequency of heat waves (Harrington et al., 2016; Russo et al., 2019).

The UHI effect and intensifying heat waves can exacerbate thermal stress, which not only causes significant thermal discomfort but also alters the patterns of outdoor physical and social activities in urban public spaces (Dunjić, 2019; Kim & Brown, 2021; Kotharkar et al., 2019). For pedestrians, excessive heat stress has been reported as a critical barrier to walking activity, which, in turn, can deteriorate walkability, street livability, and urban vitality (Paul et

* Corresponding author: Shivanjali Mohite; e-mail: shivanjali.mohite@students.vnit.ac.in

al., 2025; Tumini et al., 2016). Improving Pedestrian Thermal Comfort (PTC), which is defined as the microclimatic state in which individuals can walk the maximum distance without discomfort or being compelled to modify their environment (Vasilikou & Nikolopoulou, 2020), is therefore essential for urban planning and design.

PTC is governed by a complex interaction between meteorological factors, such as air temperature (Ta), relative humidity (RH), solar radiation (SR), and wind speed and street geometry (Aghamolaei et al., 2023; Khaire et al., 2024; Zhao et al., 2024). Key geometric parameters, including the aspect ratio (AR), street orientation, and the Sky View Factor (SVF), regulate the microclimate within urban canyons by controlling solar access and wind flow (Achour-Younsi & Kharrat, 2016a; Albdour & Baranyai, 2019; Porwal et al., 2025).

Among these variables, solar radiation has the most significant impact on outdoor human thermal sensation (Arif & Yola, 2020; Lin, 2009; Yilmaz et al., 2023). To mitigate discomfort from direct solar exposure, pedestrians consistently exhibit a preference for moving into shaded areas (Hess et al., 2023; Jamei & Rajagopalan, 2017; Watanabe & Ishii, 2016). Thus, effective shading is a fundamental requirement for sustaining long-term outdoor thermal comfort (Lin et al., 2010). The shaded pedestrian environments attract people and encourage walking, yielding direct co-benefits for public health, local economies, and environmental sustainability (Kim & Brown, 2021). The primary mechanism of shading is the reduction of the Mean Radiant Temperature (Tmrt), which represents the sum of all shortwave and longwave radiation in the pedestrian environment. Effective shading not only blocks direct sunlight but also keeps adjacent urban surfaces cooler, which in turn reduces local air temperatures.

Numerous studies have emphasized the significance of shading. For instance, a study conducted in the hot-arid climate of Cairo found that shading can improve thermal comfort by up to 2.3°C on the PET index scale (Elrefai & Nikolopoulou, 2023). Similarly, in Cordoba, Spain, shading interventions achieved up to a 16°C reduction in ground surface temperatures and up to a 6°C reduction on building façades during peak summer (Srivanit & Jareemit, 2019). Field surveys in Arizona also observed the positive impact of shading on enhancing PTC, with no reported difference in perceived comfort due to the type of shade (tree or solar canopy) in the hot-dry climate (Dzyuban et al., 2022). Urban shading can be achieved through a combination of factors, including geometric configurations such as aspect ratio and orientation, vegetative shading through street trees and green corridors, and artificial systems such as arcades, canopies, and other shading structures (Li et al., 2023; Siqi et al., 2023).

Though the efficiency of shading is well documented along with the ways to achieve it, designing thermally comfortable street spaces remains an adaptive challenge in urban design and microclimate studies. Building upon the previous part of this study on PTC, which established thermal comfort thresholds (Mohite & Surawar, 2024a) and utilized machine learning for evaluation of the thermal comfort index - modified Physiological Equivalent Temperature (mPET) (Mohite & Surawar, 2024b). This study aims to assess street geometry and shading strategies to determine configurations that provide the highest thermal benefits. The following background study examines the roles of street geometry and vegetation in shaping the urban microclimate.

Background Study

Impact of street geometry on microclimate and pedestrian thermal comfort

Street geometry is mainly quantified through parameters such as sky view factor (SVF), aspect ratio (AR), street orientation, building typology, and vegetation, etc. (Achour-Younsi & Kharrat, 2016b; Albdour & Baranyai, 2019). These parameters regulate the degree of street

shading and influence microclimate conditions, particularly mean radiant temperature (Tmrt), surface temperature, and airflow patterns (Aicha et al., 2022; Bourbia & Awbi, 2004). The studies on PTC in urban canyons are categorized into two categories. The first category focuses on urban geometry parameters such as AR and street orientation and aims to optimize different building heights with orientation to determine which urban geometry combination reduces thermal stress (Chen et al., 2012; Y. Zhang et al., 2017). The second type of study focuses on optimizing thermal comfort using different types of vegetation, their placement, and other factors (Sayad et al., 2021; Segura et al., 2022).

Street geometry plays an important role in controlling the amount of solar radiation received and reradiated by urban structures. In an urban canyon, the surface temperatures of nearby buildings and the heat they transfer to the air significantly affect the air temperature (Ta). This influence is largely determined by the presence or absence of direct solar exposure.

Sky View Factor

Sky View Factors (SVF) indicate the proportion of the visible sky at a particular location. It is a ratio of the radiation received at a given point to the overall radiation in the hemispheric area surrounding that point (Johnson & Watson, 1984). This ratio ranges from 0 to 1, where 0 indicates a completely obstructed sky, and 1 denotes a completely clear sky. The SVF is crucial in influencing PTC in urban environments. Studies have shown that modifications in SVF can significantly impact outdoor thermal comfort (Arif & Yola, 2022; Ratnayake et al., 2022). Higher SVF values, indicating a more visible sky area, are associated with a high thermal comfort index value and vice versa (Aicha et al., 2022). SVF modifications through urban vegetation, such as street trees, have been identified as effective strategies to enhance PTC, especially in warm and humid climates (Ratnayake et al., 2022). Additionally, SVF is significantly correlated with thermal comfort parameters like Tmrt, emphasizing its importance in creating comfortable outdoor spaces for pedestrians. In a study in the warm and humid context of Colombo, Sri Lanka, the correlation between the SVF modifications and outdoor thermal comfort was analyzed in the context of street tree planting, and it was identified that trees modifying SVF enhance daytime thermal comfort for pedestrians significantly (Ratnayake et al., 2022). Similarly, in a study in the tropical climate of Singapore and India, SVF was identified as a major factor influencing thermal comfort, particularly on E-W-oriented streets (Xu et al., 2023).

Street orientation and Aspect Ratio

Aspect ratio (AR) is the ratio between the canyon walls' average height (H) and width (W). Studies have shown that the AR and orientation of streets significantly impact thermal comfort in urban environments (Chatzidimitriou & Yannas, 2017; Lobaccaro et al., 2019). Abdollahzadeh & Biloria (2021) found that among four design factors, street orientation is the most influential (46.42%), followed by AR (30.59%). According to Sharmin & Steemers (2013) N–S streets have a lower Tmrt than E–W streets, and the thermal comfort index physiological equivalent temperature (PET) is mostly influenced by shade availability. Srivanit & Jareemit (2019) observed that an N–S-oriented canyon has the lowest Tmrt, followed by NW–SE- and NE–SW-oriented canyons, and the worst situation is in the E–W canyon. Raising H/W also considerably reduces Tmrt in all canyon orientations except E–W. Also, Achour-Younsi & Kharrat (2016a) found that the N–S streets with the highest AR ratio have the most comfortable values, and those with E–W orientation are the least pleasant. In Egypt, an AR of 2.5 was found to provide the best thermal conditions in both Alexandria and Aswan (Abdelhafez et al., 2022). In a study in Malaysia, it was observed that asymmetrical streets with an AR of 0.8–2 reduce morning microclimate and night heat islands, and an AR

of 2-0.8 reduces surface temperature by 10-14°C (Qaid & Ossen, 2015). Similarly, a study in Kolkata, India, observed that the AR of 2.5 reduces the thermal comfort index value (PET) by 5-9°C, and the orientation angle of 30-60° with wind direction improves the microclimate (De & Mukherjee, 2018). Furthermore, studies in Saudi Arabia emphasized the importance of multi-asymmetrical aspect ratios in improving urban pedestrian microclimates, with a gradual increase in ARs leading to reduced air temperatures and increased wind velocities (Abdelhafez et al., 2022).

Building typology

The building typology (BT) refers to how compactly the buildings are placed along the street; thus, it is categorized as linear, where there is no gap between adjacent buildings; singular, where there are appropriate setbacks between buildings; and scattered, where the buildings are placed far from each other. It governs microclimate by solar permeability, heat-trapping, and wind flow throughout the length of a street (Albdour & Baranyai, 2019). Zhang et al. (2022) indicated that the microclimate clearly differed with variations in building arrangement and enclosure. The building typology for each side of the street is determined using the Building Surface Area Fraction (BSF). BSF is a portion of the sidewalk with a building adjacent to it (Kotharkar et al., 2023).

$$\text{BSF} = \frac{\text{Length of total building surface facing the street}}{\text{Total length of sidewalk}} \qquad \text{(Equation 1)}$$

Impact of shading intervention on microclimate and pedestrian thermal comfort

Vegetation

Vegetation, primarily trees helps to cool the surrounding air as their canopy blocks radiation and evapotranspiration, where the water released from leaves absorbs heat from air (Armson et al., 2012; Konarska et al., 2016). Trees alter the microclimate by changing the amount of solar and terrestrial radiation received on the ground through shading (Speak et al., 2020). Most of these studies reported that the cooling capacity of the trees depends mainly on the canopy coverage and planting density, etc. (Raman et al., 2021). A study in the tropical city of Bangalore, India, showed that street segments with trees recorded lower ambient air temperature by 5.6 °C on average (Vailshery et al., 2013). Field measurements in the hot-humid climate of Singapore showed a temperature difference of 1.5–2.8 °C between tree canopies and surrounding areas (Lindberg & Grimmond, 2011). Similarly, a study in Roorkee highlights the role of green-blue infrastructure, particularly the combination of low sky-view factor (SVF), dense canopy trees, and proximity to water, in reducing heat stress (Manavvi & Milosevic, 2025).

Artificial Shading Structures

Artificial shading is created by permanent built structures such as arcades, awnings, and pedestrian canopies. This approach offers a controllable solution that can be precisely designed to match specific street geometry. Its cooling mechanism relies solely on blocking solar radiation; unlike vegetation, it does not provide additional cooling through evapotranspiration. In Cairo, overhead shading improved thermal comfort by up to 2.3°C on the PET scale (Galal et al., 2020). Field studies in Arizona reported that pedestrian comfort under canopies was perceived to be equal to comfort under tree shade, highlighting that blocking radiation is the primary factor (Middel et al., 2016).

Therefore, achieving optimal PTC requires the strategic integration of shading design with urban geometry. While prior research mentioned above has established the importance of

individual parameters, their synergistic combination through specific shading strategies is critical. This study addresses this necessity by evaluating the effectiveness of various shading strategies across different street geometric combinations.

Methodology

This study aims to determine street geometry and shading strategies to identify configurations that provide the highest thermal benefits in an urban street on hot summer days through ENVI-met simulation. The methodology consists of four integrated phases: (1) field data collection and model validation; (2) generation and simulation of urban canyon scenarios combining key geometric and shading variables; (3) evaluation of the modified Physiological Equivalent Temperature (mPET) index using a pre-trained machine learning model; and (4) comparative analysis to rank scenario performance. This combinatorial approach is used to provide design guidance based on descriptive analysis.

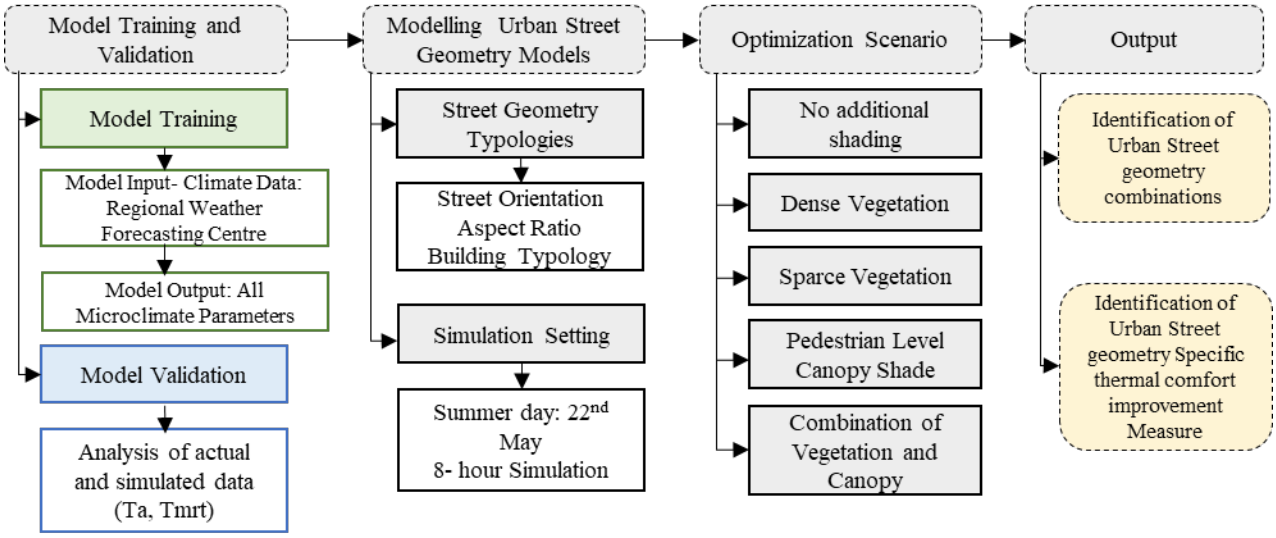

Figure 1. Proposed methodology for the study

Study area

The study area is located in Nagpur City. It is the winter capital of Maharashtra state, situated in central India (21.1458° N, 79.0882° E). It is characterized by a tropical savannah (Aw) type of climate as per Koppen climate classification. Nagpur is known for extreme annual temperature variability, with recorded lows of 4°C in winter (December-February) and highs reaching 48°C during the summer (March-May). May is the hottest month with an average maximum air temperature of about 42°C. These hot summers frequently feature severe, city-wide heatwaves (ICLEI, 2021). The selection of New Shukrawari Street in Nagpur as a case study is based on the following criteria: Mixed land use on the street and in the neighbourhood, availability of a metro station for better connectivity, and availability of pedestrian sidewalks on both sides of the street. The street was 20 m wide and 1000 m in length, the average AR on the street was 0.8, and the SVF was 0.65.

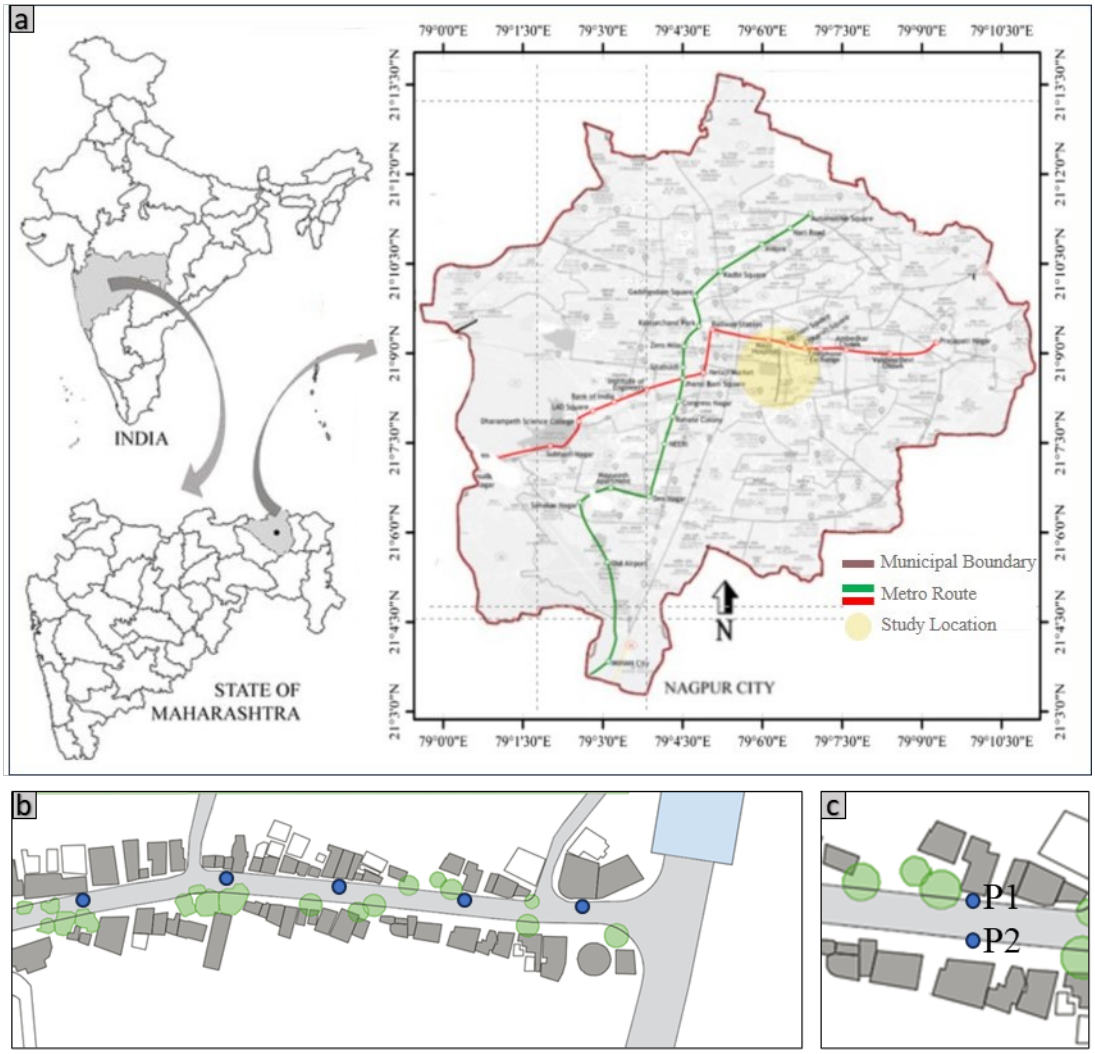

Figure 1. a. Location of Nagpur city with the studied location (Source: Meshram, 2011), b. Studied location: New Shukrawari Street, c. Points studied for validation.

Data collection and analysis

The field survey was conducted on May 22, 2022, under typical summer conditions, i.e., hot sunny days and cloudless. The data collection includes mapping of both street geometry and microclimate data. The microclimatic parameters (Ta, Rh, Ws) were measured at 1.2 m above the ground level, as it's the center of gravity of a standing human (ISO 1998). The data were collected at four different time slots between 09:00 and 18:00. To collect data, the street was divided into a grid of 100 m, and the data was collected on both sides of the street. The microclimate data was collected using MS6252B digital anemometer (Ta, Rh, Ws) and Lazer IR thermal gun (Ts). The street geometry data was collected using a Nikon DSLR with a fish-eye lens. The field data was then evaluated for Tmrt and mPET index using RayMan pro tool (Matzarakis, 2009). The mPET enhances accuracy of thermal comfort assessment by considering thermo-physiological parameters of the human body and climatic factors. Unlike other indices, mPET incorporates a multi-node heat transport model and a self-adapting multi-layer clothing model, providing a more realistic analysis of the impact of climate on humans (Pecelj et al., 2021). This particular index is used and validated in previous part of this study (Mohite & Surawar, 2024c). RayMan requires all microclimate parameters along

with the fish eye lens image as input. The microclimate data and mPET values of the studied street are given in Table 1.

Table 1. Observed Values of Microclimate and thermal comfort index -mPET

Location	Time		Ta	Ts	RH	Ws	MRT	mPET
New Shukrawari Street	9 am-10 am	East	37.4°C	40.7°C	32.64%	0.91m/s	54.7°C	38.9
		West	38.1°C	45.8°C	32.07%	0.62m/s	58.9°C	40.6
	11.30 am - 12.30 pm	East	42.9°C	57.3°C	24.68%	0.7m/s	57.5°C	42.3
		West	42.9°C	57.2°C	24.84%	0.67m/s	61.4°C	43.3
	2.30 pm - 3.30 pm	East	41.7°C	56.4°C	25.7%	1.64m/s	64.5°C	44.1
		West	41.3°C	54.1°C	25.7%	1.04m/s	59.6°C	42.5
	5 pm-6 pm	East	38.9°C	52.5°C	24.6%	1.04m/s	53.0°C	41.2
		West	40.0°C	49.4°C	25.2%	1.19m/s	47.15°C	38.0

Simulation setting and model validation

ENVI-met 5.6.1 microclimate modeling software is used to simulate three-dimensional surface–air interaction representing the proposed scenarios in the study (Fig. 3a). This simulation method was previously used in various microclimate studies and has shown the credibility of the ENVI-met model. For instance, Ma et al. (2020) reported a slight variation between simulated and measured values of Ta, with R^2 values ranging from 0.76 to 0.98. Galal et al. (2020) found that the simulated Ta closely matched the measured diurnal temperature, achieving an index of agreement (IA) ranging from 0.96 to 0.98. Elnabawi et al. (2013) demonstrated a strong correlation for the anticipated mean radiant temperature (Tmrt) up to sunset (6:00 PM).

In this study, the model was validated by simulating the partial area of the surveyed street. Two measurement points were selected (P1 and P2) to simulate the model using local weather station data of May 2022 and record the model output for microclimatic (Ta, Ts, Tmrt) and urban geometry parameters (SVF) (Fig. 2). Ta and Tmrt play a major role in determining the performance of the accuracy analysis. The simulation process was run on May 22, 2022, on a typical hot day of the hottest summer month. May is the month with the most sunshine, with 11.8 hours of sunshine per day, and it has maximum Ta and Tmrt. During this month, Nagpur City has experienced heatwaves for the past 30 years, as per IMD data (Surawar et al., 2017). The simulation began at 10:00 a.m. since the morning hours of summer days stimulate a slight warm-to-warm thermal sensation (Mohite & Surawar, 2024a).The simulations were run for 8 hours until sunset to assess the data. The simulated weather data were obtained from the Regional Weather Forecasting Centre in Sonegaon, Nagpur. The mean values of Ta, RH and Va were utilized as input parameters for the ENVI-met simulation model. The models examined via ENVI-met had 50 × 50 × 40 grid units with a suitable resolution of 1 × 2 × 2 m grid. The input data for materials, vegetation, and microclimate is given in the table. Results are extracted for a height of 1.2 m (K=5) on the sidewalk, representing a standing person to evaluate the comfort degree for outdoor space users (Fig. 3b).

ENVI-met Model

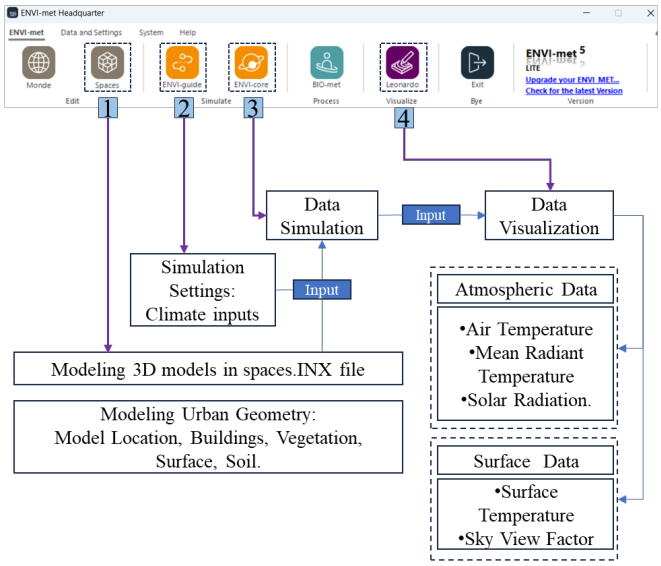

ENVI-met Model: Simulation Settings

Location	Nagpur, Maharashtra, India
Geographical Location	21.1458° N, 79.0882° E
Climate Type	Tropical savannah (AW)
Total Simulation Duration	8 hours
Spatial resolution	1m X 2m X 1m
Model Dimension (Number of grid cell)	X = 50, Y= 50, Z= 40
Date	22nd May, 2022
Building Material	Concrete Wall
Sidewalk Material	Concrete pavement Light
Vegetation Specification	
Type	Evergreen tree
Tree Height	6m
Crown Width	6m
Basic Meteorological Inputs	
Wind Speed	2.8 m/s
Wind Direction	295°C
Air temperature for 24h	Simple Forcing
Relative Humidity for 24h	Simple Forcing
Maximum air temperature	42°C
Minimum air temperature	30°C
Maximum relative humidity	48°C
Minimum relative humidity	22°C
Sky Condition	Clear Sky

Figure 2. ENVI-met model (a) and Simulation Setting (b)

In order to evaluate the performance of the model, various statistical parameters were used in the calibration of the observed (O) and predicted (P) data. These statistical parameters include the agreement index (d), the coefficient of determination (R^2), mean bias error (MBE), and mean absolute error (MAE). This agreement index method, developed by Willmott in 1982, uses a specific formula for analysis (Willmott, 1982). The agreement index (d) is a descriptive measure indicating the extent to which the simulated values are free from error, ranging from 0 to 1. A value of 1 signifies perfect agreement, meaning the simulated values (s) are identical to the observed values (o). As the first indicator, the agreement index (d) ranges from 0 to 1, with values closer to 1 indicating higher accuracy. The higher coefficient of determination (R^2) value represents that the differences between the observed data (O) and the predicted data (P) are smaller and unbiased. The mean bias error (MBE) shows whether the values from the model are higher or lower than the observed data. The mean absolute error (MAE) is the same as the MBE indicator but takes into account the absolute difference between predicted and observed values (Battista et al., 2023). The MBE/MAE value must be between 0 and 1. If this value is 1 or close to 1, it shows the accuracy of the model.

These statistical parameters are calculated using the following equations:

$$d = 1 - \frac{(\sum_{i=1}^{n}(O_i - P_i)^2)}{(\sum_{i=1}^{n}(|P_i - \bar{O}| + |O_i - \bar{O}|)^2)} \quad ,0 \leq d \leq 1 \qquad \text{(Equation 2)}$$

$$\mathrm{MAE} = (1/n) \times \sum_{i=1}^{n}|O_i - P_i| \qquad \text{(Equation 3)}$$

$$MBE = (1/n) \times \sum_{i=1}^{n}(P_i - O_i) \qquad \text{(Equation 4)}$$

Where,
d: Index of agreement
MAE: Mean absolute error

MBE: Mean bias error
ND: Number of analysed data
Ō: Mean of the observed variable
Oj: Observed variables for each instant j
Pj: Model-predicted variables for each instant j

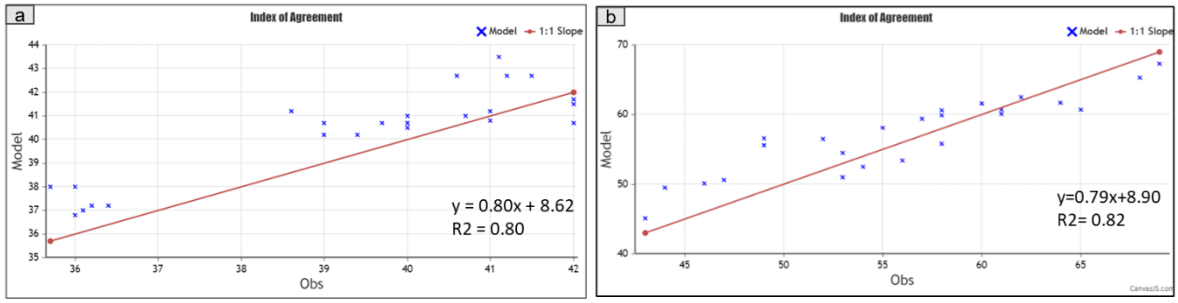

Figure 3. Results of model validation using the Index of Agreement (a) Air Temperature (b) Mean radiant temperature

The observed (O) and the predicted (P) values indicate the coefficient of determination (R^2) for Ta is 0.80, and R^2 for Tmrt is 0.82. In the analyses, the R^2 is very close to 1, which shows that they are statistically significant. In addition, the fit index (d) was determined as 0.85 for Ta and 0.89 for Tmrt (Fig. 4). The MBE and MAE for Ta are 0.92 and 1.44, respectively, whereas for Tmrt they are 0.73 and 1.02. These results show that the software has been well verified and the work can be run with these software outputs.

Modelling Street Geometry and Proposed Scenarios

The proposed scenarios are identified considering the primary factor affecting PTC: solar exposure. To reduce solar exposure on the pedestrian level, natural and artificial shading strategies are considered, which include shading through buildings, vegetation, pedestrian canopy, and a combination of vegetation and canopy. The study has considered two orientations (N-S and E-W), three ARs (shallow, uniform, and deep), and three building typologies (singular, linear, and scattered) for simulation. The ARs considered in this research are consistent with the prior part of the research (Mohite & Surawar, 2024c), with the primary considerations such as: if AR of a street canyon is below 0.5, the canyon is considered shallow, if it is approximately equal to 1, the canyon is considered uniform; and if the AR is equal to or more than 2, the canyon is considered deep, being maintained. The considered setbacks between adjacent buildings vary with building typologies, ranging from no setback for linear buildings to 4M in singular buildings and 14M in scattered buildings. The building length is 20 m; these considerations are based on the studied streets in the prior part of the research. The scenarios were designed by permuting three geometric factors and five shading strategies, resulting in 90 combinations (2 Orientations × 3 Aspect Ratios × 3 Building Typologies × 5 Shading Strategies) that are considered for simulation in ENVI-met (Fig. 5 and 7).

a. Singular building typology with H/W of (shallow, uniform, and deep), two street orientations (N–S, E–W), and five mitigation scenarios (models 1 to 30);

b. Linear building typology with H/W of (shallow, uniform, and deep), and two street orientations (N–S), and five mitigation scenarios (models 31 to 60);

c. Scattered building typology with H/W of (shallow, uniform, and deep) and two street orientations (N–S), and five mitigation scenarios (models 61 to 90).

The building material was specified as concrete, reflecting common construction in Nagpur, with an albedo of 0.3. Vegetation was modeled using the evergreen tree profile within ENVI-met, with a height and crown width of 6m. Canopies were modeled as horizontal planes at 3m height.

For all scenario simulations, a consistent protocol was followed to ensure comparability. Each of the 90 scenarios was simulated for 8 hours, considering climate of May 22, 2022 (10:00 a.m.–6:00 p.m.). Microclimate data for PTC analysis was extracted for every hour and the average for entire period was considered for comparison. To ensure data representativeness, output parameters (microclimate data) were extracted at 1.2 m height for ten receptor points per sidewalk (points were positioned at 10m intervals on either side), and then average was considered (Fig. 6).

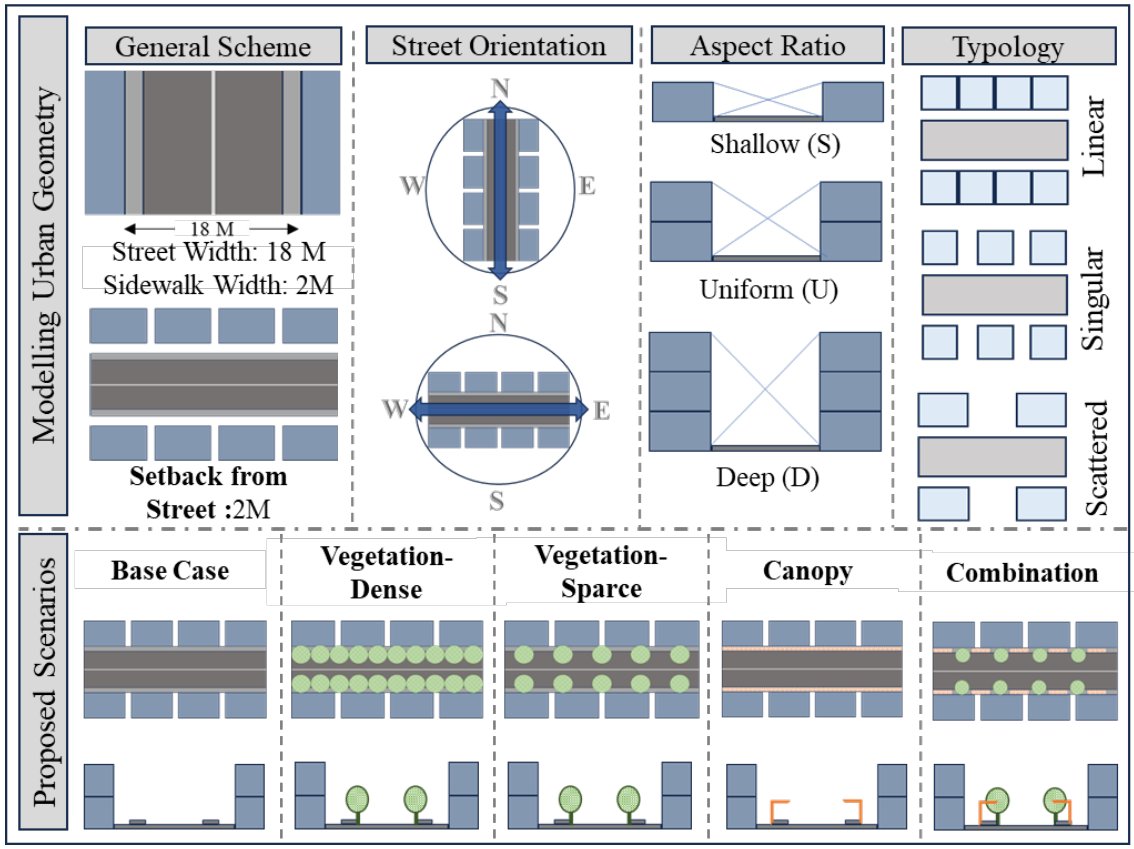

Figure 4. Proposed urban street geometry and shading strategies for the study

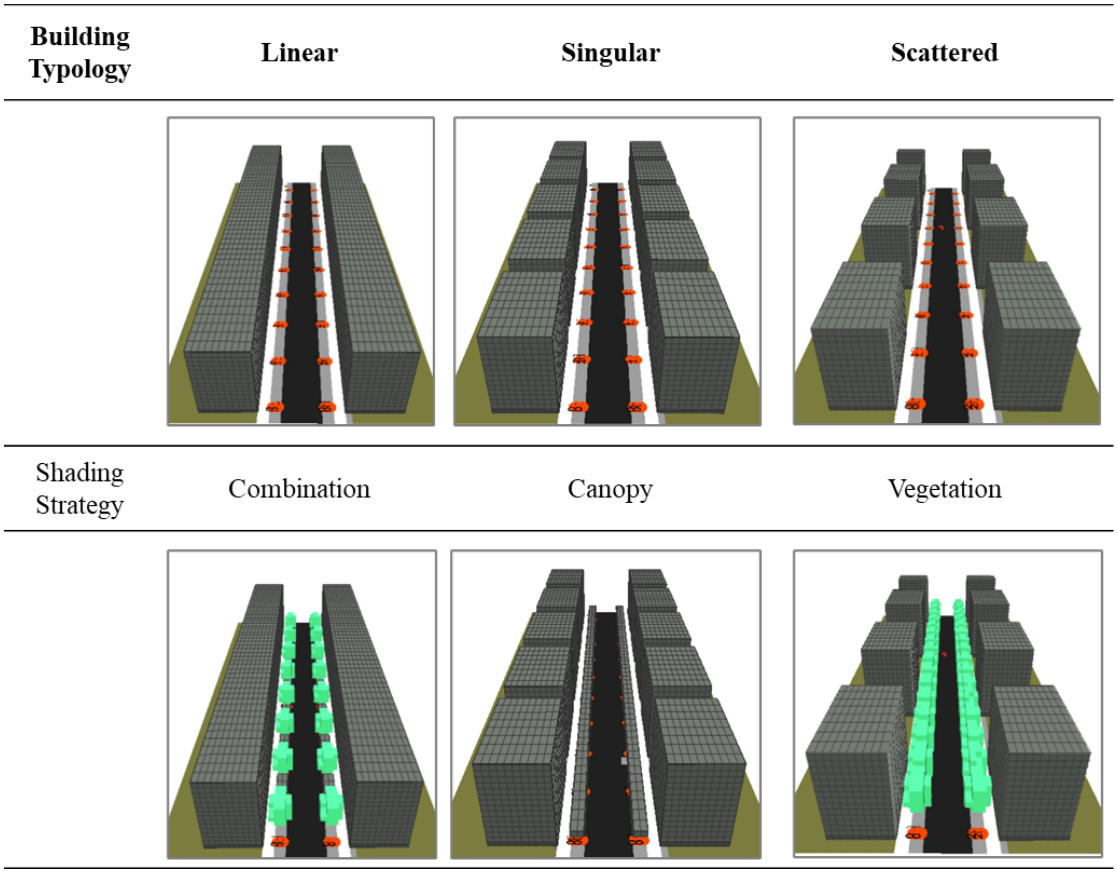

Figure 5. The Representative space setting input files of the ENVI-met 3D model: a) Base case with three building typologies; b) three representative shading strategies- vegetation, canopy and combination

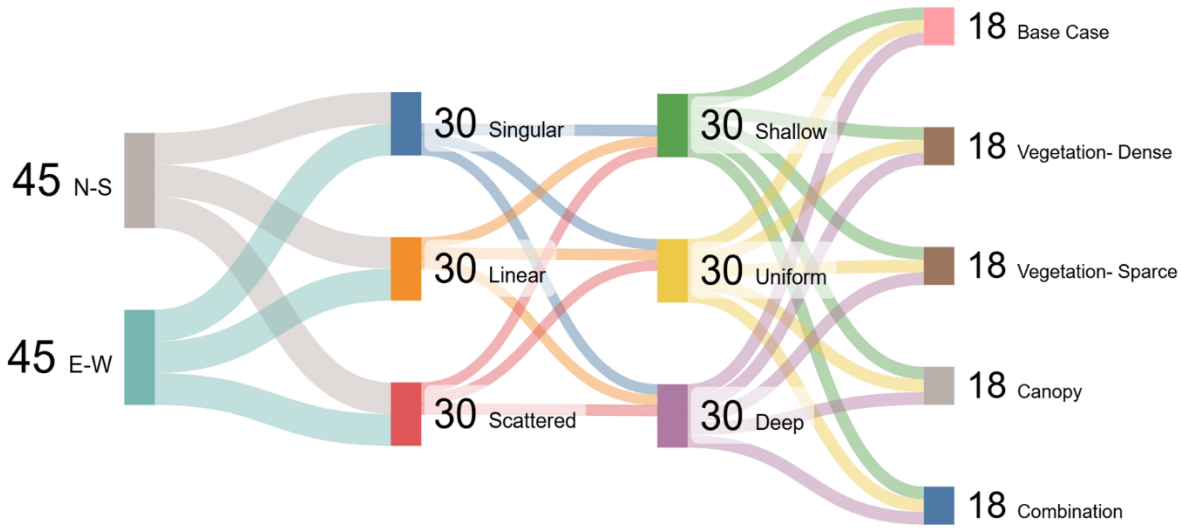

Figure 6. Designed combinations of urban street geometry and shading strategies

Evaluation of mPET values

In the previous part of this study, a machine learning model was developed using Random Forest (RF) algorithm for assessing and predicting PTC. The model was trained using urban geometry and microclimate data (Mohite & Surawar, 2024b). The model was validated for unseen data and showed a high level of accuracy ($R^2 > 0.90$ at training phase and $R^2 > 0.80$ at prediction phase, low mean squared error values - overall MSE < 1.4). Thus, in this study, the pre-trained RF model was used to evaluate mPET alongside of the street, using the microclimate parameters from the simulated model. The model utilizes simulated hourly values of Ta and solar radiation from ENVI-met outputs, along with the predefined SVF and AR for each scenario, were given as input into this model to generate corresponding mPET values at the receptor points (Fig. 1). These mPET values are then used for analyzing the influence of urban geometry and shading strategies.

Results

Influence of Aspect Ratio and Street Orientation

The AR is essential in shaping PTC by influencing solar exposure, shading, and wind movement within urban streets. The effects vary significantly depending on the street orientation. Shallow street canyons, characterized by an AR of 0.5 or lower, exhibit poor shading due to their low building heights relative to street width. In N-S-oriented shallow streets, maximum exposure to solar radiation leads to mPET values ranging between 36.9°C and 42.9°C. Similarly, Shallow E-W streets experienced the highest mPET values, ranging from 37.9°C to 43.9°C.

Uniform street canyons, with an AR close to 1.0, offered better thermal comfort than shallow canyons. In N-S oriented uniform streets, mPET values ranged from 34.1°C to 41.4°C, representing a reduction of 2–3°C compared to shallow N-S streets. In E-W uniform streets, mPET values drop by 1-2°C compared to their shallow counterparts, ranging from 35.1°C to 43.3°C. However, persistent solar exposure in E-W orientations keeps thermal conditions in the "hot" to "very hot" range on the mPET index, highlighting the limitations of this orientation despite improved AR.

Deep street canyons, with an AR of 1.2 or higher, offer the most significant improvements in thermal comfort by maximizing shading. N-S-oriented deep AR streets achieve the lowest mPET values, ranging from 33.1°C to 40.1°C. On-E-W-oriented street as increased building heights provided marginal improvements, with mPET values ranging from 35.8°C to 43.2°C.

The interaction between AR and street orientation is essential in determining thermal comfort. Shallow canyons, particularly in E-W orientations, perform poorly, leading to mPET increases of up to 3-4°C compared to deep canyons. Uniform canyons provide moderate improvement, especially in N-S orientations, though E-W orientations still experience thermal stress. Deep canyons offer the best thermal performance, particularly in N-S orientations, where mPET values are significantly lower. However, E-W deep canyons remain thermally challenging due to persistent solar exposure (Fig. 7).

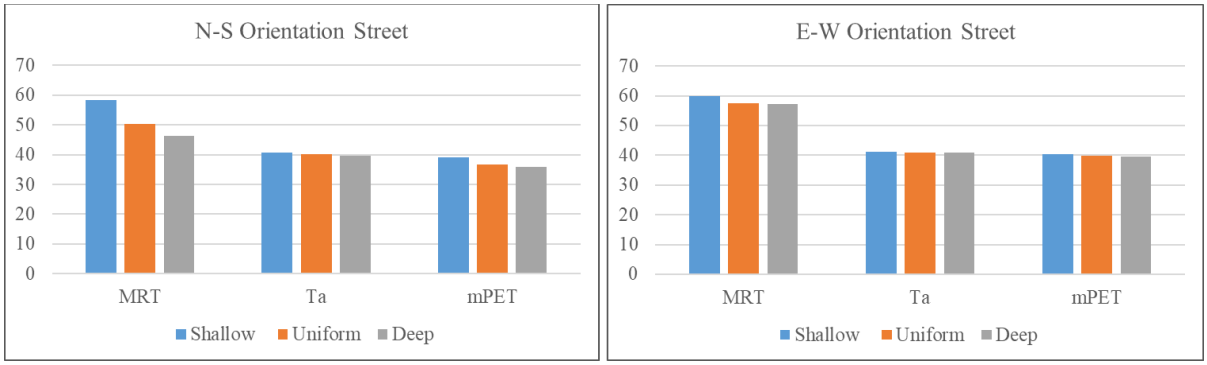

Figure 7. Influence of Aspect Ratio and Street Orientation on Microclimate and mPET Index

Influence of Building Typology on Thermal Comfort

The BSF for each building typology was evaluated using Equation 1. The linear typology depicts dense building typology having no gaps in buildings; these typologies have a BSF value of 1; the singular typology has minimum setbacks between buildings and has a BSF value of 0.84. The scattered typology has high gaps between buildings, leading to a BSF value of 0.57.

N-S Orientation

For N-S-oriented streets, the linear typology (BT2) remains the best performer across all scenarios, as minimum Ta (39.7°C) and Tmrt (48.5°C) were observed. This typology has the highest BSF values, creating continuous street canyons that limit solar penetration and maintain consistent shading on the southern side of the street throughout the day. The singular typology (BT1) shows higher Tmrt (50.8°C) and Ta (40.15°C) values than linear typologies. The scattered typology (BT3) performs worst for N-S streets, primarily due to the large setbacks between buildings, leading to low BSF values. These open spaces allow for continued solar exposure, leading to increased Tmrt values (56.2°C) and increased Ta (41.8°C) (Fig. 8a).

E-W Orientation

For E-W-oriented streets, solar exposure and its impact on Tmrt are more pronounced due to their alignment with the sun's path. The singular typology (BT1) is the most thermally favorable option, with reduced Tmrt (56.2°C) and Ta (40.8°C) values compared to other typologies. The linear typology (BT2) also performs better, with slightly higher Tmrt (57°C) and Ta values (40°C) compared to singular typologies. The scattered typology (BT3) exhibits maximum mPET values in E-W streets. The large setbacks exacerbate solar exposure, leading to the highest Tmrt (58.5°C) and Ta (58.5°C) values across all typologies (Fig. 8b).

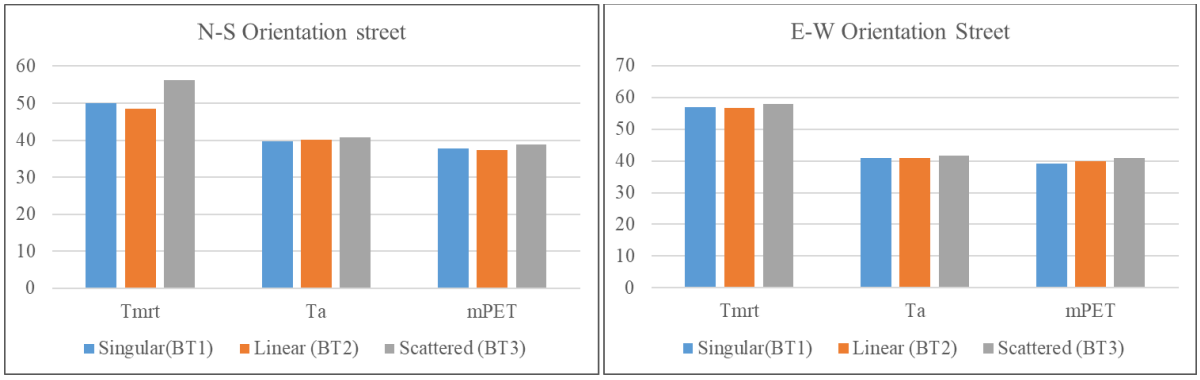

Figure 8. Influence of Building Typology on Microclimate Parameters and mPET index- (a: N-S-Orientation Street, b: E-W-Orientation Street)

Proposed Shading Scenario

The thermal performance analysis on two different street orientations reveals distinct variations in outdoor thermal comfort due to differences in solar exposure and urban configurations.

N-S oriented streets

In the base case scenario, where there was no vegetation or canopy, street geometry heavily influenced the thermal environment. For singular building typologies, mPET values ranged from 38.28°C on the west-facing sidewalk in deep AR to 41.5°C on the east-facing sidewalk in shallow AR. For Linear typologies, on the other hand, displayed mPET values ranging between 37.8°C (west-facing sidewalk) and 42.2°C (east-facing sidewalk). Scattered typologies recorded the highest mPET values, with all AR configurations reaching up to 42.9°C.

The sparse vegetation (4m apart) provides minor cooling benefits. For singular building typologies, the mPET was reduced to 37.28°C on the west-facing sidewalk in deep AR and 41.3°C on the east-facing sidewalk in shallow and deep AR. Linear typologies experienced slightly better thermal performance, with mPET ranging from 36.7°C to 41.0°C. Scattered typologies showed a slight reduction in mPET, ranging from 37.9°C to 41.5°C. Dense vegetation shows significant improvement in thermal comfort across all typologies, particularly in deep AR. In singular building typologies, the mPET reduced further to 34.2°C on the west-facing sidewalk of deep AR and 39.9°C on the east-facing sidewalk of shallow AR. Similarly, in linear typologies, mPET values ranged from 34.9°C to 40.3°C, with deep AR benefiting the most from dense vegetation's shading and cooling-enhancing effects. For scattered typologies, while dense vegetation led to mPET reductions ranging from 36.9°C to 40.6°C, the irregular shading distribution limited its potential to create uniform cooling.

The canopy shading shows improved values of mPET in all AR's. For singular building typologies, mPET decreased to 34.2°C on the west-facing sidewalks of deep ARs and 38.4°C on the east side of shallow layouts. Canopies provided consistent shading and effectively blocks direct sunlight. Linear typologies benefited the most, with mPET values ranging from 33.1°C to 38.2°C. Scattered typologies, while benefiting from canopies, recorded slightly higher mPET values ranging between 35.5°C and 38.6°C due to the irregular shading distribution.

The combination of vegetation and canopies proved to be an effective strategy for improving thermal comfort in N-S-oriented streets. For singular building typologies, the mPET decreased to 34.28°C in deep layouts and 39.94°C in shallow ARs. Linear typologies

exhibited consistent cooling benefits, with mPET values ranging from 33.8°C to 39.3°C, as the combination of vegetation and canopies ensured even shading and reduced heat accumulation. Scattered typologies displayed improvements with mPET ranging from 36.3°C to 40.1°C, but they still lagged slightly behind singular and linear typologies (Fig. 9).

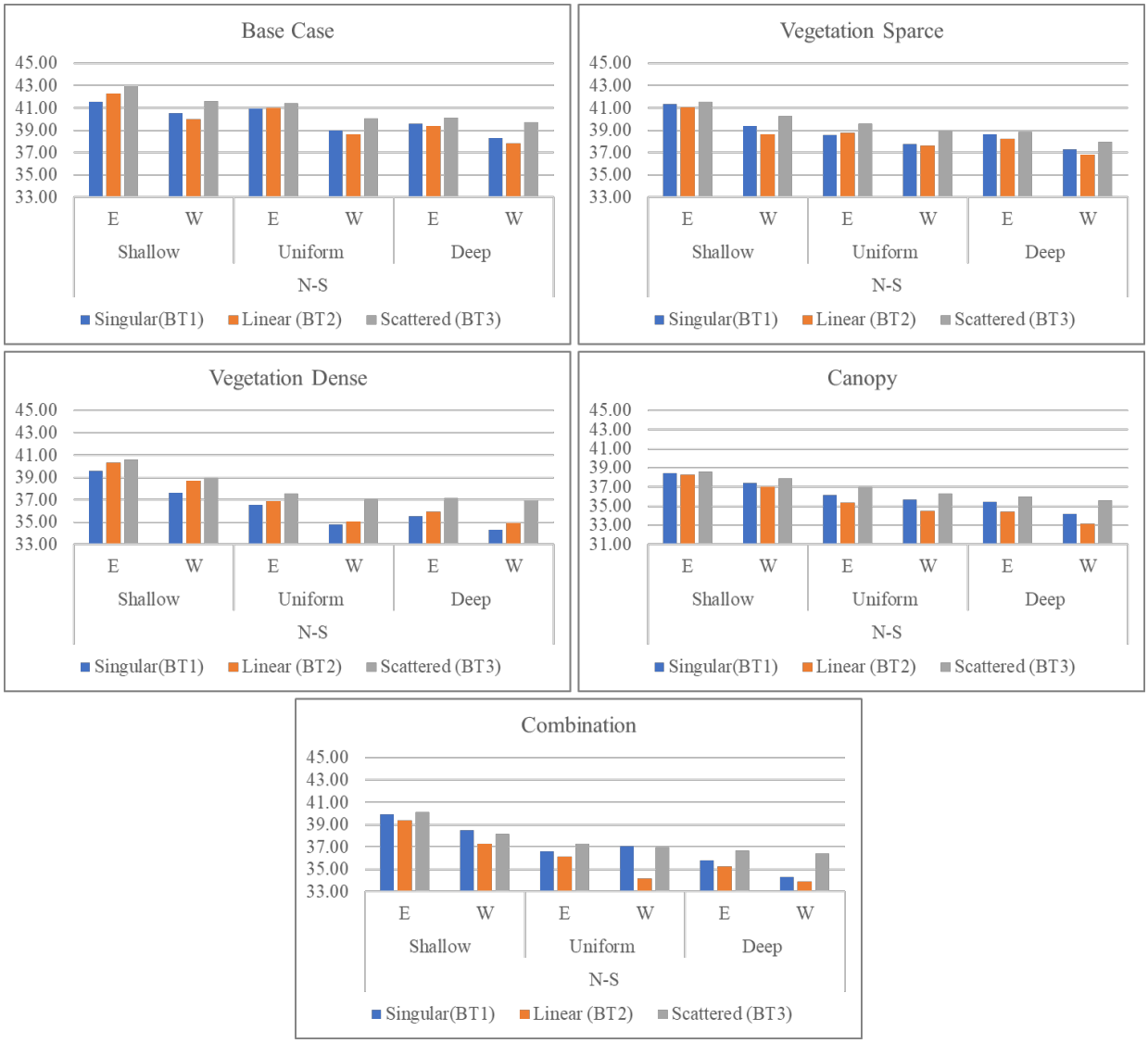

Figure 9. Comparison of Effect of no-shade and shading strategies on mPET on N-S-Orientation Street

E-W streets

For E-W-oriented streets, mPET was significantly influenced by building typology and shading interventions, and side of the street. In the base case scenario, the mPET values reflected the direct impact of the sun's trajectory. For singular building typologies, mPET values ranged from 43.40°C on the shallow north-facing sidewalk to 41.9°C on the deep south-facing sidewalk. The north-facing sidewalk consistently exhibited higher mPET values (43.2°C), while the south-facing sidewalk had relatively lower values (42.5°C). The linear typology (BT2) demonstrates mPET values varying between 43.9°C on the north-facing sidewalk and 42.5°C on the south-facing sidewalk. Scattered typologies recorded the highest

mPET values, ranging from 43.2°C south-facing sidewalk to 44°C on a north-facing sidewalk, especially in shallow and uniform configurations.

With sparse vegetation, the result shows a slight reduction in mPET values. For the singular typology (BT1), mPET decreases by approximately 2.5°C to 3°C, ranging between 40.8°C on the south- facing sidewalk of deep AR and 40.12°C on the north-facing sidewalk of shallow AR. The linear typology (BT2) achieves a reduction of around 2°C to 3°C, ranging from 42.2°C to 40.3°C. The scattered typology (BT3) exhibits similar reduction, ranging between 42.7°C and 40.7°C.

Dense vegetation considerably improves thermal comfort in E-W streets. In singular building typologies, mPET values further decreased to 38.97°C on the south side of deep AR and 38°C on the north side of shallow AR. Similarly, the linear typology (BT2) records temperatures between 40.4°C and 38.4°C, while the scattered typology (BT3) registers values ranging from 40.9°C to 38.7°C. The overall reduction is approximately 4°C to 5°C compared to the base case scenario.

With the canopy shading scenario, the singular typology (BT1) records the lowest mPET values, ranging from 37.6°C to 35.04°C, achieving a reduction of approximately 6°C to 7°C compared to the base case. The linear typology (BT2) ranged from 38.6°C to 36.3°C, while the scattered typology (BT3) records values between 38.3°C and 37.2°C.

The combination of vegetation and canopies emerged as an effective strategy for mitigating heat stress in E-W streets. It significantly reduces mPET values across both south- and north-facing sidewalks. The singular typology (BT1) records mPET values ranging from 38.4°C to 38.1°C, indicating reductions of over 5°C to 7°C compared to the base case. Similarly, the linear typology (BT2) ranged between 40.1°C and 38.3°C, while the scattered typology (BT3) records values ranging from 39.8°C to 38.9°C (Fig. 10).

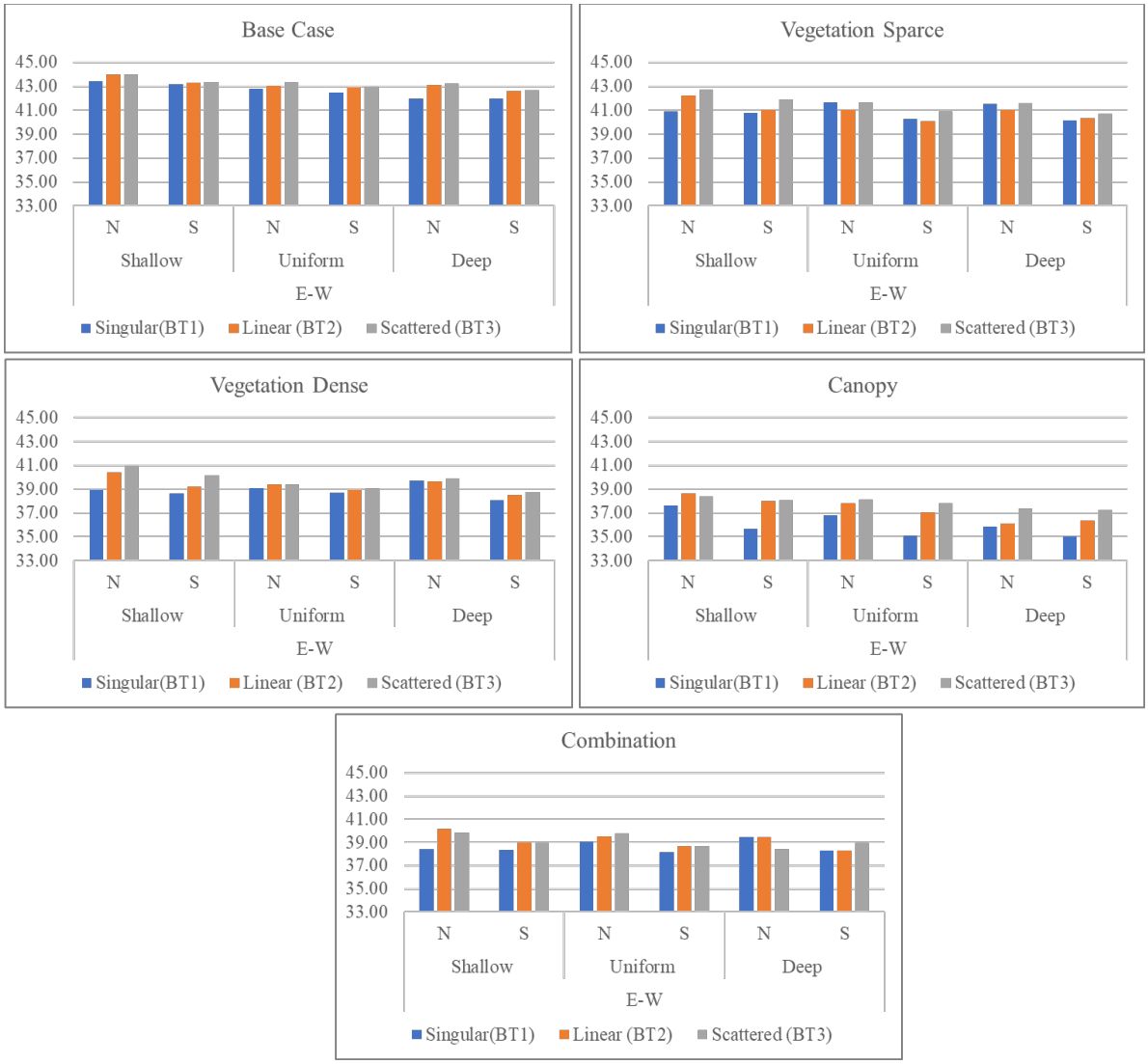

Figure 10. Comparison of the Effect of No-Shade (base case) and Shading Strategies on mPET on E-W-Orientation Street

Identification of Street-Specific Shading Strategies

The comprehensive analysis of ENVI-met results for all 90 scenarios provided critical insights into the effectiveness of various shading strategies in enhancing thermal comfort on urban streets. Each strategy provided a different level of thermal comfort improvement; thus, each strategy was evaluated using a detailed rating system. The mPET values are categorized into ratings based on the accepted thermal comfort range for summer, identified earlier in the study as 24.1°C–36.8°C (Mohite & Surawar, 2024a). The observed thermal comfort ranges from this study were then divided into 5 equal categories. Ratings 4 and 5 fall within this thermal comfort range, while ratings 1, 2, and 3 represent increasingly warmer conditions beyond the comfort zone. The rating categories are as follows:

Table 2. Categorization of mPET Values into Thermal Comfort Ratings

Rating	mPET Range (°C)	Range of Thermal perception as per mPET
5	33.8–35.82	Slightly warm - warm
4	35.82–37.84	Warm
3	37.84–39.86	Hot
2	39.86–41.88	Hot
1	41.88–43.9	Very Hot

Source: Matzarakis & Mayer, 1996; Lin & Matzarakis, 2008; Mohite & Surawar, 2024a

The evaluation accounted for variations in street orientation, AR, and BT, providing an understanding of the performance of shading strategies under diverse urban conditions, as illustrated in Table 3.

In N-S-oriented streets, vegetation and canopy shading consistently performed better. In contrast, on E-W-oriented streets, canopy shading was more effective due to its ability to block direct solar radiation as the sun travels along its path. The effectiveness of dense vegetation in N-S streets varied, with ratings typically between 2 and 5 and often achieving ratings of 4 and 5. This higher efficiency was particularly noted in streets with higher AR values and compact building typologies, where the interaction between urban geometry and greenery maximized shade coverage. For E-W streets, dense vegetation is effective, with scores ranging from 2 to 3. This reduced efficiency compared to N-S-oriented streets can be attributed to the sun's east-west movement, which limits the shading benefits during the early morning and late afternoon hours.

Canopy shading demonstrated similar orientation-based differences. N-S streets consistently received ratings of 4 or 5, as canopies provided continuous shading throughout the day by aligning with the solar path. In E-W streets, the effectiveness of canopies was slightly improved, with ratings ranging from 3 to 4, as shading coverage was uniform during certain times of the day, highlighting the orientation-specific interaction between canopy placement and sun angles.

In N-S-oriented streets, the Combination Strategy demonstrates performance levels similar to Dense Vegetation, achieving ratings between 3 and 5 across most configurations. This similarity can be attributed to the substantial shading provided by the interplay of tree and pedestrian-level canopies, which creates a stable microclimate, effectively reducing heat stress. However, canopy shading consistently outperforms both dense vegetation and the combination Strategy, receiving higher ratings. In E-W streets, the combination strategy performed high, with ratings of 3.

Sparse vegetation is moderately effective, scoring between 2 and 3 on N-S, whereas it scores 1 and 2 on E-W orientation. The sparse tree cover could partially mitigate heat during peak afternoon hours. However, sparse vegetation remained insufficient to meet the accepted thermal comfort range, demonstrating limited applicability for high-density urban areas or streets with higher AR values.

The analysis highlights that the highest-rated strategies (5) align with the accepted thermal comfort range but are fewer in number due to the inherent complexity of achieving thermal comfort solely through shading. This shows the need to consider other environmental factors, such as wind patterns, reflective materials, and the cooling effects of water bodies, to enhance the overall microclimate. While shading remains a critical component of thermal comfort, it must be integrated into a holistic urban design approach to achieve maximum efficiency.

The findings highlight the importance of horizontal shading solutions like canopies, particularly in E-W streets, where they provide the most effective mitigation against solar exposure. This analysis emphasizes the importance of modifying shading strategies to specific street characteristics and integrating them with complementary environmental interventions to create resilient and thermally comfortable urban environments.

Table 3. Thermal Comfort Evaluation Matrix Based on mPET Ratings Across Building Typologies and Vegetation Scenarios

Street Orientation	Aspect Ratio (AR)	Building Typology (BT)	Side of the Street	Base Case	Vegetation (Sparse)	Vegetation (Dense)	Canopy	Combination
N-S	Shallow	BT1 (Singular)	E	1	1	2	3	2
			W	2	3	3	3	3
		BT2 (Linear)	E	1	2	2	3	3
			W	2	3	3	4	3
		BT3 (Scattered)	E	1	1	2	3	2
			W	1	2	3	3	3
	Uniform	BT1 (Singular)	E	2	3	4	4	4
			W	3	3	5	5	5
		BT2 (Linear)	E	2	3	4	4	4
			W	3	3	4	5	5
		BT3 (Scattered)	E	1	2	3	4	3
			W	2	3	4	4	4
	Deep	BT1 (Singular)	E	2	3	4	5	4
			W	3	3	5	5	5
		BT2 (Linear)	E	3	3	4	5	4
			W	3	4	5	5	5
		BT3 (Scattered)	E	2	3	4	4	4
			W	2	3	4	4	4
E-W	Shallow	BT1 (Singular)	N	1	2	2	3	3
			S	1	2	3	4	3
		BT2 (Linear)	N	1	1	2	3	2
			S	1	2	3	4	3
		BT3 (Scattered)	N	1	1	2	3	2
			S	1	1	2	3	3
	Uniform	BT1 (Singular)	N	1	1	3	4	3
			S	1	2	3	4	3
		BT2 (Linear)	N	1	2	3	4	2
			S	1	2	3	4	3
		BT3 (Scattered)	N	1	1	2	3	2
			S	1	2	3	3	3
	Deep	BT1 (Singular)	N	1	1	3	4	3
			S	1	2	3	4	4
		BT2 (Linear)	N	1	2	3	4	3
			S	1	2	3	4	4
		BT3 (Scattered)	N	1	1	2	3	3
			S	1	2	3	3	3

Rating with respective mPET Ranges: **5**- 33.8–35.82; **4**- 35.82–37.84; **3**- 37.84–39.86; **2**- 39.86–41.88; **1**- 41.88–43.9

Discussion and Conclusion

This paper investigated the influence of urban street geometry and shading strategies on pedestrian thermal comfort through microclimate simulations using ENVI-met 5.6.1 and the mPET index evaluation using trained machine learning model. The study analyzed 90 urban scenarios, varying building typologies (singular, linear, scattered), aspect ratios (shallow, uniform, deep), street orientations (N–S, E–W), and shading interventions (vegetation, canopies, or combined). The simulation of 90 urban scenarios revealed that pedestrian thermal comfort (mPET) is most effectively improved through the synergistic integration of street geometry and targeted shading strategies, rather than either approach in isolation. The results support the critical role of street orientation in influencing outdoor thermal comfort, especially in hot climates. The N–S orientation consistently exhibited better thermal performance, as indicated by lower mPET values (Minimum up to 33.1°C) and reduced exposure to direct solar radiation during a significant duration of the day. These orientations benefit from prevailing wind direction, leading to increased wind velocity (Va), which plays a significant role in convective cooling. Whereas, E–W-oriented streets presented the most thermally stressful conditions, with mPET values peaking at 43.9°C, primarily due to elevated mean radiant temperatures (Tmrt) and significantly reduced wind flow. This is consistent with previous studies, (Elnabawi & Hamza, 2020; Elraouf et al., 2022; Mahmoud & Ghanem, 2019; Sharmin & Steemers, 2013), confirming the negative effect of E–W orientation on thermal comfort environment. The higher aspect ratio shows improved thermal comfort due to increased self-shading of the canyon walls, reducing Tmrt. This aligns with findings from other climatic contexts, (Achour-Younsi & Kharrat, 2016b; De & Mukherjee, 2018a, 2018b; Galal et al., 2020b; Lobaccaro et al., 2019; Qaid & Ossen, 2015c) supporting the use of shaded street profiles to mitigate solar radiation exposure. However, additional shading measures such as tree planting or overhead canopies are necessary, especially in E–W-oriented streets, where solar exposure remains high during afternoon hours regardless of aspect ratio(Mohite & Surawar, 2024c). The results also showed that the benefit of a deep aspect ratio is strongly moderated by orientation. While deep canyons provided the greatest improvement in N-S streets, their efficacy in E-W streets was limited, demonstrating that geometry alone cannot overcome the solar exposure inherent to east-west orientation.

The role of building typology further complements the findings on street geometry. The results align with (Abd Elraouf et al., 2022b; Abdollahzadeh & Biloria, 2021) indicated that the linear typology of buildings provides the highest level of comfort among the other alternatives. Meanwhile, the singular typology is the best option for E–W-oriented streets, as it generates the least Tmrt value and the highest Va value in these orientations.

Among shading strategies, canopy shading was most impactful, reducing mPET by up to 7°C, particularly in E–W streets where horizontal shading proved most useful. Dense vegetation also improved comfort but was less effective than canopies in E–W orientations due to solar path alignment.

This performance difference can be attributed to the distinct cooling mechanisms. Canopies provide continuous, horizontal obstruction of the sun's path, directly and consistently reducing Tmrt. Vegetation, while offering shading and evaporative cooling, casts dynamic, vertical shadows that provide less complete coverage against the low-angle morning and afternoon sun prevalent in E–W streets, explaining its relative lower efficacy in these orientations. The findings emphasize that optimal thermal comfort requires context-specific solutions. The thermal comfort rating matrix (Table 3) operationalizes this principle, providing a decision-support tool. It translates complex interactions into actionable guidance, showing, for example, that for an existing E–W street with a shallow aspect ratio, canopy shading (Rating 3-4) is a more reliable intervention than sparse vegetation (Rating 1-2).

While this study demonstrated the effectiveness of shading strategies in general, it was assumed that shading is either uniform or sparse considering fixed distance between two trees, along the entire street length. However, in reality, length, type of shading, placement, and frequency significantly influence localized thermal discomfort. This study focused on continuous shading elements and used wind data as a model input rather than analyzing ventilation interplay in detail. Future research should investigate the microclimate effects of various shade patterns, such as varying tree types, spacing or canopy gaps, on transient thermal perception.

Therefore, future studies may investigate the role of shading length and frequency by assessing localized skin temperature variations and transient thermal discomfort. This analysis may provide practical guidelines for optimizing shading distribution by ensuring consistent thermal comfort rather than relying solely on full-length shading solutions.

In conclusion, for the tropical savanna climate, development of thermally comfortable streets shall prioritize important actions such as actions favoring N–S orientations with deep canyons where possible, and deploying extensive horizontal shading like canopies as the primary mitigation for unavoidable E–W streets. The findings and the rating matrix shows that effective design requires moving beyond generic solutions to strategically align geometric form with specific, climate-responsive shading interventions. Street designs that will enable pedestrians to walk around comfortably in terms of thermal comfort are important. People working in the planning and design discipline should conduct even more research on this subject. Especially in urban renewal and transformation areas, better space designs should be made for people by increasing their thermal comfort.

References

Abdelhafez, M. H. H., Altaf, F., Alshenaifi, M., Hamdy, O., & Ragab, A. (2022). Achieving Effective Thermal Performance of Street Canyons in Various Climatic Zones. *Sustainability*, *14*(17), 10780–10780. https://doi.org/10.3390/SU141710780

Abdollahzadeh, N., & Biloria, N. (2021). Outdoor thermal comfort: Analyzing the impact of urban configurations on the thermal performance of street canyons in the humid subtropical climate of Sydney. *Frontiers of Architectural Research*, *10*(2), 394–409. https://doi.org/10.1016/J.FOAR.2020.11.006

Achour-Younsi, S., & Kharrat, F. (2016a). Outdoor Thermal Comfort: Impact of the Geometry of an Urban Street Canyon in a Mediterranean Subtropical Climate – Case Study Tunis, Tunisia. *Procedia - Social and Behavioral Sciences*, *216*(October 2015), 689–700. https://doi.org/10.1016/j.sbspro.2015.12.062

Achour-Younsi, S., & Kharrat, F. (2016b). Outdoor Thermal Comfort: Impact of the Geometry of an Urban Street Canyon in a Mediterranean Subtropical Climate – Case Study Tunis, Tunisia. *Procedia - Social and Behavioral Sciences*, *216*, 689–700. https://doi.org/10.1016/J.SBSPRO.2015.12.062

Aghamolaei, R., Azizi, M. M., Aminzadeh, B., & O'Donnell, J. (2023). A comprehensive review of outdoor thermal comfort in urban areas: Effective parameters and approaches. *Energy and Environment*, *34*(6), 2204–2227. https://doi.org/10.1177/0958305X221116176

Aicha, C., Moussadek, B., & Djamila, D. (2022). The Effect of Sky View Factor on the Thermic Ambiances: Case of Batna City. *International Journal of Innovative Studies in Sociology and Humanities*, *7*(8), 209–220. https://doi.org/10.20431/2456-4931.070820

Albdour, M. S., & Baranyai, B. (2019). Impact of street canyon geometry on outdoor thermal

comfort and weather parameters in Pécs. *Pollack Periodica*, *14*(3), 177–187. https://doi.org/10.1556/606.2019.14.3.17

Arif, V., & Yola, L. (2020). The Primacy of Microclimate and Thermal Comfort in a Walkability Study in the Tropics: A Review. *Journal of Strategic and Global Studies*, *3*(1). https://doi.org/10.7454/jsgs.v3i1.1025

Arif, V., & Yola, L. (2022). The Impact of Sky View Factor on Pedestrian Thermal Comfort in Tropical Context: A Case of Jakarta Sidewalk. *Lecture Notes in Civil Engineering*, *161*, 27–33. https://doi.org/10.1007/978-981-16-2329-5_4

Armson, D., Stringer, P., & Ennos, A. R. (2012). The effect of tree shade and grass on surface and globe temperatures in an urban area. *Urban Forestry & Urban Greening*, *11*(3), 245–255. https://doi.org/10.1016/J.UFUG.2012.05.002

Battista, G., de Lieto Vollaro, E., Ocłoń, P., & de Lieto Vollaro, R. (2023). Effects of urban heat island mitigation strategies in an urban square: A numerical modelling and experimental investigation. *Energy and Buildings*, *282*, 112809. https://doi.org/10.1016/J.ENBUILD.2023.112809

Bourbia, F., & Awbi, H. B. (2004). Building cluster and shading in urban canyon for hot dry climate Part 2: Shading simulations. *Renewable Energy*, *29*(2), 291–301. https://doi.org/10.1016/S0960-1481(03)00171-X

Chatzidimitriou, A., & Yannas, S. (2017). Street canyon design and improvement potential for urban open spaces; the influence of canyon aspect ratio and orientation on microclimate and outdoor comfort. *Sustainable Cities and Society*, *33*, 85–101. https://doi.org/10.1016/j.scs.2017.05.019

Chen, L., Ng, E., An, X., Ren, C., Lee, M., Wang, U., & He, Z. (2012). Sky view factor analysis of street canyons and its implications for daytime intra-urban air temperature differentials in high-rise, high-density urban areas of Hong Kong: A GIS-based simulation approach. *International Journal of Climatology*, *32*(1), 121–136. https://doi.org/10.1002/joc.2243

De, B., & Mukherjee, M. (2018). "Optimisation of canyon orientation and aspect ratio in warm-humid climate: Case of Rajarhat Newtown, India." *Urban Climate*, *24*, 887–920. https://doi.org/10.1016/J.UCLIM.2017.11.003

Dunjić, J. (2019). Outdoor Thermal Comfort Research in Urban Areas of Central and Southeast Europe: A Review. *Geographica Pannonica*, *23*(4), 359–373. https://doi.org/10.5937/GP23-24458

Dzyuban, Y., Hondula, D. M., Vanos, J. K., Middel, A., Coseo, P. J., Kuras, E. R., & Redman, C. L. (2022). Evidence of alliesthesia during a neighborhood thermal walk in a hot and dry city. *Science of The Total Environment*, *834*, 155294. https://doi.org/10.1016/J.SCITOTENV.2022.155294

Elnabawi, M. H., Hamza, N., & Dudek, S. (2013). Use and evaluation of the ENVI-met model for two different urban forms in Cairo, Egypt: Measurements and model simulations. *Proceedings of Building Simulation 2013: 13th Conference of IBPSA*, 13, 2800–2806. https://doi.org/10.26868/25222708.2013.1237

Elrefai, R., & Nikolopoulou, M. (2023). A simplified outdoor shading assessment method (OSAM) to identify outdoor shading requirements over the year within an urban context. *Sustainable Cities and Society*, *97*, 104773.

https://doi.org/10.1016/j.scs.2023.104773

Galal, O. M., Sailor, D. J., & Mahmoud, H. (2020). The impact of urban form on outdoor thermal comfort in hot arid environments during daylight hours, case study: New Aswan. *Building and Environment*, *184*, 107222. https://doi.org/10.1016/J.BUILDENV.2020.107222

Glen T. Johnson and Ian Watson. (1984). The determination of view factor in urban canyons. *Americal Metrological Society*. https://www.ptonline.com/articles/how-to-get-better-mfi-results

Harrington, L. J., Frame, D. J., Fischer, E. M., Hawkins, E., Joshi, M., & Jones, C. D. (2016). Poorest countries experience earlier anthropogenic emergence of daily temperature extremes. *Environmental Research Letters*, *11*(5), 055007. https://doi.org/10.1088/1748-9326/11/5/055007

Hess, J., Meister, A., Melnikov, V. R., & Axhausen, K. W. (2023). Geographic Information System-Based Model of Outdoor Thermal Comfort: Case Study for Zurich. *Transportation Research Record*, *2677*(3), 1465–1480. https://doi.org/10.1177/03611981221125211

ICLEI. (2021). *Climate resilient city action plan: Nagpur, Maharashtra, India* (Supported and jointly implemented). http://southasia.iclei.org

IPCC. (2022). *Climate Change 2022: Impacts, Adaptation and Vulnerability*. https://doi.org/ISBN 978-92-9169-161-6

Jamei, E., & Rajagopalan, P. (2017). Urban development and pedestrian thermal comfort in Melbourne. *Solar Energy*, *144*, 681–698. https://doi.org/10.1016/j.solener.2017.01.023

Khaire, J. D., Ortega Madrigal, L., & Serrano Lanzarote, B. (2024). Outdoor thermal comfort in built environment: A review of studies in India. *Energy and Buildings*, *303*, 113758. https://doi.org/10.1016/J.ENBUILD.2023.113758

Kim, Y. J., & Brown, R. D. (2021). A multilevel approach for assessing the effects of microclimatic urban design on pedestrian thermal comfort: The High Line in New York. *Building and Environment*, *205*, 108244. https://doi.org/10.1016/j.buildenv.2021.108244

Konarska, J., Uddling, J., Holmer, B., Lutz, M., Lindberg, F., Pleijel, H., & Thorsson, S. (2016). Transpiration of urban trees and its cooling effect in a high latitude city. *International Journal of Biometeorology*, *60*(1), 159–172. https://doi.org/10.1007/S00484-015-1014-X/FIGURES/8

Kotharkar, R., Bagade, A., & Agrawal, A. (2019). Investigating Local Climate Zones for Outdoor Thermal Comfort Assessment in an Indian City. *Geographica Pannonica*, *23*(4), 318–328. https://doi.org/10.5937/gp23-24251

Kotharkar, R., Dongarsane, P., & Keskar, R. (2023). Determining influence of urban morphology on air temperature and heat index with hourly emphasis. *Building and Environment*, *233*, 110044. https://doi.org/10.1016/j.buildenv.2023.110044

Li, Y., Huang, N., & He, J. (2023). Analytical evaluation of thermal comfort in the pedestrian environment using pedestrian shade space distribution. *Urban Climate*, *51*, 101665. https://doi.org/10.1016/J.UCLIM.2023.101665

Lin, T. P. (2009). Thermal perception, adaptation and attendance in a public square in hot and humid regions. *Building and Environment*, *44*(10), 2017–2026. https://doi.org/10.1016/J.BUILDENV.2009.02.004

Lin, T. P., & Matzarakis, A. (2008). Tourism climate and thermal comfort in Sun Moon Lake, Taiwan. *International Journal of Biometeorology*, *52*(4), 281–290. https://doi.org/10.1007/s00484-007-0122-7

Lin, T. P., Matzarakis, A., & Hwang, R. L. (2010). Shading effect on long-term outdoor thermal comfort. *Building and Environment*, *45*(1), 213–221. https://doi.org/10.1016/j.buildenv.2009.06.002

Lindberg, F., & Grimmond, C. S. B. (2011). The influence of vegetation and building morphology on shadow patterns and mean radiant temperatures in urban areas: Model development and evaluation. *Theoretical and Applied Climatology*, *105*(3), 311–323. https://doi.org/10.1007/S00704-010-0382-8/FIGURES/12

Lobaccaro, G., Acero, J. A., Martinez, G. S., Padro, A., Laburu, T., & Fernandez, G. (2019). Effects of orientations, aspect ratios, pavement materials and vegetation elements on thermal stress inside typical urban canyons. *International Journal of Environmental Research and Public Health, 16*(19), 3574. https://doi.org/10.3390/ijerph16193574

Ma, X., Zhao, J., Zhang, L., Wang, M., & Cheng, Z. (2020). *The Deviation between the Field Measurement and ENVI-met Outputs in Winter- A Cases Study in a Traditional Dwelling Settlement of China*. https://doi.org/10.21203/RS.3.RS-94479/V1

Manavvi, S., & Milosevic, D. (2025). Chasing cool: Unveiling the influence of green-blue features on outdoor thermal environment in Roorkee (India). *Building and Environment*, *267*, 112238. https://doi.org/10.1016/J.BUILDENV.2024.112238

Marcotullio, P. J., Keßler, C., Quintero Gonzalez, R., & Schmeltz, M. (2021). Urban Growth and Heat in Tropical Climates. *Frontiers in Ecology and Evolution*, *9*, 616626. https://doi.org/10.3389/FEVO.2021.616626/BIBTEX

Matzarakis, A. (2009). Additional features of the RayMan model. *The Seventh International Conference on Urban*, *July*, 3–6. http://www.urbanclimate.net/matzarakis1/papers/ICUC7_rayman_374543-1-090330185705-002.pdf

Matzarakis, A., & Mayer, H. (1996, December). *Another kind of environmental stress: Thermal stress*. WHO Collaborating Centre for Air Quality Management and Air Pollution Control, Institute for Water, Soil and Air Hygiene – Federal Environmental Agency (Newsletter No. 18).

Meshram, D. S. (2011). Institute of Town Planners. *India Journal 8-4*, 1–20.

Middel, A., Selover, N., Hagen, B., & Chhetri, N. (2016). Impact of shade on outdoor thermal comfort—a seasonal field study in Tempe, Arizona. *International Journal of Biometeorology*, *60*(12), 1849. https://doi.org/10.1007/S00484-016-1172-5

Mohite, S., & Surawar, M. (2024a). Assessing Pedestrian Thermal Comfort to Improve Walkability in the Urban Tropical Environment of Nagpur City. *Geographica Pannonica*, *28*(1), 71–84. https://doi.org/10.5937/gp28-48166

Mohite, S., & Surawar, M. (2024b). Assessment and prediction of pedestrian thermal comfort through machine learning modelling in tropical urban climate of Nagpur City.

Theoretical and Applied Climatology, *2006*, 1–23. https://doi.org/10.1007/s00704-024-04967-x

Mohite, S., & Surawar, M. (2024c). Impact of urban street geometry on outdoor pedestrian thermal comfort during heatwave in Nagpur city. *Sustainable Cities and Society*, *108*(April), 105450. https://doi.org/10.1016/j.scs.2024.105450

Paul, T., Daketi, S., Rao, K. M., & Chundeli, F. A. (2025). A qualitative approach for investigating thermal discomfort in the outdoor environment of a World Heritage Site: A case study of Hampi, India. *Geographica Pannonica, 29*(3), 172–193. https://doi.org/10.5937/gp29-57738

Porwal, S., Mandal, S. K., Banerjee, S., & Abdul, A. P. J. (2025). Factors Influencing Outdoor Thermal Comfort: A Review. *International Research Journal of Multidisciplinary Scope (IRJMS)*, *6*(2), 478–487. https://doi.org/10.47857/irjms.2025.v06i02.03123

Qaid, A., & Ossen, D. R. (2015). Effect of asymmetrical street aspect ratios on microclimates in hot, humid regions. *International Journal of Biometeorology*, *59*(6), 657–677. https://doi.org/10.1007/S00484-014-0878-5/FIGURES/15

Raman, V., Kumar, M., Sharma, A., & Matzarakis, A. (2021). A quantitative assessment of the dependence of outdoor thermal-stresses on tree-building morphology and wind: A case-study in sub-tropical Patna, India. *Sustainable Cities and Society*, *73*, 103085. https://doi.org/10.1016/J.SCS.2021.103085

Ratnayake, C. W., Perera, N. G. R., & Emmanuel, R. (2022a). Street Tree Planting Patterns to Modify the Sky View Factor for Outdoor Thermal Comfort Enhancement. *FARU Journal*, *9*(2), 1–1. https://doi.org/10.4038/FARUJ.V9I2.167

Russo, S., Sillmann, J., Sippel, S., Barcikowska, M. J., Ghisetti, C., Smid, M., & O'Neill, B. (2019). Half a degree and rapid socioeconomic development matter for heatwave risk. *Nature Communications*, *10*(1), 1–9. https://doi.org/10.1038/s41467-018-08070-4

Sayad, B., Alkama, D., Ahmad, H., Baili, J., Aljahdaly, N. H., & Menni, Y. (2021). Nature-based solutions to improve the summer thermal comfort outdoors. *Case Studies in Thermal Engineering*, *28*. https://doi.org/10.1016/J.CSITE.2021.101399

Segura, R., Krayenhoff, E. S., Martilli, A., Badia, A., Estruch, C., Ventura, S., & Villalba, G. (2022). How do street trees affect urban temperatures and radiation exchange? Observations and numerical evaluation in a highly compact city. *Urban Climate*, *46*, 101288. https://doi.org/10.1016/J.UCLIM.2022.101288

Sharmin, T., & Steemers, K. (2013). Effect of Canyon Geometry on Outdoor Thermal Comfort. *PLEA2013 - 29th International Conference Proceedings: Sustainable Architecture for a Renewable Future, Munich, Germany. 10-12 September 2013*, *September*. https://mediatum.ub.tum.de/doc/1169310/file.pdf

Siqi, J., Yuhong, W., & Nyuk Hien, W. (2023). The effect of urban greening on pedestrian's thermal comfort and walking behaviour. *E3S Web of Conferences*, *396*. https://doi.org/10.1051/e3sconf/202339605013

Speak, A., Montagnani, L., Wellstein, C., & Zerbe, S. (2020). The influence of tree traits on urban ground surface shade cooling. *Landscape and Urban Planning*, *197*, 103748. https://doi.org/10.1016/J.LANDURBPLAN.2020.103748

Srivanit, M., & Jareemit, D., (2019, December 1). Modelling the Urban Microclimate Effects of Street Configurations on Thermal Environment in the Residential Townhouse of Bangkok, Thailand. *1st International Conference on Recent Advances in Science and Technology (ICORAST 2019), MalaysiaAt: Kuala Lumpur, Malaysia*. https://doi.org/10.13140/RG.2.2.17499.21283

Surawar, Meenal; Kotharkar, R. (2017). Assessment of Urban Heat Island through Remote Sensing in Nagpur Urban Area Using Landsat 7 ETM+ satellite images. *International Journal of Urban and Civil Enginering*, *11*(7), 868–874. https://doi.org/10.5281/ZENODO.1131073

Tumini, I., Higueras García, E., & Baereswyl Rada, S. (2016). Urban microclimate and thermal comfort modelling: strategies for urban renovation. *International Journal of Sustainable Building Technology and Urban Development*, *7*(1), 22–37. https://doi.org/10.1080/2093761X.2016.1152204

Vailshery, L. S., Jaganmohan, M., & Nagendra, H. (2013). Effect of street trees on microclimate and air pollution in a tropical city. *Urban Forestry & Urban Greening*, *12*(3), 408–415. https://doi.org/10.1016/J.UFUG.2013.03.002

Vasilikou, C., & Nikolopoulou, M. (2020). Outdoor thermal comfort for pedestrians in movement: thermal walks in complex urban morphology. *International Journal of Biometeorology*, *64*(2), 277–291. https://doi.org/10.1007/s00484-019-01782-2

Watanabe, S., & Ishii, J. (2016). Effect of outdoor thermal environment on pedestrians' behavior selecting a shaded area in a humid subtropical region. *Building and Environment*, *95*, 32–41. https://doi.org/10.1016/j.buildenv.2015.09.015

Willmott, C. J. (1982). Some comments on the evaluation of model performance. *Bulletin - American Meteorological Society*, *63*(11), 1309–1313. https://doi.org/10.1175/1520-0477(1982)063<1309:SCOTEO>2.0.CO;2

Xu, L., Gopalakrishnan, S., & Schroepfer, T. (2023). *Assessment of overhead environments on pedestrian thermal comfort in a dense urban district*. https://doi.org/10.1051/e3sconf/202339605012

Yilmaz, S., Kurt, A., & Gölcü, M. (2023). ENVI-met Simulations of the Effect of Different Landscape Design Scenarios on Pedestrian Thermal Comfort: Haydar Aliyev Street. *Yuzuncu Yil University Journal of Agricultural Sciences*, *33*(3), 338–353. https://doi.org/10.29133/yyutbd.1265752

Zhang, M., You, W., Qin, Q., Peng, D., Hu, Y., Gao, Z., & Buccolieri, R. (2022). Investigation of typical residential block typologies and their impact on pedestrian-level microclimate in summers in Nanjing, China. *Frontiers of Architectural Research*, *11*(2), 278–296. https://doi.org/10.1016/J.FOAR.2021.10.008

Zhang, Y., Du, X., & Shi, Y. (2017). Effects of street canyon design on pedestrian thermal comfort in the hot-humid area of China. *International Journal of Biometeorology*, *61*(8), 1421–1432. https://doi.org/10.1007/S00484-017-1320-6

Zhao, H., Zhao, L., Zhai, Y., Jin, L., Meng, Q., Yan, J., Wu, R., & Brown, R. D. (2024). The impact of dynamic thermal experiences on pedestrian thermal comfort: A whole-trip perspective from laboratory studies. *Building and Environment*, *258*, 111599. https://doi.org/10.1016/J.BUILDENV.2024.111599

INTERNATIONAL SCIENTIFIC JOURNAL | GEOGRAPHICA PANNONICA

Bridging Disciplines: Inter–Multi–Transdisciplinary Pathways for Sustainable Urban Development in the Western Balkans

Dragan Milošević[A, B*]

[A] Meteorology and Air Quality Section, Wageningen University, Wageningen, The Netherlands
[B] Hydrology and Environmental Hydraulics Section, Wageningen University, Wageningen, The Netherlands; ORCID: 0000-0001-5050-0052

Received: November 27, 2025| Revised: January 13, 2026| Accepted: January 14, 2026

doi: 10.5937/gp29-64068

Abstract

Western Balkan cities currently stand at a critical inflection point, characterized by the convergence of intensifying climate and hydrometeorological hazards, acute environmental pollution, and profound demographic imbalances. This article argues that the region's persistent implementation gap—frequently described as being "full of plans but short of traction"—is not primarily a technological deficiency but a structural crisis of knowledge integration and governance. By analyzing the compounding nature of risks, where environmental stressors cascade across interdependent infrastructure systems, the study demonstrates that traditional, siloed policy responses are insufficient. Instead, it posits that achieving urban resilience requires a fundamental shift from technocratic management to inter-, multi-, and transdisciplinary frameworks. Four practical pathways are proposed to operationalize this shift: (1) embedding environmental and social risk assessment into the core of sustainable urban development; (2) integrating service delivery to simultaneously support livelihoods and sustainability; (3) establishing 'frugal' urban observatories that bridge official monitoring gaps with citizen science, providing a resource-efficient counterpart to expensive 'smart city' architectures; and (4) institutionalizing co-production to ground policy in local realities. Ultimately, the paper suggests that by treating integration as a delivery mechanism rather than an academic ideal, Western Balkan cities can transform into "integration laboratories," demonstrating how to govern sustainability transitions effectively under strict fiscal and administrative constraints.

Keywords: Sustainable Urban Development; Urban Climate Resilience; Transdisciplinary Governance; Nature-based Solutions (NBS); Western Balkans

Cities at a convergence point

Western Balkan cities are becoming the places where multiple pressures collide—and where their interactions become visible, lived, and politically consequential. Climate-related shocks and slow-onset stressors are expected to intensify together, with extreme heat, flash floods, wildfire, drought, and landslide hazards worsening and increasingly occurring simultaneously. These compounding hazards matter because infrastructure systems fail as systems: disruptions can

* Corresponding author: Dragan Milošević; e-mail: dragan.milosevic@wur.nl

cascade across transport, energy, food supply, and livelihoods when interdependent networks are stressed at the same time (World Bank, 2024a).

Urban concentration is amplifying these risks. Capital cities in Western Balkans now hold a disproportionate share of national urban populations—approaching half in cities such as Podgorica and Skopje—while many smaller cities are shrinking and losing economic vitality. At the same time, extreme heat days have increased sharply, from only a few days per year in the 1990s to more than 40 days per year on average in the 2010s, intensifying exposure precisely where population density and built surfaces are highest (World Bank, 2024b). The health burden that urban residents carry is already stark. In 19 assessed towns and cities, air pollution is estimated to reduce life expectancy by up to 13–16 months, with nearly 5,000 premature deaths per year directly attributable to air pollution (UNEP, 2022).

At the same time, demographic change is tightening constraints on municipal capacity just as the problem set expands. Rapid population ageing—driven by low fertility and sustained emigration—raises the dependency ratio and increases pressure on social expenditure and health systems over time (OECD, 2021). If the region's cities feel like they are "full of plans but short of traction," part of the explanation sits in governance capacity. The practical work of preparing mature projects, evaluating environmental impacts, and monitoring delivery is often weakest at the municipal level, even when formal compliance frameworks exist (Mildner et al., 2023).

This makes the constraint structural: sustainable, resilient, healthy and inclusive urban development in the Western Balkans is not primarily a technology problem—it is also a knowledge-integration and governance problem.

Why the bottleneck is integration, not information

Evidence is growing across climate risk, pollution, mobility, and sectoral transitions, but it often arrives in disconnected streams. The region's adaptation challenge is clearly framed as one of compounding risk and high costs of inaction, with damages projected to rise sharply without adaptation investments (World Bank, 2024a). Cities across the region score high on composite climate-hazard indices that combine heat, drought, floods, wildfire, and water stress, with most Western Balkan cities falling into high-risk or red-flag categories compared with cities elsewhere in Europe (World Bank, 2024b). These risks, however, are unevenly distributed across capitals, shrinking cities, coastal areas, and mountain basins, meaning that averages hide sharp local vulnerabilities.

What looks like "multiple problems" is often the same system showing up in different forms. Energy systems shape air quality and household affordability; transport choices shape exposure and access; land take and infrastructure form shape heat and flood impacts; monitoring capacity shapes what is visible and governable. The region's own Green Agenda reporting increasingly treats implementation as a coordination challenge—calling for stronger cross-sector collaboration and multi-level governance to accelerate progress and avoid duplication (Regional Cooperation Council, 2025). For example, urban nature-based solutions (NBS) can provide a pathway to cleaner environments and lower carbon emissions, helping cities move toward climate neutrality and circularity over the coming decades (Pearlmutter et al., 2021; Savić et al., 2024).

As a result, policy implementation becomes a coordination challenge rather than a technical one. Plans exist in abundance, but the absence of cross-sectoral, multi-level integration makes it difficult to translate them into investments that address compound risks rather than isolated symptoms.

The case for inter-, multi- and transdisciplinarity

Urban form, emissions, and environmental stress are tightly coupled. Cities that expand outward in low-density patterns generate higher $PM_{2.5}$ and CO_2 emissions from both transport and residential energy use, while more compact cities perform better on air quality and carbon intensity. At the same time, green cover declines as cities grow, reducing natural cooling and pollution absorption precisely where exposure is rising (World Bank, 2024b). These patterns link land-use planning, energy systems, transport, public health, and ecosystem management into a single system. Air pollution and climate change share sources; waste mismanagement contributes to methane emissions, fire risk, and local toxicity; housing quality determines vulnerability to both heat and cold. Polluted air shows why integration is non-negotiable. Pollution sources range from thermal power generation and industrial facilities to traffic emissions, mining and household heating, with seasonal variation and city-specific mixes that demand different combinations of energy, housing, transport, and health interventions (UNEP, 2022). Another example is related to urban mobility. Transport systems in many cities fail to provide adequate capacity and service quality, contributing to congestion, air pollution, and unequal accessibility—while the absence of coherent policy and investment frameworks keeps cities stuck in incremental responses (World Bank, 2024c).

No single discipline can capture these interactions, and no single agency can manage them alone. In this context, transdisciplinarity becomes a necessity rather than an aspiration. Local authorities, utilities, civil society, and residents hold critical knowledge about how systems actually function on the ground—where heat accumulates, where waste is burned, where transport fails, where energy poverty bites. Co-producing knowledge with these actors strengthens both the accuracy of diagnosis and the legitimacy of solutions (Mildner et al., 2023). Gathering the perspectives of key stakeholders and local population before implementing solutions, such as NBS, increases their effectiveness and supports efforts to address climate change, biodiversity loss, and growing pressures on water and food resources (Megyesi et al., 2024). This approach should be included in decision-making processes to develop climate-sensitive urban services that are place-based, people-centric, and facilitate planning towards green, resilient, and inclusive cities (Milošević et al., 2022).

Data gaps—and frugal pathways to smarter governance

A recurring constraint is not simply "lack of data," but inconsistent monitoring, fragile maintenance financing, and uneven analytical capacity. Urban environmental monitoring is particularly underdeveloped despite being central to adaptation and public health. Most Western Balkan cities lack dense, locally calibrated observations of temperature, humidity, heat stress, precipitation, and urban surface conditions, even though heatwaves and pluvial flood effects are becoming dominant climate risks (Milošević et al., 2023; Arsenović et al., 2023; Allen et al., 2024; Tošić et al., 2025). These risks do not affect urban populations evenly: poorer households, informal neighborhoods, and elderly populations are far more exposed because of housing quality, location, and limited access to cooling, green space, and healthcare. Air-quality reporting across the region also highlights inconsistent data due to station maintenance financing gaps and the absence of certified calibration laboratories and air-quality modelling capacity—limitations that compromise trend analysis and targeted policy design (UNEP, 2022).

Most Western Balkan cities still lack integrated data that links environmental hazards with population characteristics, health outcomes, and service access, making it difficult to identify who is most at risk and to design targeted interventions. Without exposure and vulnerability mapping, investments in resilience risk protecting infrastructure rather than people. Thus, rather than just importing an expensive "smart city" model built on dense proprietary sensor networks, the Western Balkans context points toward frugal, layered observatories: strengthen fit-for-purpose official monitoring, targeted low-cost deployments where decisions require granularity, use crowdsourcing and citizen science, and harmonize reporting for comparability and learning.

Practical pathways where integration can move the needle

What, then, would integration look like as an urban practice—not just an academic preference? Four practical pathways are provided below and visualized in Figure 1.

1. Resilient Cities Start with Smarter Development. In Western Balkan cities, heatwaves, floods, droughts, and air pollution already affect who stays healthy, who finds work, and which neighborhoods continue to attract investment. These pressures will intensify for future generations if today's planning ignores them. Sustainable development therefore requires that urban growth, housing, and infrastructure decisions be guided not only by short-term economic returns but by where people are most exposed and vulnerable. Integrating environmental and social risk into urban development helps protect today's residents while preventing tomorrow's costs from being passed to future generations.

2. Deliver urban services in ways that support both livelihoods and long-term sustainability. Energy, water, housing, transport, waste, and healthcare are the everyday foundations of prosperity and wellbeing. When these services are planned in isolation, cities waste resources, deepen inequality, and increase environmental damage. Coordinated service provision—such as cleaner heating, efficient buildings, reliable public transport, and safe public space—allows Western Balkan cities to reduce pollution and climate stress while improving affordability, access to jobs, and quality of life. This is how economic growth, social inclusion, and environmental protection can reinforce rather than undermine each other.

3. Build frugal, transparent urban data systems to guide fair and effective decisions. Meeting today's needs without harming tomorrow requires knowing where problems and progress actually lie. Yet many Western Balkan cities lack reliable local data on air quality, heat, infrastructure performance, and social vulnerability. Frugal urban observatories that combine public data, low-cost sensors, and citizen reporting can provide the evidence needed to prioritize investments, track whether policies work, and ensure that resources are directed to the communities that need them most. Good data is not just about technology—it is also about accountability to both present and future residents.

4. Make co-production the backbone of urban sustainability. The transition toward more sustainable cities will only succeed if it reflects local realities and builds public trust. Municipal governments, scientists, businesses, and communities all hold knowledge that matters. In Western Balkan cities, where institutional capacity is often stretched, co-producing solutions—such as climate adaptation plans, nature-based projects, and service improvements—helps ensure that policies are practical, socially fair, and environmentally effective. Involving people in shaping their cities strengthens democracy today while creating more resilient and inclusive urban futures for the next generation.

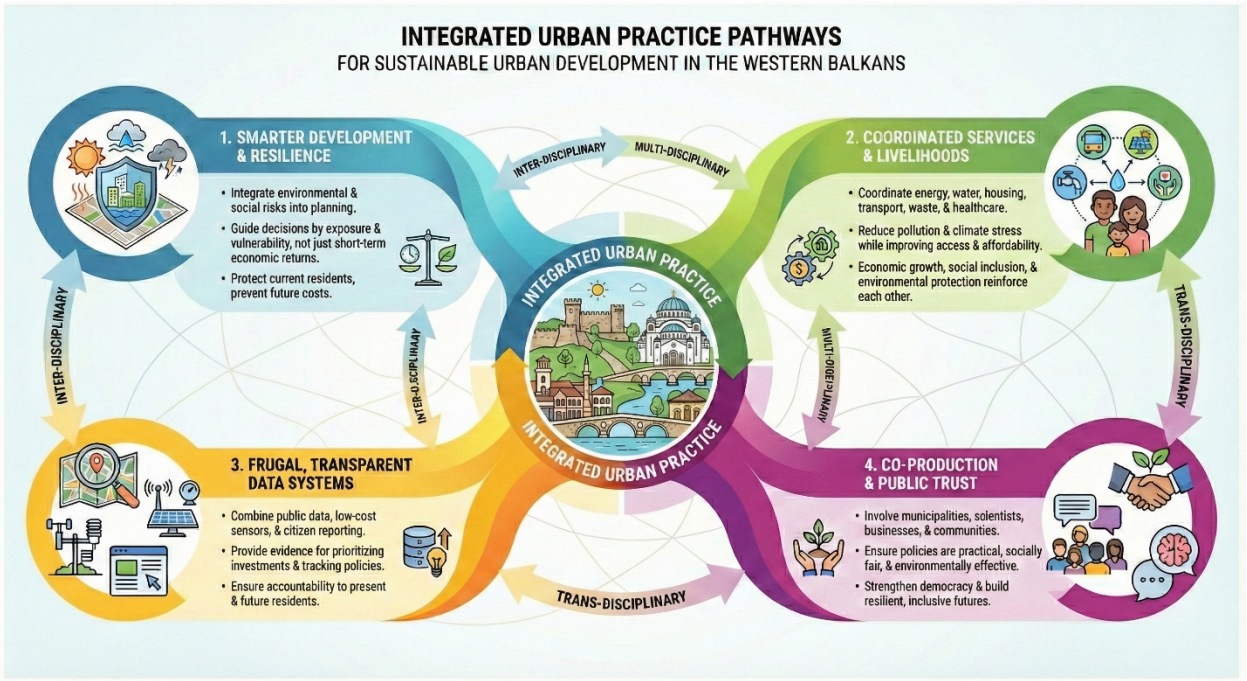

Figure 1. Conceptual framework for sustainable urban development in the Western Balkans. *Note: The graphical representation of this framework was developed by the author with visualization assistance from Google Gemini*

Conclusion: Western Balkan cities as "integration laboratories"

Western Balkan cities are not short of strategies or technical pilots; they are short of integration capacity—the ability to connect risk, health, mobility, energy, land, and monitoring into coherent governance that can deliver, learn, and adjust under tight fiscal and administrative constraints. Because hazards are compounding, infrastructure is interdependent, and health burdens are immediate, the cost of staying siloed is rising. If inter-, multi- and transdisciplinary approaches are treated as delivery tools—paired with frugal, reliable data ecosystems—Western Balkan cities can become "integration laboratories" that demonstrate how to govern sustainability transitions under constraint, rather than waiting to become idealized "smart cities" first.

References

Allen, M. J., Arsenović, D., Savić, S., & Nikitović, V. (2024). Mortality risk during heatwaves: An evaluation of effects by heatwaves characteristics in Serbia. *Geographica Pannonica, 28*(4), 284-293. https://doi.org/10.5937/gp28-52729

Arsenović, D., Lužanin, Z., Milošević, D., Dunjić, J., Nikitović, V., & Savić, S. (2023). The effects of summer ambient temperature on total mortality in Serbia. *International Journal of Biometeorology*, *67*(10), 1581-1589. https://doi.org/10.1007/s00484-023-02520-5

Megyesi, B., Gholipour, A., Cuomo, F., Canga, E., Tsatsou, A., Zihlmann, V., Junge, R., Milosevic, D. & Pineda-Martos, R. (2024). Perceptions of stakeholders on nature-based solutions in urban planning: A thematic analysis in six European cities. *Urban Forestry & Urban Greening*, *96*, 128344. https://doi.org/10.1016/j.ufug.2024.128344

Mildner S-A, Bories T, Sass M, Engstrom A, Neumann-Wengler S., & Gordon-Forbes, D. (Eds.). (2022). *GreenAgenda for the Western Balkans. The Road Toward Effective and Sustainable Implementation*. AspenInstitute Deutschland e.V. ISSN 2940-4169. *Available at: www.aspeninstitute.de/wp-content/uploads/Green-Agenda-for-the-Western-Balkans_2023.pdf*

Milošević, D., Dunjić, J., Stojsavljević, R., Žgela, M., Savić, S., & Arsenović, D. (2023). Analysis of long-and short-term biometeorological conditions in the Republic of Serbia. *International Journal of Biometeorology*, *67*(6), 1105-1123. https://doi.org/10.1007/s00484-023-02482-8

Milošević, D., Middel, A., Savić, S., Dunjić, J., Lau, K. & Stojsavljević, R. (2022). Mask wearing behavior in hot urban spaces of Novi Sad during the COVID-19 pandemic. *Science of the Total Environment*, *815*, 152782. http://dx.doi.org/10.1016/j.scitotenv.2021.152782

OECD (2021). *Multi-dimensional Review of the Western Balkans: Assessing Opportunities and Constraints, OECD Development Pathways*. OECD Publishing, Paris, https://doi.org/10.1787/4d5cbc2a-en.

Pearlmutter, D., Pucher, B., Calheiros, C. S. C., Hoffmann, K. A., Aicher, A., Pinho, P., Stracqualursi, A., Korolova, A., Pobric, A., Galvão, A., Tokuç, A., Bas, B., Theochari, D., Milosevic, D., Giancola, E., Bertino, G., Castellar, J. A. C., Flaszynska, J., Onur, M., ... & Nehls, T. (2021). Closing Water Cycles in the Built Environment through Nature-Based Solutions: The Contribution of Vertical Greening Systems and Green Roofs. *Water, 13*(16), 2165. https://doi.org/10.3390/w13162165

Regional Cooperation Council. (2025). *2024 report on the implementation of the Green Agenda for the Western Balkans Action Plan (GARI). Available at: https://www.rcc.int/pubs/218/2024-report-on-the-implementation-of-the-green-agenda-for-the-western-balkans-action-plan-gari*

Savić, S., Krstić, H., Šećerov, I. & Dunjić, J. (2024). Decreasing the energy demand in public buildings using nature-based solutions: Case studies from Novi Sad (Republic of Serbia) and Osijek (Republic of Croatia). *Energy, sustainability and society*, *14*(1), 23. https://doi-org.ezproxy.library.wur.nl/10.1186/s13705-024-00455-2

Tošić, I., da Silva, A.S.A., Filipović, L., Putniković, S., Stošić, T., Stošić, B. & Đurđević, V. (2025). Extreme precipitation events in Novi Sad during the period 1961-2020. *Geographica Pannonica*, *29*(3). 10.5937/gp29-57395

United Nations Environment Programme (2022). *Air pollution in the Western Balkans: Key messages for policymakers and the public.* Available at: https://www.ccacoalition.org/resources/air-pollution-western-balkans-key-messages-policy-makers-and-public

World Bank. (2024a). *Country Climate and Development Report: Western Balkans 6 background note—Adapting to a changing climate: The case for urgent action.* Available at: https://documents1.worldbank.org/curated/en/099092624072026025/pdf/P179205-f9cb3642-1bdb-4724-93c6-deec380abe55.pdf

World Bank. (2024b). *Reshaping Cities: Readying Cities in the Western Balkans for a Changing Climate*. World Bank. Available at: https://www.worldbank.org/en/region/eca/publication/reshaping-cities-readying-cities-in-the-western-balkans-for-a-changing-climate

World Bank. (2024c). *Western Balkans Urban Mobility Initiative: Summary report.* Available at: https://documents.worldbank.org/en/publication/documents-reports/documentdetail/099060624074022601